FLOW RESISTANCE OF DUNES IN ALLUVIAL STREAMS

Thesis by

Li-San Hwang

In Partial Fulfillment of the Requirements

For the Degree of

Doctor of Philosophy

California Institute of Technology

Pasadena, California

1965

ACKNOWLEDGMENT

The writer wishes to express his profound indebtedness and sincere appreciation for the helpful guidance and generous assistance offered by his advisor, Professor Vito A. Vanoni, throughout the course of this research.

Special appreciation is expressed for the valuable criticism and suggestions given by Professor Norman H. Brooks during the progress of this investigation.

Furthermore, the writer would like again to express his sincere thanks to both Professors Vito A. Vanoni and Norman H. Brooks for the use of their unpublished experimental results which were obtained in research carried out with the aid of National Science Foundation Grant G-1709.

In addition, the writer would like to thank Dr. Fredric Raichlen for his help in the instrumentation, Mr. Elton Daly for the assistance in developing apparatus and the technique of stabilizing dune beds and Mr. Robert Greenway for the construction of the experimental equipment.

For the assistance in preparing the figures for this thesis, the writer would like to extend his gratitude to Mr. Carl Eastvedt and Mr. Fred Cammack.

The laboratory investigation was carried out with the support of National Science Foundation Grants G19194 and GK89. The 130-foot flume used in the study was built with the support of National Science Foundation Grant G19821.

ABSTRACT

Studies were made of the hydrodynamic resistance of channels with beds covered with dunes generated by flows over granular sediments of the kind normally found in alluvial rivers. The principal objectives of the studies were to determine the pertinent geometric properties of a dune bed by means of which one can express the dune resistance and to establish a quantitative relation between resistance and these geometric quantities. The main results reported here were obtained through experiments in laboratory flumes.

A series of 23 experiments with flows over dune-covered beds of fine sand were performed in tilting flumes 130 ft. and 40 ft. in length respectively. In addition, two dune beds generated by different flows were stabilized chemically without disturbing their surface configurations and texture. By doing this, it was possible to explore velocity and pressure distributions in the flow fields and to determine the effect of Reynolds number on the friction factor of the dune beds.

It was found that the hydrodynamic roughness of a dune field can be described by the average dune height and the exposure parameter which is the fraction of the total bed area occupied by the horizontal projection of the steep lee slopes of the dunes. It was also found from the results of flume experiments that the bed friction factor due to dunes is a function of the modified relative roughness, $r_b/e\overline{H}$, where r_b is the bed hydraulic radius, e is the exposure parameter defined above and $\overline{H}$ is the average dune height.

A function for dune resistance in straight uniform channels, that is, Equation (6-1) was established from experimental results obtained in the flume. Friction factors for typical alluvial rivers cannot be calculated from Equation (6-1) above because some important features of streams, such as meandering, which contribute to resistance are not reproduced in flumes.

TABLE OF CONTENTS

LIST OF FIGURES

LIST OF FIGURES (cont'd)

LIST OF FIGURES (cont'd)

LIST OF FIGURES (cont'd)

LIST OF FIGURES (cont'd)

LIST OF TABLES

CHAPTER I

INTRODUCTION

Due to increasing activities in the development of water resources and in the construction of hydraulic projects, the problem of sediment transportation in alluvial streams has increased considerably in importance in the last decades. Some knowledge of the general mechanism of sediment transportation has been obtained through intensive studies both in the laboratory and in the field, but there are still many fundamental questions remaining without satisfactory answers. In order to manage rivers intelligently, knowledge is needed of the fundamental laws governing the transportation of sediment by water and governing the flow of water in the presence of sediment.

Observations in alluvial channels show that water flowing over a sand bed interacts with the bed in various ways. Such interactions result in bed configurations which depend on conditions such as velocity, depth of flow and properties of the sediment. When the velocity near the bed is only slightly greater than that required to initiate movement of the sediment, it deforms into a series of waves which are triangular in profile with gentle upstream slopes, steep downstream or lee slopes and sharp crests. These are called dunes or ripples and are familiar to many people since they are often observed in small streams with sandy beds. Sediment is moved up the upstream side of dunes to the sharp crest where it slides down the steep lee side. In this way dunes move slowly downstream. The flow separates at

the sharp crest forming an eddy or wake on the lee side of the dune. The size of dunes varies with flow conditions and sand properties and is not uniform for a particular flow. Furthermore, shapes and geometric arrangement of dunes in sand beds vary with flow conditions and sediment properties in a way that is not understood. The presence of dunes generated by the flow itself will affect the flow pattern and the resistance to the flow. Under some conditions a further increase of the velocity to a certain value will cause the dunes to disappear abruptly and the bed to become flat. This limiting velocity at which the bed becomes flat depends on the characteristics of sand and on the depth of flow. By still further increasing the velocity, other bed forms will be generated. These will not be described since they are not of interest to this study.

Brooks [1] has called attention to the effect of dunes on flow resistance, but no quantitative studies of this effect have been made. The objectives of this research are: (1) to determine the pertinent geometric properties of dune fields by means of which one can express the resistance to flow offered by dune fields and (2) to establish a quantitative relationship between the resistance to flow and these geometric quantities.

Because of the complexity of the flow system under consideration, the method of solving this problem depends largely on experiments. Most of the data used in this study were obtained from experiments in flumes with loose beds of fine sands. Series of experiments were made with two different solidified or stabilized dune beds without any sediment in motion. These made it possible to change flow velocity,

depth and fluid properties while the bed configuration remained fixed. With fixed beds it was also possible to explore velocity and pressure distributions in the flow fields. This is not possible in flows with loose beds because the dunes are moving and also because disturbances due to an instrument near the bed will destroy or modify the dunes near the instrument.

In Chapter II, analytical considerations of the problem are presented. Chapters III and IV describe experimental apparatus and techniques, and experimental procedures respectively. In Chapter V, the experimental data are presented and discussed briefly. In Chapter VI, a resistance function is given for straight channels with dune covered beds. Chapter VII deals mainly with the discussion of field observations. And finally, the conclusions and results are summarized in Chapter VIII.

CHAPTER II

ANALYTICAL CONSIDERATIONS

A. Resistance of Sand Roughness Elements

The problem of the hydrodynamic resistance offered to a steady uniform turbulent flow by a bed composed of closely packed sand grains has been solved and the results are to be found in many textbooks. These results show that when the ratio of the sand grain size, d_s, to the thickness of the laminar sublayer, δ, exceeds about 5 the resistance to flow depends only on the mean velocity, pipe diameter, fluid density and d_s. In this region, the resistance is independent of the fluid viscosity and the bed is said to be hydrodynamically rough. The resistance is usually expressed by the friction factor, f, defined by the Darcy-Weisbach formula

$$h_f = f \frac{l}{4r} \frac{U^2}{2g} \tag{2-1}$$

in which h_f is the drop in piezometric head in a distance l, r is the hydraulic radius of the pipe cross section defined by the total cross-sectional area divided by the wetted perimeter, g is the acceleration of gravity and U is the average velocity. For hydrodynamically rough channels with walls roughened with closely packed sand of size d_s, the friction factor can be expressed as a function of relative roughness $\frac{4r}{d_s}$ only, that is

$$f = F\left(\frac{4r}{d_s}\right) \tag{2-2}$$

Although the values of f in this equation have been determined for circular pipes it has been found that they also are valid for flows with non-circular cross sections like those of open channels[2]. Based on experi-

ments in pipes by Nikuradse[3], von Karman[4] established the functional relationship of Equation (2-2) as follows:

$$f = \frac{1}{(1.16 + 2\log 4r/d_s)^2} \tag{2-3}$$

The friction factor for the closely packed sand roughness elements can be expressed in terms of $4r/d_s$ alone because all surfaces covered with closely packed uniform sand grains are geometrically similar. However, if the sand particles on a boundary are not closely packed, the resistance to flow offered by the boundary will not depend simply on the size of the sand grain, d_s, alone. Other geometric quantities such as the areal density of the sand grains and their geometrical arrangement will also affect the resistance and will have to be considered.

The very useful idea of equivalent sand roughness size, k_s, introduced by von Karman[2] can be applied to this problem. To explain this idea suppose one has the value of the friction factor, f, of a rough channel with roughness elements other than of closely packed sand grains. Then the equivalent sand roughness size for this surface is equal to the sand size, d_s, of a hydrodynamically rough bed of closely packed sand grains which will have the same friction factor, f, when the flow has the same hydraulic radius, r. By this procedure one can calculate the equivalent sand roughness size of a bed made of any elements including one made of sand grains with arbitrary spacing. Obviously the equivalent sand roughness size of a bed of sand grains which are not closely packed is not the same as the sand size, d_s.

In order to solve for the friction factor of a bed covered with arbitrarily spaced sand grains, it is necessary to obtain a relation between the equivalent sand roughness size, k_s, the sand size d_s, the area density of the grains and their arrangement pattern. Such a relation can be expressed as

$$\frac{k_s}{d_s} = F\left(\frac{A_s}{A}, A_r\right) \tag{2-4}$$

in which $\frac{A_s}{A}$ is the areal density of the grains, A_s is the wall area covered by roughness elements in the total wall area A and A_r is a dimensionless parameter which describes the arrangement pattern of sand grains and which for intricate patterns may need to be expanded to several terms.

In his Study of Flow in Rough Conduits, Morris[5] found that the flow over discrete roughness elements can be classified into three basic regimes dependent on the area density and the size of roughness elements. He denoted these regimes as (1) isolated roughness flow, (2) wake interference flow, and (3) skimming flow. The second and third types are those in which the roughness elements are so closely packed that the wake behind one roughness element interferes with that of its neighbors. In these two types of flow, the resistance depends not only on the area density of sand particles but also on the arrangement of the particles because a different arrangement pattern will result in a different pattern of wake interference. The roughness elements in Morris' first type are sufficiently far apart so that the wake behind each roughness element does not interfere with that of its neighbors and hence the

arrangement will have little effect on the resistance. Therefore, for the first type of roughness, the resistance will largely depend on the areal density of the roughness elements, and for this case Equation (2-4) can be simplified to

$$\frac{k_s}{d_s} = F\left(\frac{A_s}{A}\right) \tag{2-5}$$

Furthermore, the drag due to the roughness elements will increase if the areal density of the roughness elements increases. Therefore, the equivalent sand roughness size, k_s, will also increase as the areal density of the roughness elements increases. Taylor[6] plotted experimental results obtained by Schlichting[7] and Colebrook and White[8] for isolated sand like roughness elements, and found that the value k_s/d_s is proportional to A_s/A. Through this linear relationship, one can find the equivalent sand roughness size, k_s, once $\frac{A_s}{A}$ and d_s are given and then the friction factor can be estimated from Equation (2-3) through the use of k_s in place of d_s.

B. Resistance of Sediment-Laden Streams

The resistance of a sediment-laden stream not only involves the effect of the roughness of the channel boundary, but also the effect of the suspended sediment[9]. Fortunately, in dune covered beds, the latter effect is relatively small[9] and may be neglected thus simplifying the problem.

The resistance which the boundary of an alluvial stream exerts on the flow can be divided into two parts: that due to the sides or banks and that due to the bed. In experiments the mean resistance over the boundary is measured and expressed in terms of a mean friction factor,

f , defined by Equation (2-1). The total resistance is separated into wall resistance and bed resistance by so-called side-wall correction method outlined by Einstein[10] and Johnson[11]. These resistances are also expressed in terms of friction factors f_w for the walls and f_b for the bed where the friction factors also are defined by equations similar to Equation (2-1).

The friction factor f_b for a dune covered bed can further be divided into two parts: (1) a part f'_b due to sand particles and (2) the remainder $f_b - f'_b$ due to the form drag of the dunes. An exact evaluation of f'_b for dune covered beds is rather difficult because the velocity profile near the dune surface and hence the resistance or shear stress caused by the grains is highly modified by the presence of the dunes. The distribution of the shear stress over a typical dune may be visualized qualitatively through observations and through measurements of velocity profiles. On the lee side of the dune, there is a stable wake which introduces a relatively low reversed velocity near the wall and therefore a small negative shear stress on the boundary within the wake. Downstream from the stagnation point where the dividing streamline of the wake meets the boundary, the flow is accelerated on the sloping upstream side of the dunes. Therefore, in this zone the shear stress is zero at the stagnation point and then gradually increases until the crest is reached[12]. When dunes are present, the resistance created by the sand grains is small[13] in comparison to that created by dune roughness. Also direct measurements of shear stress over idealized two-dimensional dunes[12] show that the shear stress due to grain roughness can be estimated reasonably well from the standard pipe friction chart, assuming

that there are no dunes. If the sand grain surface is hydrodynamically rough, f'_b can be approximated from Equation (2-3). When the bed material has a large range of sizes, the geometric mean sieve diameter, D_g, is used in place of d_s. To calculate f'_b where the bed is not completely rough, the value of the Reynolds number $\frac{4r_bU}{\nu}$ and the relative roughness $\frac{4r_b}{D_g}$ are first calculated from experimental data. The chart is then entered with these two values and a value of the friction factor, f , is read. This is denoted as f'_b, the bed friction factor due to the sand grain roughness.

It is clear that the error resulting from the inaccuracy of evaluating the relatively small grain friction factor, f'_b , will not introduce large error in predicting the total bed friction factor. Now the problem remaining is to establish the relationship between $f_b - f'_b$ due to the drag of the dunes and the dune dimensions and their spacing. Because dune dimensions are much larger than the thickness of the laminar boundary layer, it is reasonable to assume that a dune covered bed is hydrodynamically rough. If the dunes and dune patterns generated by different flows were similar, the dune friction factor, $f_b - f'_b$, would be expected to be a function of the relative roughness $\frac{r_b}{h}$ only, that is,

$$f_b - f'_b = F\left(\frac{r_b}{h}\right) \tag{2-6}$$

in which r_b is called the bed hydraulic radius and is obtained by the side-wall correction procedure[13] and h is a characteristic dimension of the dune field. In this case one may choose the average height, $\overline{H}$, as the characteristic length because of the similarity of dunes and their

pattern of arrangement. Actually, the shape and the pattern of arrangement of dunes generated under different flow conditions are different and hence the average dune height, $\overline{H}$, alone can not describe the hydraulic behavior of dune beds.

From observations it was found that the wakes behind the dunes in general do not interfere with one another. Therefore, the effect of their pattern of arrangement on the dune friction factor, $f_b - f'_b$, is probably small. On the basis of this information it seems reasonable to omit the arrangement parameter A_r so that the variables remaining to describe the roughness of the dune configuration are the areal density of the dunes and their height.

The form drag on one dune can be expressed as the product of a drag coefficient, the exposed area, and the dynamic pressure, $\frac{1}{2}\rho U^2$, acting on the dune surface, where ρ is the mass density of the water. From the observation of flow over a dune bed, it seems reasonable to use the vertical component of the area of the lee sides of dunes as the exposed area. However, the lee slopes of dunes observed in the flume are inclined at the angle of repose of the bed material and hence must vary very little. Hence the vertical components of the lee sides are proportional to the horizontal components and one can just as well use the horizontal components in the drag relation. As will be seen later this has the advantage that it can be determined from horizontal photographs. The total drag of the dunes in an area A which contains many dunes will increase as a_s, the sum of horizontal components of the lee sides area of all dunes in the area A, increases. And the mean dune drag per unit area will increase with a_s/A which will be called the

exposure parameter and designated by "e". Based on this discussion, the exposure parameter, e, of the dune is essentially equivalent to the areal density, A_s/A as it appears in the sand roughness elements. Therefore, it is reasonable to assume that the characteristic roughness of the dune, h, divided by the average dune height, $\overline{H}$, is proportional to the exposure parameter, e, that is

$$\frac{h}{\overline{H}} = C e \tag{2-7}$$

where C is a constant. Substituting this relationship into Equation (2-6), one obtains

$$f_b - f_b' = F\left(\frac{r_b}{Ce\overline{H}}\right)$$

or simply

$$f_b - f_b' = F\left(\frac{r_b}{e\overline{H}}\right) \tag{2-8}$$

The problem remaining is to find the functional relationship between $f_b - f'_b$ and $\frac{r_b}{e\overline{H}}$. This will be determined experimentally in Chapter VII.

CHAPTER III

APPARATUS AND TECHNIQUE

A. The 130-foot Flume and Accessories

1. General Description of the 130-foot Flume:

The flume is 43 5/16 inches wide, 24 inches deep and 130 feet long. A schematic diagram of the flume is shown in Fig. (3-1) and an oblique view of the entire flume taken from the downstream end is shown in Fig. (3-2). A detailed description of this flume has been given by Vanoni [14].

The entire floor of the flume is made of stainless steel and the side walls of the flume are of glass in panels of 5 feet long, except near the inlet and the outlet, where stainless steel sides are installed. The glass walls permit a clear side view of the bed configuration over most of the flume. The flume is supported on two 30-inch I-beams which are supported on a central pivot and four pairs of screw jacks spaced 28 feet apart. The jacks are operated through rigid hollow drive shafts by an electric motor located at the pivot point. Through this support system, the flume can be tilted continuously to a maximum slope of 2 percent.

Fig. (3-3) is a photograph of the control console. Through this console, the slope of the flume and the speed of the pump can be adjusted. The slope of the flume can be read directly to the nearest 0.00001 from a dial installed on the console. A more accurate value of slope can be read from a veriner, which gives the vertical displacement of the flume near the inlet end. With this scale, one can obtain

the slope to 0.000002. A portable remote control box is also available by means of which the slope and the pump speed can be varied.

As shown in Fig. (3-1), the water and the sediment flow from left to right in the open channel portion of the flume and down into the outlet tank. Then the water and the sediment which it carries pass through the pump into one of the return pipes and flow back to the flume inlet. The circuit is completely closed so that the water and the sediment are continuously recirculating. This feature is very important in sediment transportation experiments because the sediment is introduced to the flume at the same rate that it is discharged from the flume.

As shown in Fig. (3-1), there are two return pipes of 16- and 8-inch diameter, respectively, and each pipe is connected to a pump. The discharge is varied by changing the rotation speed of the pump shaft rather than by throttling. The 8-inch return system is used in sediment experiments with low discharge in order to avoid disposition which may form in the larger pipe due to the lower velocity. In the present investigation, only the 16-inch pipe was used and the other one was disconnected. The discharge in the 16-inch pipe was measured by a venturi meter, the location of which is shown in Fig. (3-1). The head difference across the meter was measured with an air-water manometer. The meter was calibrated in place against a weir installed in the flume section. At the upstream end of the venturi meter, a section of transparent lucite pipe 6 inches long and 16 inches in diameter is installed for the observing if sand has deposited in the

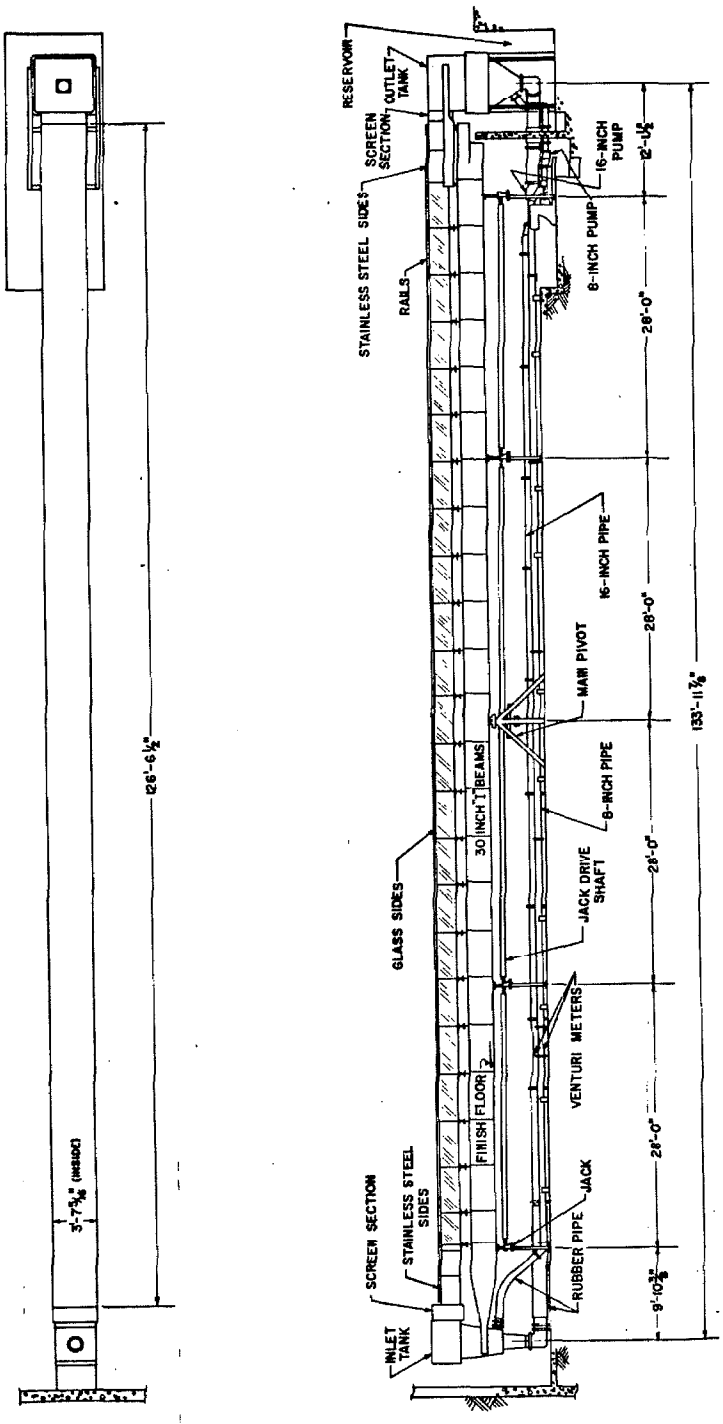

Fig.(3-1) 130-foot precision tilting flume

Fig. (3-2) Oblique view of the 130-foot flume from the downstream end.

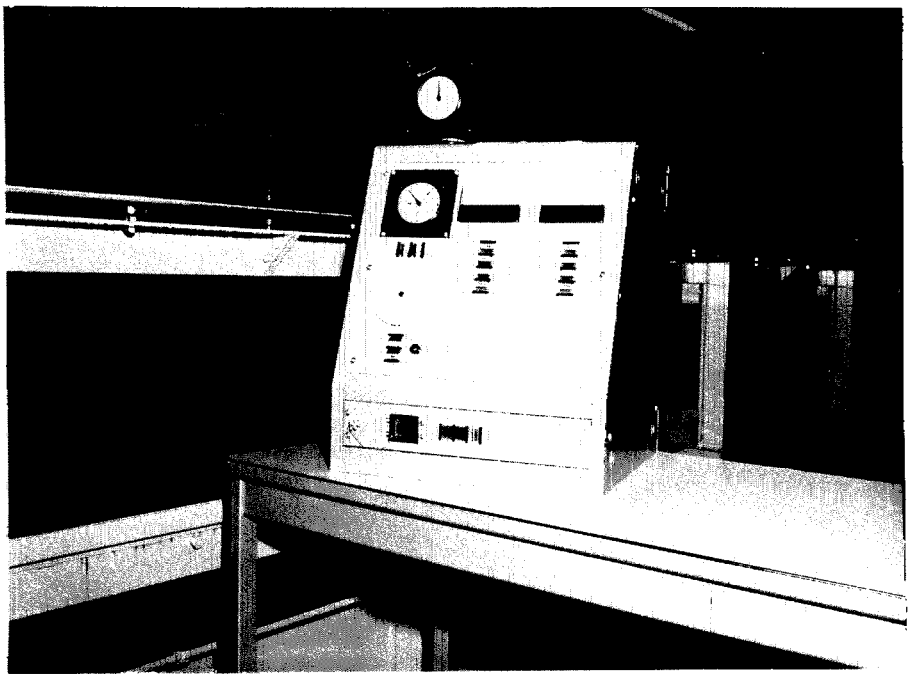

Fig. (3-3) Control console beside the 130-foot flume.

venturi meter and the pipe. The flexible rubber pipes shown in Fig. (3-4) are installed in both of the return pipes near the inlet tank to allow the necessary motion between the fixed pipes and the flume cuased by the adjusting of the slope of the flume.

A pair of rails $1\frac{1}{2}$ inches in diameter are installed on each side of the flume to provide the support for the instrument carriage. The instrument carriage shown in Fig. (3-5) and Fig. (3-2) can be moved on the rails along the entire length of the flume and its position can be read from a metric scale on the flume side. The point gauge which is mounted on the carriage can be moved both transversely across the flume and normally to the flume bottom. Metric scales on the carriage and the point gauge enable one to locate a point anywhere within the flume cross section to the nearest 0.0001 meter. The position along the flume can be determined to the nearest mm.

2. Inlet and Outlet Arrangements:

Fig. (3-6) shows an oblique view of the inlet end of the flume, which consists of an inlet tank, a screen section and a regulating sluice gate. A detailed longitudinal section of the inlet is shown in Fig. (3-7).

In order to minimize the disturbance in the flow entering the flume, some special baffles were used. Two baffles were installed in the bottom portion of the inlet tank as shown in Fig. (3-7). These were made of a square mesh of wood strips $2\frac{3}{8}$ inches wide by $\frac{3}{4}$ inches thick spaced $2\frac{3}{8}$ inches apart. In addition,a square mesh screen with 16 meshes per inch and one with 8 meshes per inch were placed in the screen section. With these baffles,large scale inlet disturbances are

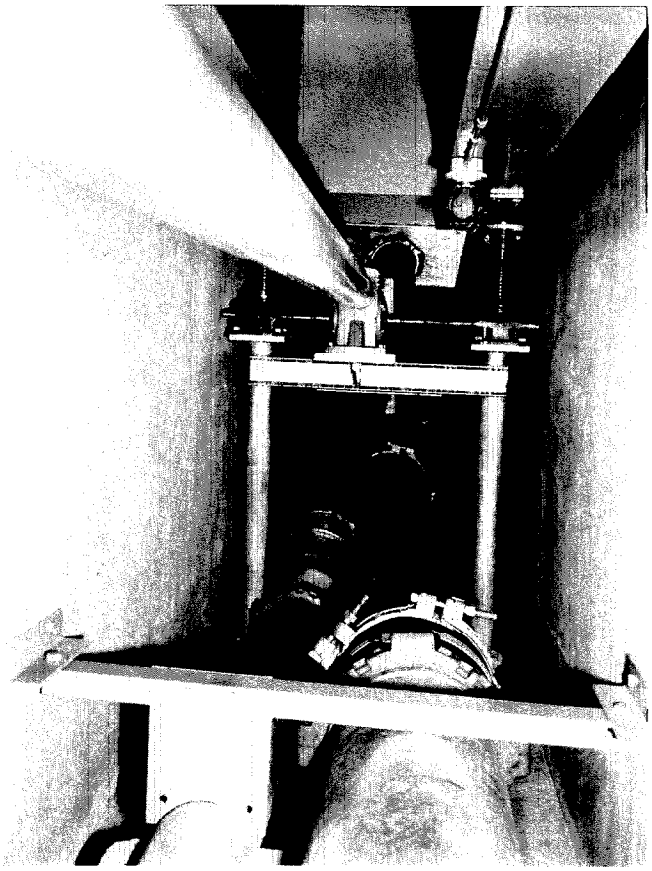

Fig. (3-4) 8-in. and 16-in. flexible rubber pipes in return lines. A pair of screw jacks and the drive shaft are also shown.

Fig. (3-5) Movable instrument carriage on the 130-foot flume.

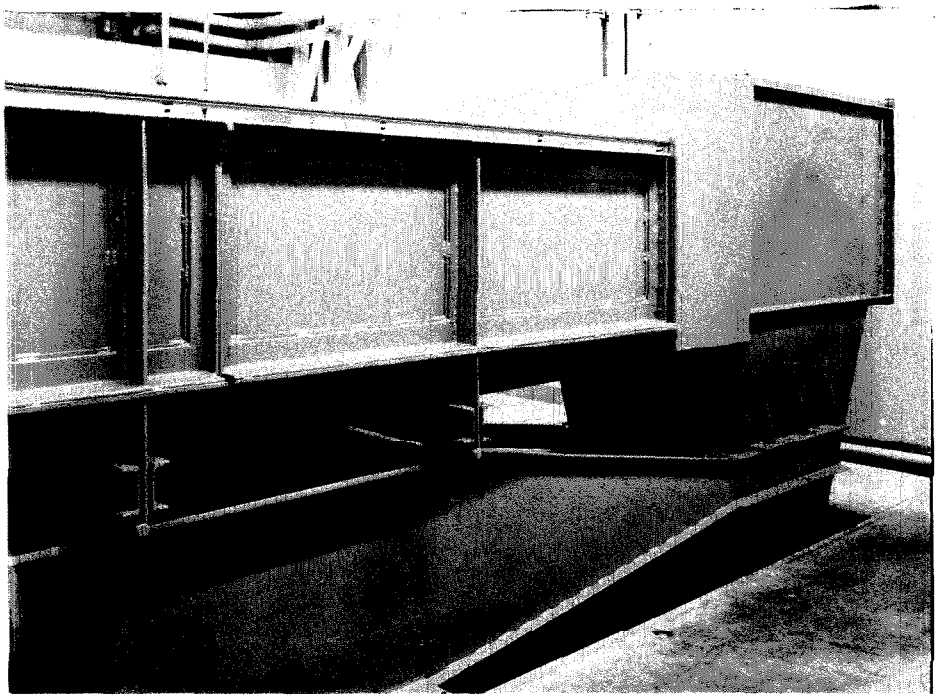

Fig. (3-6) View of the inlet end of the 130-foot flume.

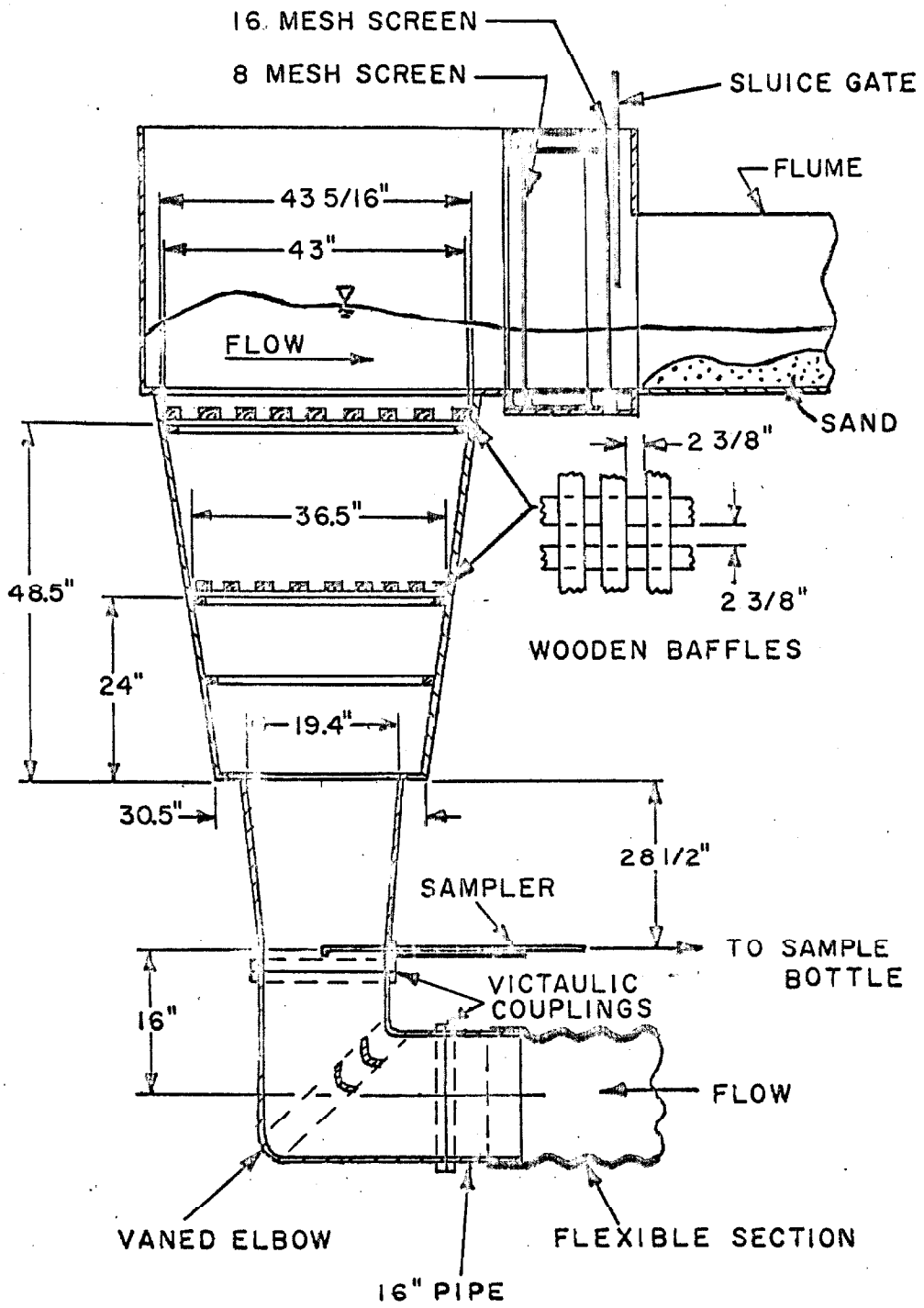

Fig. (3-7) Longitudinal section of the upstream end of the 130-foot flume.

eliminated in a relatively short distance. A detailed discussion of the function of such baffles has been given by Brooks[15].

The water surface in the screen section drops in elevation as it flows across the screens. Disturbances in this drop generate small waves downstream from the screen, especially for higher velocities. These waves increase the error in measuring the water surface elevation. To avoid these waves, a board approximately 43 in. x 40 in. size was placed floating on the water surface downstream of the screen section.

Fig. (3-8) shows an oblique view of the flume outlet tank. The enlarged section between the flume and the outlet tank is for inserting screens or other baffles. However, no screen was installed in performing the present experiments. The outlet tank which is 6.5 feet square is made of two portions. The upper portion which is attached to the flume is connected to the lower fixed portion by a rubber sheet to allow the necessary motion when the slope is adjusted.

3. Sampling Device:

The sediment discharge concentration was obtained by sampling the flow in the short vertical 16-inch pipe at the entrance to the diffuser of the inlet tank as shown in Fig. (3-7). As may be seen in this figure, the sampler is located just downstream from a 90° vane elbow which turns the flow vertically upward.

The general features of the sampler are shown in Fig. (3-9). The sampler tube is of hard-drawn brass tubing, $\frac{1}{2}$ in. outside diameter and $\frac{3}{8}$ in. inside diameter. The tube is kept horizontal and the end is bent through 90 degrees and is beveled to give a sharp edge, near

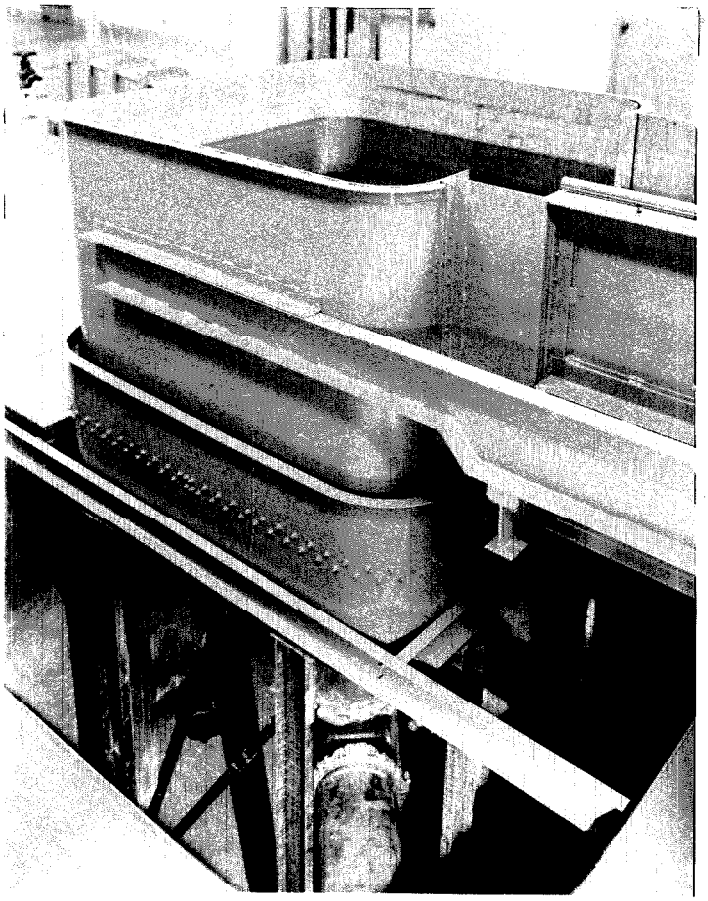

Fig. (3-8) View of the outlet tank of the 130-foot flume.

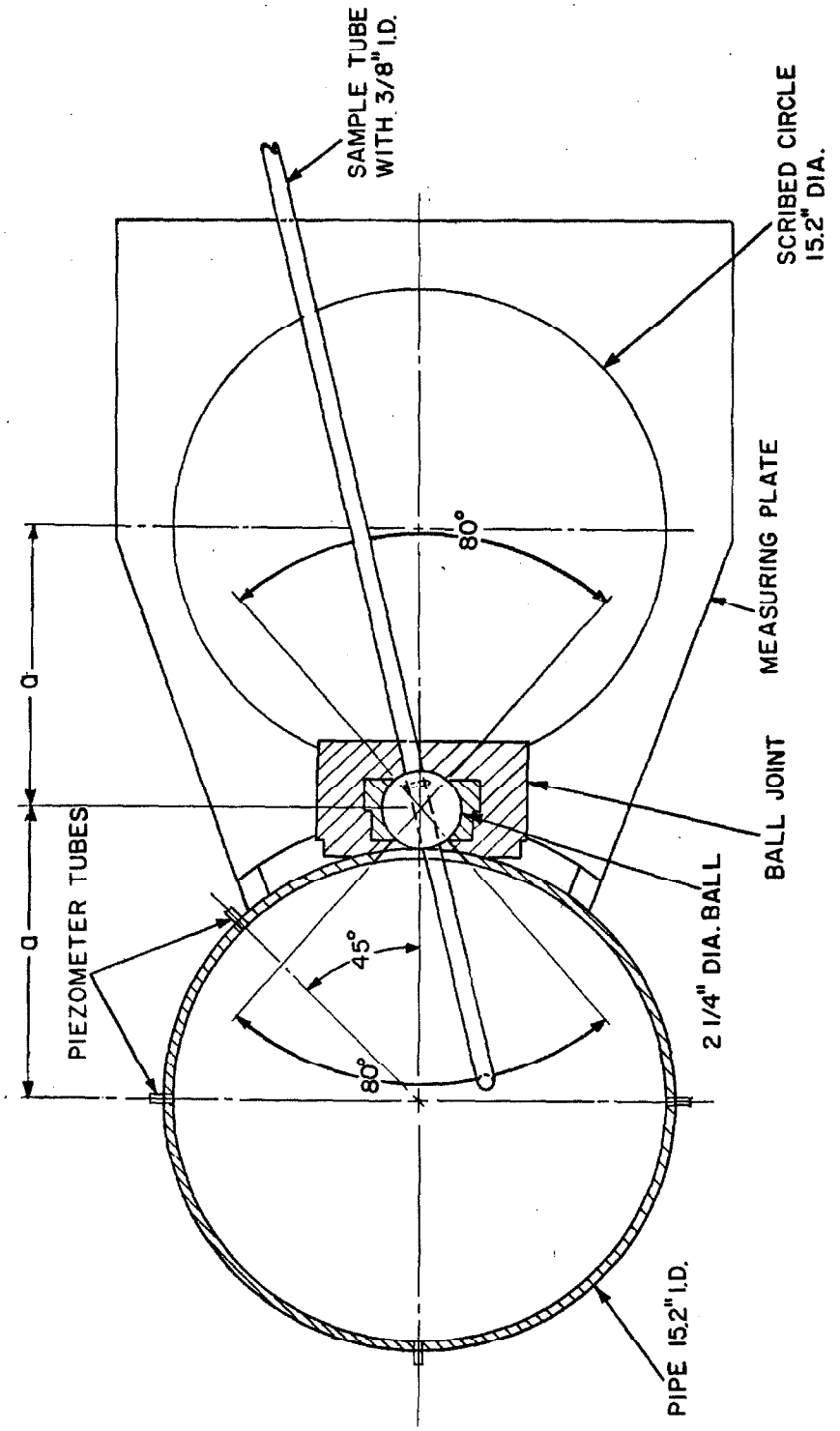

Fig. (3-9) Sampler and positioning plate used in the 130-foot flume.

inside wall. As shown in the figure, the tube passes through a stainless steel ball and an "O" ring seal is provided to prevent leakage of water. The ball can be rotated in a socket which also serves as a seal. The entire ball and socket assembly is bolted to the pipe and sealed with a gasket. A slotted hole in the pipe wall permits the sampler tube to swing in the horizontal plane through a total angle of 80°. Four piezometers were installed in the pipe wall at the level of the inlet end of the sampler tube. The sampler was also used as a total head pitot tube to determine point velocities in the pipe at the sampling section. In doing this, the difference between the total head and the static head at the pipe wall obtained with a water manometer was taken as the velocity head.

Fig. (3-9) also shows a circle on a steel plate fastened to the pipe just below the sampler. This is an image of the pipe section, that is, it has the same diameter as the inside of the pipe and its center is the same distance "a" from the ball center as that of the pipe. An index on the sampler tube, that is distance "2a" from the inlet of the sampler tube will indicate the location of the sampler inlet in the pipe cross section. By swinging the sampler and moving it longitudinally, it was possible to reach 83 percent of the pipe area.

A baffle was installed after completing Run no. 1 in the return pipe near the inlet to the 16-inch rubber pipe about 2.5 feet upstream from the sampling point. This was made of one thickness of stainless steel sheet perforated with 3/16-inch-diameter holes spaced such that the holes occupied 33 percent of the area. The baffle was installed in an attempt to spread the sediment load over the pipe cross section at the sampling section and this to improve sampling accuracy.

4. Sand Leveler:

By definition the mean elevation of the bed is taken as the elevation of the plane for which the volume of the depressions below the plane is just equal to the volume of sediment above the plane. This is just the plane of the leveled sand surface. The device used to level the bed in the 130-foot flume is shown in Fig. (3-10). The entire frame is supported by four rollers on the rails on the two sides of the flume. Two blades of aluminum plate, $1\frac{1}{2}$ inches wide, serve as scrapers to move sand into the depressions. The blades are supported near the bed by two vertical rods. Each rod is threaded and can be raised or lowered at the same time by turning the crank located at a transverse bar as shown in the figure. A rubber roller at each of the four corners of the frame guides the leveler by rolling on the side walls.

5. Camera Holder:

Fig. (3-11) shows the camera holder designed for taking plan-view pictures of the bed of the 130-foot flume. The camera is supported by the holder about $7\frac{1}{2}$ feet above the sand bed. This enables one to take an over-head picture of a section of the bed 69 inches long. A 4 by 5 in. view camera with a 203 mm, f/7.7 Kodak Ektor lens was used to take the over-head pictures.

B. The 40-foot Flume and Accessories

1. General Description of the 40-foot Flume:

A schematic diagram of the 40-foot flume is shown in Fig. (3-12). As shown in the figure, the water flows from left to right in the open channel section, then flows down through the pump, and returns to the inlet of the channel through a 4-inch pipe. The circuit

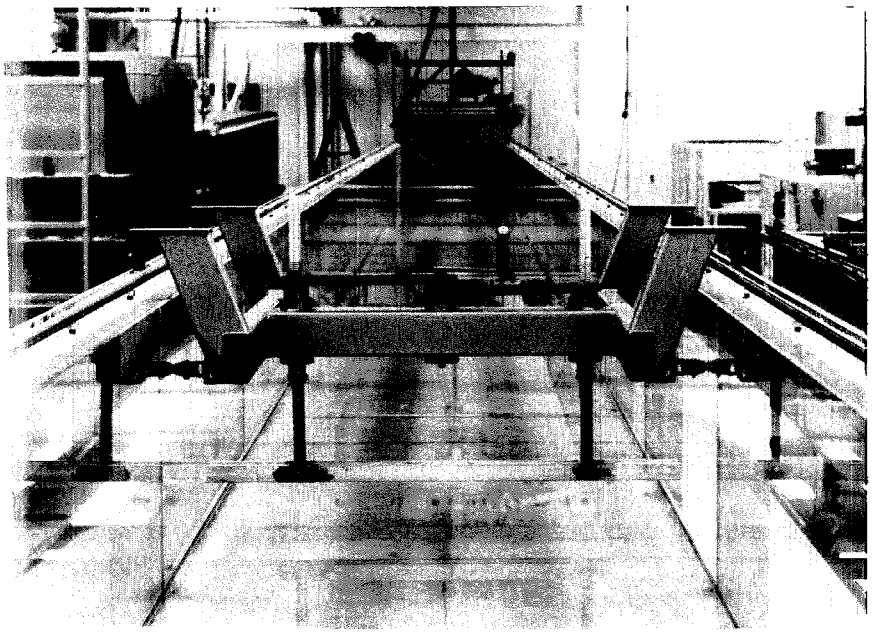

Fig. (3-10) Sand leveler for the 130-foot flume.

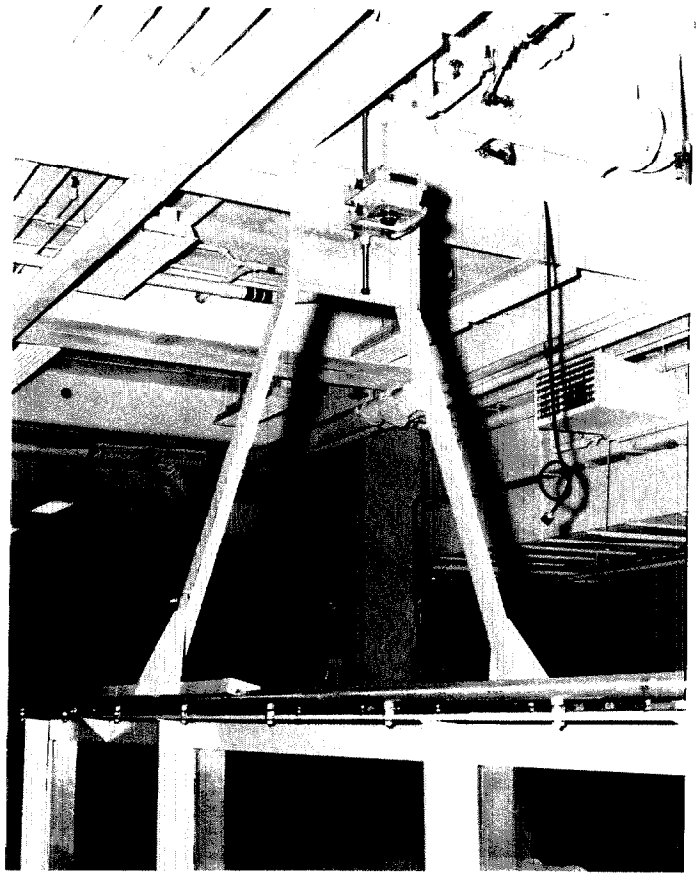

Fig. (3-11) Camera holder and the camera used in the 130-foot flume for taking plan-view pictures of the sand bed.

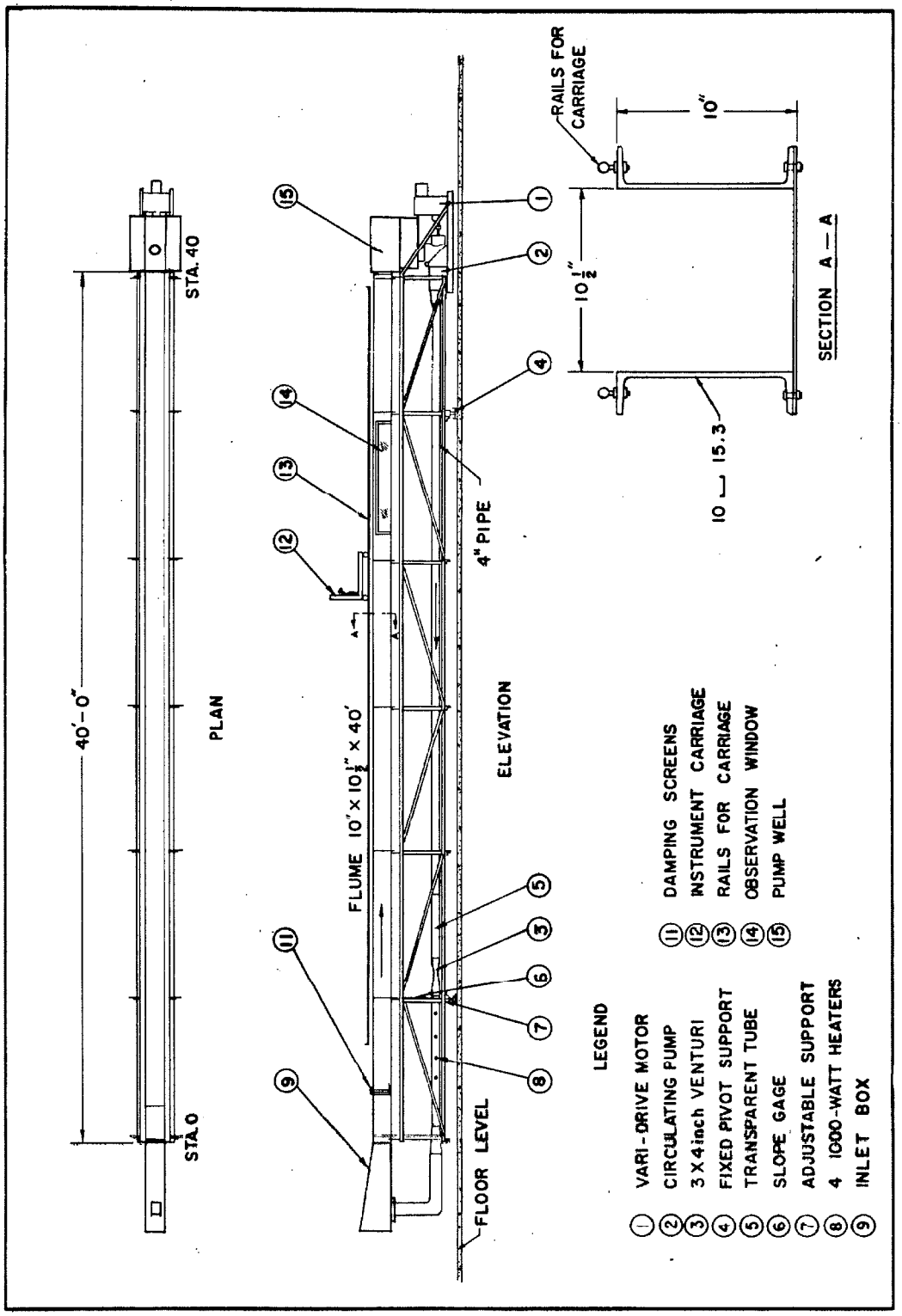

Fig. (3-12) Schematic diagram of the 40-foot flume.

is closed so that the water as well as the sediment being carried is re-circulated by the pump at the outlet of the channel.

The open channel portion of the flume consists of two 10-inch steel channels attached to a bottom plate with bolts. The dimensions of the channel are shown in section A-A of Fig. (3-12). The inside surfaces of the flume are painted with an epoxy resin paint which gives a hydrodynamically smooth surface.

The entire flume assembly including the pump and the motor is supported on a rigid truss which itself is mounted on a pivot near one end of the flume and on a jack on the other end. A steel scale installed near the jack is calibrated so that one can read the slope directly to the nearest 0.00001 by means of a vernier scale.

A transparent lucite tube, 50 inches long and 4 inches in diameter, is installed in the return pipe near the venturi meter to make it possible to observe if sufficient sand is being deposited to affect the accuracy of the venturi meter.

Along the flume, 32 stations, one foot apart, are marked starting at 64 inches from the inlet of the flume. Glass windows 5 feet long are installed in each wall between stations 20 and 25. All side-view pictures were taken at these windows.

2. Inlet and Outlet Sections:

The principal features of the inlet section of the 40-foot flume are more or less the same as those in the 130-foot flume. As shown in Fig. (3-13), the inlet box which is $10\frac{1}{2}$ inches wide has two 8-mesh screens installed in it for stilling disturbances generated by the re-entry of the flow from the return pipe. Another 4-mesh screen

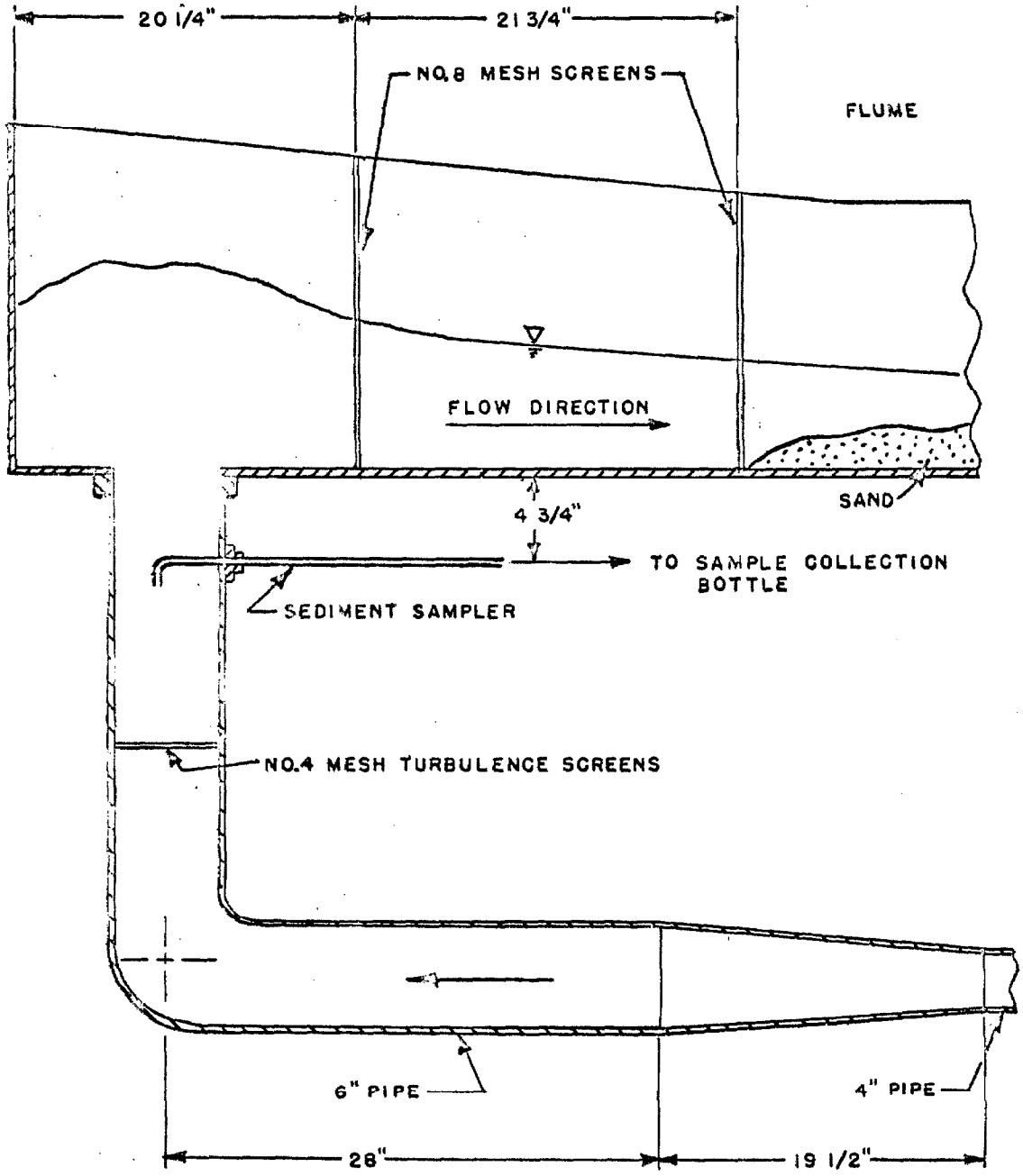

Fig. (3-13) Longitudinal section of the inlet box and sediment discharge sampler for the 40-foot flume.

was installed in the 6-inch pipe 10 inches below the sediment sampler tip in order to spread the sediment over the sampling section and hence to improve the sampling.

The construction of the outlet section is relatively simple. It consists only of a rectangular outlet tank with a plan area 6.25 square feet, which serves as a pump well. The outlet tank serves to decrease oscillations that may be created by unsteady flows in the open-channel section.

3. Heaters:

Four 1000-watt immersion heaters were installed in the 4-inch return pipe near the upstream end of the flume. Three of the heaters are wired for either 110 or 220 volts, so that each of them can produce either 250 or 1000 watts of heat. With this installation, a temperature difference of 19°C. between the water and the air can be maintained. The laboratory is air-conditioned so that the air temperature is always maintained around 21°C. Therefore, the water temperature can be raised up to around 40°C. This will decrease the kinematic viscosity of water from 1.06×10^{-5} square feet per second to 0.70×10^{-5} square feet per second.

C. Stabilization of the Sand Bed

The requirements for a stabilized bed are as follows:

(i) It should preserve its surface configuration and texture.

(ii) It should preserve the porosity of sand so that water and air can seep through the stabilized layer.

(iii) It should last for a long period without changing its surface characteristics and configuration while the experiments are being carried out.

(iv) It should be strong enough to allow the installation of the pressure taps on the bed surface.

The method of stabilizing the sand bed was developed by tests of different samples in trays. Of the several materials tested, a chemical material sold commercially under the trade name "Standard Plaspreg" was found most nearly to meet the above requirements. This material is a liquid impregnant used to strengthen and harden plaster molds. "Standard Plaspreg" is a Furfural polymer, which does not activate and polymerize with sand until a weak organic acid called "Catalyst XP-2" is added and the temperature is raised to around 140^{o} F.

The procedure in stabilizing the sand bed is described as follows:

(i) Drain the water from the flume slowly and allow the sand to dry for 1 day.

(ii) Spray over the sand with a mixture of the following materials: 5 parts by volume of "Standard Plaspreg" and one part by volume of "Catalyst XP-2". Apply this mixture to the bed with a hand sprayer until the solution has wetted the sand to a depth of about $\frac{1}{4}$ inch.

(iii) Maintain the impregnated surface at 140^{o}-160^{o} F. by use of infra-red electric lamps suspended approximately 1 foot above the sand bed. Raise the temperature slowly and then cool it slowly to avoid small cracks. Cure is not completed until the surface

becomes deep black in color. The time for curing is approximately 24 hours.

In order to determine if shrinkage of the sand bed occurred in the process of stabilization, the elevation of the bed at the centerline was measured at several points to within 0.001 of a ft. both before and after stabilization. No shrinkage was observed.

Water poured on the stabilized bed penetrated readily indicating that it was fairly permeable. However, no test was made to determine the change of the permeability through the stabilization process. Since the sand used here was fine, it is believed that the effect of the permeability on the friction factor is negligible.

Fig. (3-14) shows a magnified photograph of the surface of the stabilized bed of quartz sand with geometric mean size of 0.23 mm. This photograph was taken after finishing a series of experiments, which lasted for almost two months. Pictures (a) and (b) in Fig. (3-15) are the side views of a dune-covered bed before and after stabilization.

D. Equipment for Measuring Velocity

The point velocities were measured with a 1/8-in. diameter Prandtl pitot static tube and a pressure transducer recording system for reading the dynamic pressure. A general view of the Prandtl tube and the pressure transducer is shown in Fig. (3-16). The dynamic pressure was recorded continuously by a Sanborn recorder. A micromanometer shown in Fig. (3-17) was used for calibrating the transducer and recorder. The micromanometer described by Vanoni[16] enables one

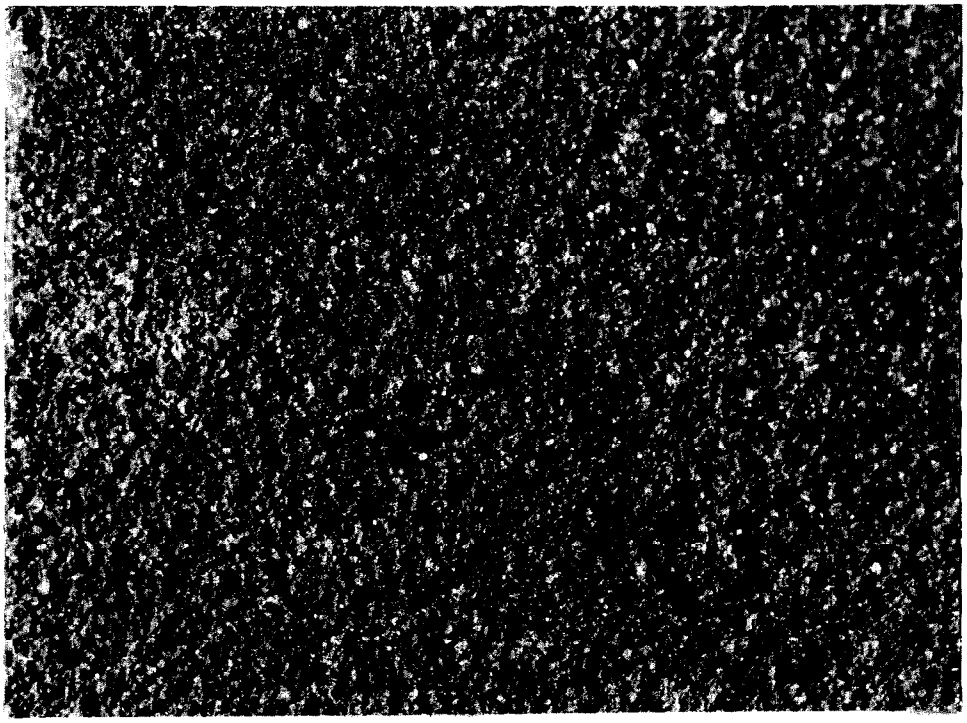

Fig. (3-14) Surface of a stabilized sand bed. Run No. 9-14, velocity = 0.749 fps., depth = 0.231 ft., magnification: 5 times.

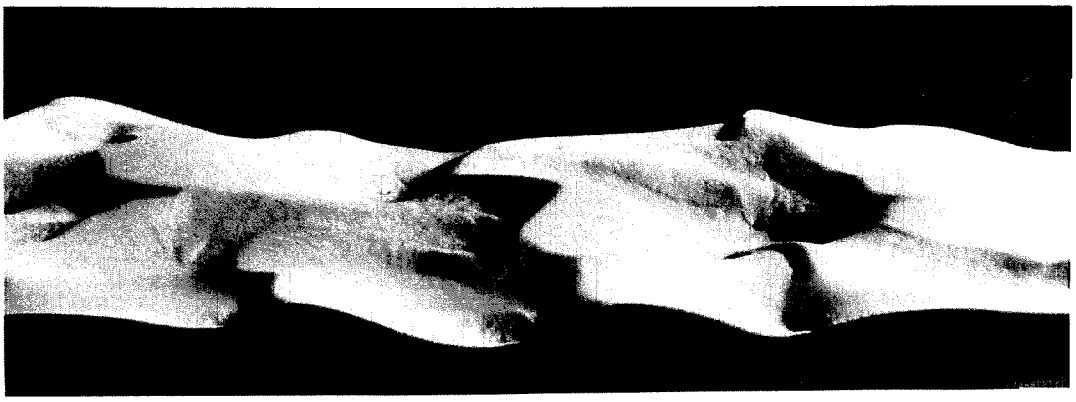

(a) Loose sand.

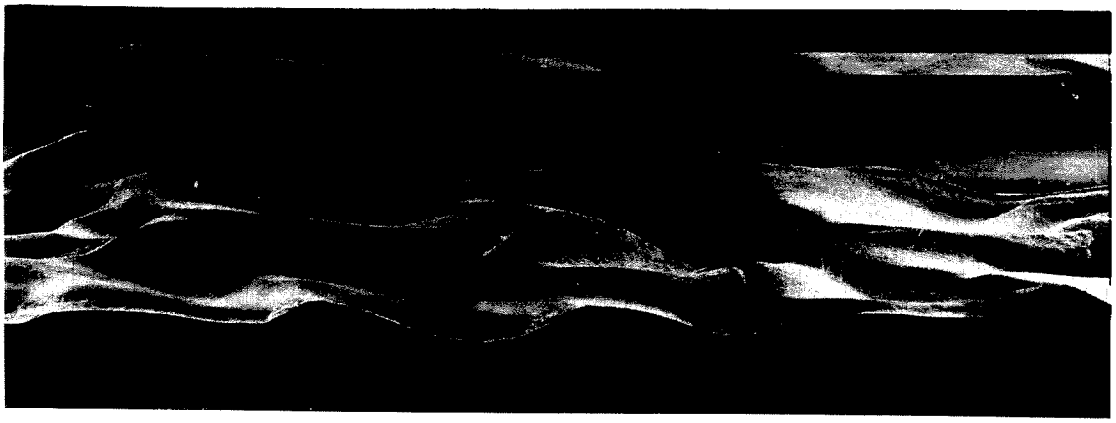

(b) Stabilized sand.

Fig. (3-15) Side views of a sand bed before and after stabilization (Run No. 9-14).

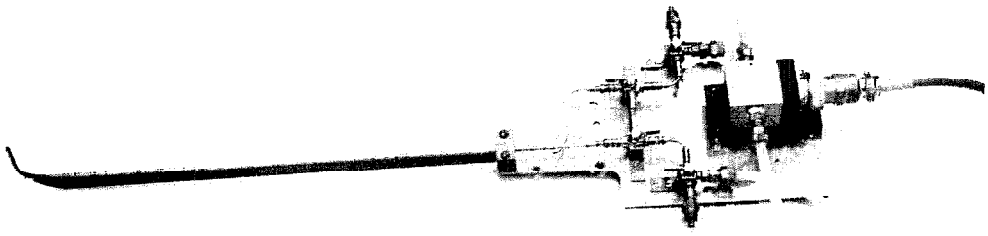

Fig. (3-16) Prandtl tube and pressure transducer.

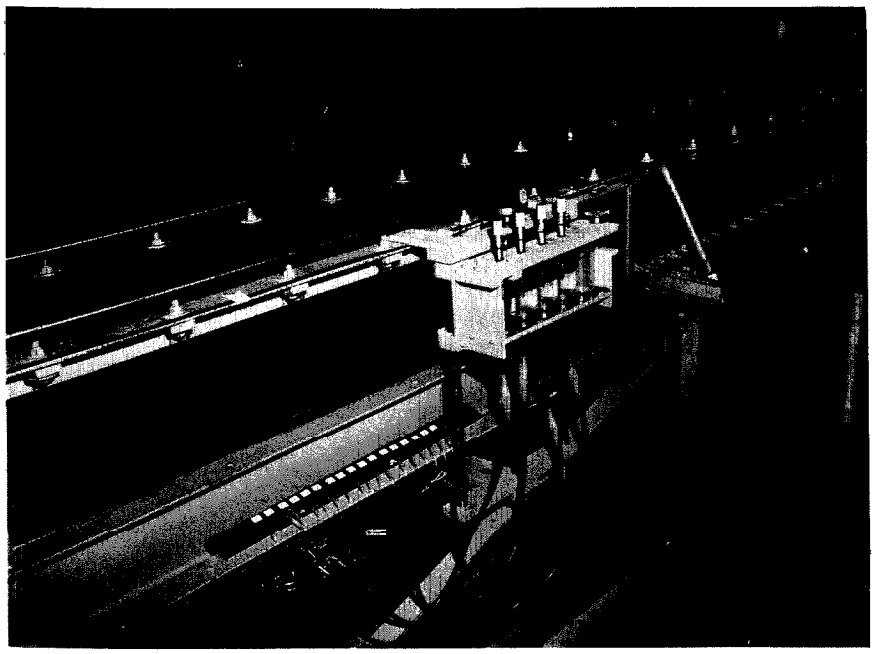

Fig. (3-17) Micromanometer and tubings used in measuring velocity and pressure distributions.

to read the differential head to 0.001 of an inch. A detailed description of this equipment is given below.

1. Prandtl Pitot Static Tube and Connecting Valves:

Since the pressure transducer used in recording the dynamic pressure does not displace an appreciable amount of water the passages in the pitot tube and the tube itself can be made small. This small instrument is very convenient in measuring the point velocity near the dune bed. In order to avoid vibration created by the vortex behind the vertical portion of the Prandtl tube, a brass hydrofoil was soldered to the trailing edge of the tube.

A valve system containing four three-way valves was designed in such a way that the operations of flushing and calibration could be carried out easily. A diagram of the valves and their connection system is shown in Fig. (3-18).

2. Pressure Transducer and Sanborn Recorder:

The pressure transducer used here is Model No. P7D manufactured by Pace Engineering Company of Los Angeles, California. It contains two gaps separated by a magnetically permeable diaphragm 0.004 of an inch. As shown in Fig. (3-19), the diaphragm supported between two symmetrical core inductance assemblies, completes a magnetic circuit with each core. The diaphragm deflects slightly when there is a difference in pressure between the static and the dynamic ports. This increases the gap in the magnetic flux path of one core, and decreases the gap equally in the other thus changing the magnetic reluctance of the magnetic circuits. The inductance can be measured by a bridge circuit which produces an output voltage related

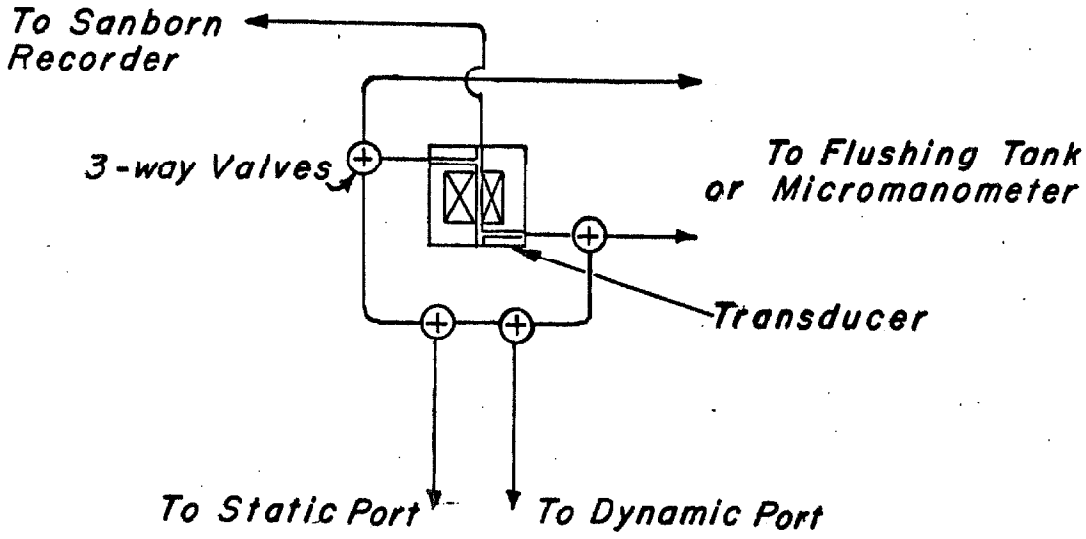

Fig. (3-18) Diagram of pressure transducer, valves and connecting tubes for velocity measurement.

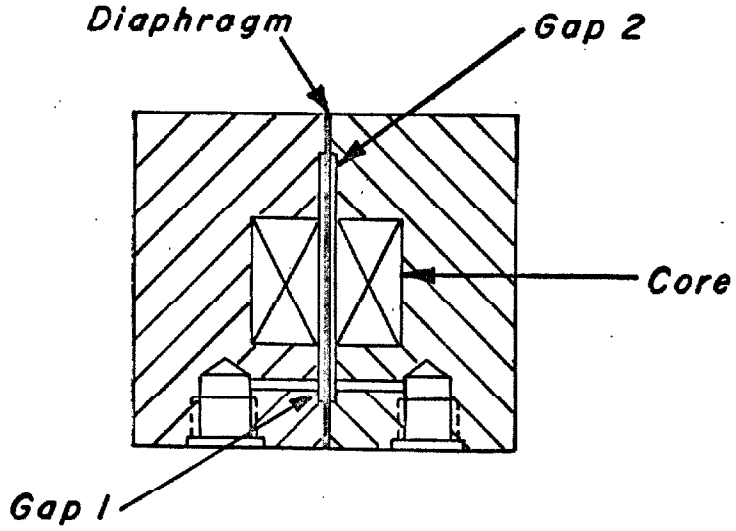

Fig. (3-19) Cross-sectional diagram of the pressure transducer.

to pressure differences. This output voltage was recorded by the Sanborn recorder.

The Sanborn recorder used here is Model 150 with 1100 AS Carrier Amplifiers. A motor with variable speeds is used for advancing the record paper.

E. Installation of Pressure Taps in a Stabilized Bed

In order to determine the pressure distribution over a dune surface, 17 pressure taps spaced 0.06 of a ft. apart were installed as shown in Fig. (3-15b). This portion of the bed was treated specially to give a stabilized crust 1/2-inch thick or double the thickness in the rest of the bed. Holes 1/8 inch in diameter were drilled through the stabilized sand bed and the steel bottom perpendicularly to the bottom of the flume as shown in Fig. (3-20). Copper tubing with an outside diameter of 1/8 inch was then inserted into each hole and the upper end of the tube was then filed until it was flush with the dune surface. The end of the tube was then filled up with solder and a hole 0.032 inches in diameter was drilled into the solder in a direction normal to the dune surface.

In order to prevent water from seeping through the gap around the tube, the tubes were coated with grease before they were inserted into the bed. The gap around the tubes was then filled with sand and the loose sand around the tap was stabilized with "Standard Plaspreg". At the steel bottom of the flume, a seal was made around the pressure tube with rubber cement.

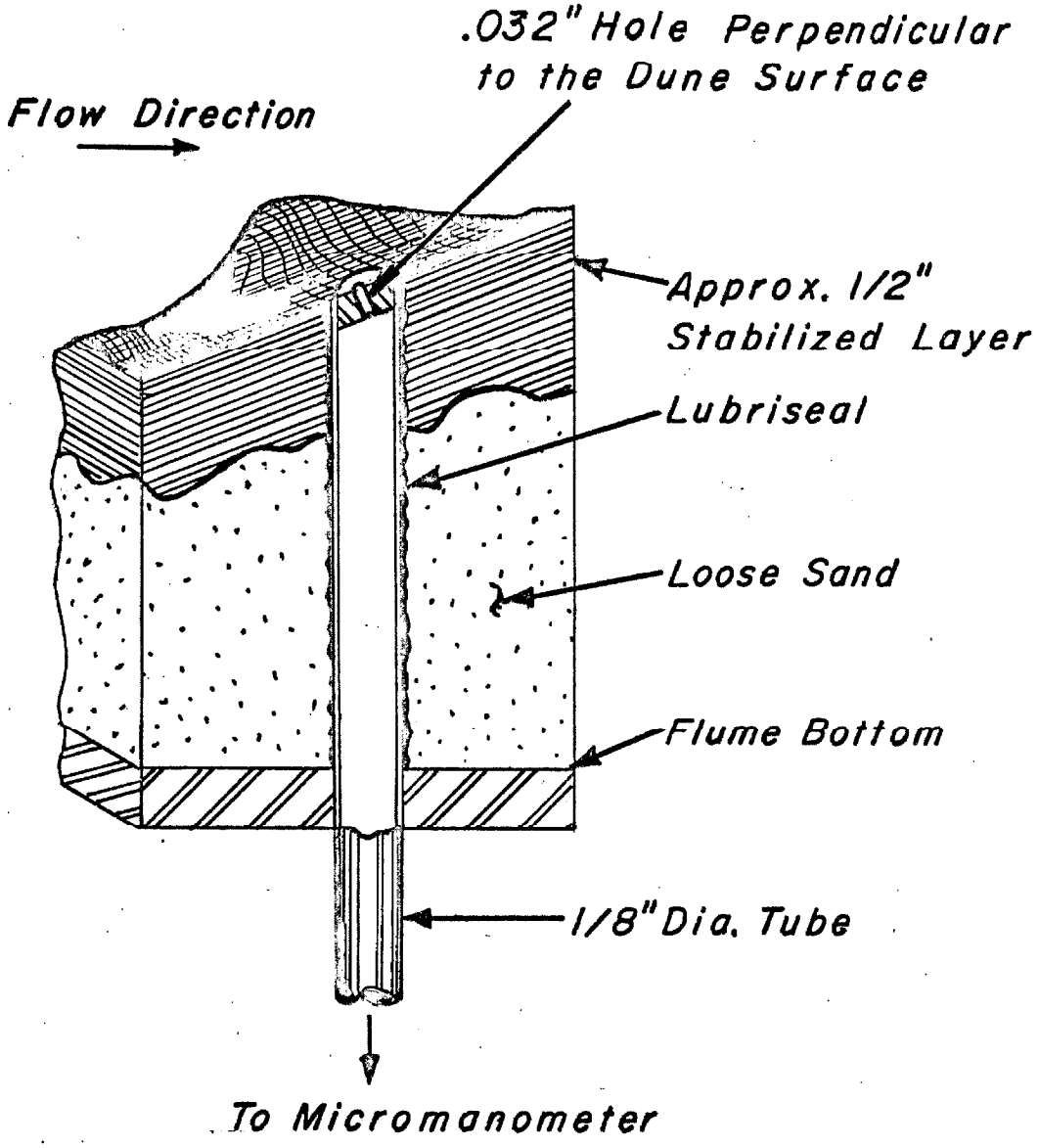

Fig. (3-20) Schematic diagram of a pressure tap on a stabilized dune.

CHAPTER IV

EXPERIMENTAL PROCEDURE

A. Establishing a Steady Uniform Flow

Since the flumes used here have closed circuits, the depth of flow is determined by the amount of water added to the flume system. If a given amount of water is added to the flume and the flow rate is kept constant, the slope is the only variable which can be adjusted in establishing a steady uniform flow. As a guide in establishing a steady uniform flow, a point gauge near the end of the flume was first set at the elevation corresponding to the mean water depth. The slope of the flume was then adjusted to keep the tip of the point gauge at the water surface until the water surface elevation at this station remained fixed. Complete water surface profiles along the flume were then measured to make sure that the flow was uniform before other measurements were made. Before stopping the pump and terminating the run, a more detailed water surface profile was measured for use in calculating average depth, velocity and the energy grade line.

In experiments with loose beds, it is very important to minimize the departure from uniform flow. This is because even small departures from uniformity may cause significant changes in bed configuration and give rise to a variation of the bed friction factor along the flow. These effects cannot be taken into account through slope correction.

B. Determination of the Depth of Flow

To determine the flow depth at a station in runs with loose sand, it was first necessary to determine the local mean bed elevation. To do this the bed was first leveled in short reaches with a leveler as described in Chapter III. In the 40-foot flume these reaches were 2 feet long and in the 130-foot flume, only alternate one-meter reaches of the bed were leveled. The local mean bed elevation was measured with a point gage at each leveled reach. The water surface elevation was measured with a point gage directly over the center of each leveled reach of bed. The local mean depth was taken as the difference between the elevations of the water surface and the leveled bed. The mean depth for the whole flume was taken as the average of the local mean depths exclusive of depths at stations near the inlet and outlet.

The elevations referred to above were determined with the point gage which gives the elevation relative to some arbitrary reference plane parallel to the flume rails and bottom. These will be referred to as elevations relative to the flume. Therefore, to obtain the elevation of a point in the bed or water surface one must add the point gage reading to the elevation of the flume at the measuring station. To determine the water depth at a station one merely takes the difference in point gage readings at the water surface and leveled bed and it is not necessary to determine the elevation of the points.

In the runs with stabilized beds, a special technique was used to determine the local mean bed elevation. A known volume of water-saturated, loose sand was added to each reach of 2 feet. Then

the sand was leveled with the sand leveler described in the previous chapter and the elevation of the surface of the leveled loose sand was measured. The local mean bed elevation of the stabilized bed was equal to the elevation of the leveled loose sand minus the mean thickness of the added sand, which was obtained by dividing the known volume of sand added to the 2-foot reach by the surface area of the reach. The volume of the sand added was determined with a graduated measuring cylinder.

C. Determination of the Slope of the Energy Grade Line

After the mean depth is calculated at a station, the average velocity, U, is determined by dividing the water discharge, Q , by the product of the width of the flume, b, and the mean depth. One can then calculate the elevation of the energy grade line, e_s, at each station, by the equation

$$e_s = y_w + \frac{U^2}{2g} \tag{4-1}$$

in which U is the average velocity in the cross section and

y_w and e_s are, respectively, the water surface elevation and the elevation of the energy grade line relative to the flume, and

g is the gravitational acceleration.

The slope of the energy grade line, S, is the sum of the slopes of the flume, S_f, and of the energy grade line relative to the flume, $\frac{d}{dx} e_s$, that is,

$$S = S_f - \frac{d}{dx}\left(y_w + \frac{U^2}{2g}\right) \tag{4-2}$$

where x is the distance along the flume taken to be positive in the direction of flow. Typical bed and water surface profiles and a typical energy grade line for the 130-foot flume are shown in Fig. (4-1). In this case the slope of the energy grade line relative to the flume is less than one percent of the flume slope.

D. Discharge Measurements

The water discharge, Q, was measured by a venturi meter installed in the return pipe in each flume. The differential piezometric head, Δh_v, across the venturi meter was measured with an air-water differential manometer which could be read to the nearest 0.001 ft.

The problem of using a venturi meter to measure sediment-laden water discharge has been thoroughly discussed by Brooks[15]. He concluded that the discharges determined by this apparatus were accurate to within one percent.

In the experiments with the water-glycerine mixture, special care was taken to ensure that the mixture of water and glycerine in the two manometer tubes was the same as that of the flowing fluid. In this way the head on the venturi meter was read directly in terms of the flowing fluid.

E. Side-Wall Corrections

If the roughness of the side wall surface is different from that of the bed, a side-wall correction must be made to determine the true resistance and friction factor of the bed. A simple correction method, which has been used by many workers in sedimentation, was devised by Johnson[11], and later modified by Brooks[15]. The procedure

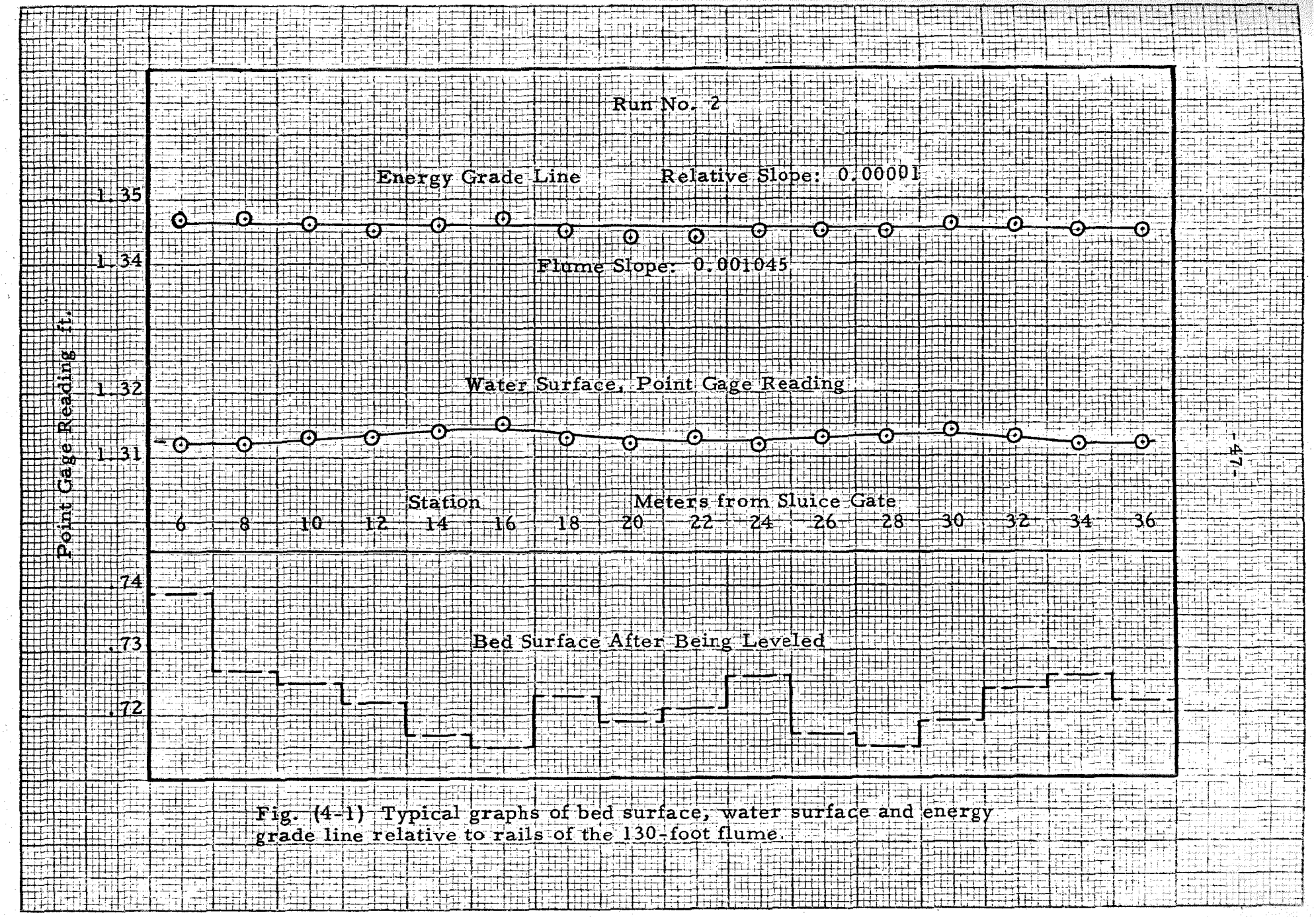

Fig. (4-1) Typical graphs of bed surface, water surface and energy grade line relative to rails of the 130-foot flume.

given by Brooks will be outlined here. The principal assumptions for this procedure are described as follows:

(i) The area of the cross section can be divided into two parts, the bed area in which the flow is resisted by the bed, and the wall area which consists of two equal sub-parts, in which the flow is resisted by the walls.

(ii) A flow formula can be applied to each part of the cross section and the average velocity and slope of the energy grade line are the same for the whole cross section and for each part.

(iii) The roughnesses of the wall and the bed are homogeneous but different.

By use of the above assumptions, the equation of the side-wall correction can be established as follows.

The Darcy-Weisbach equation for the entire channel, the bed, and the wall can be written respectively as follows:

$$f = \frac{8gSA}{\rho U^2} \tag{4-3}$$

$$f_b = \frac{8gSA_b}{\rho_b U^2} \tag{4-4}$$

and

$$f_w = \frac{8gSA_w}{\rho_w U^2} \tag{4-5}$$

in which f is the friction factor, p is the wetted perimeter, A is the cross-sectional area, the subscripts b and w refer to the bed and the wall respectively and the symbols without subscript are for the whole cross section. The symbols S, U and g denote the slope of the energy grade line, the average velocity and the acceleration of gravity respectively and are the same for the total cross section and the bed and wall sections.

From the geometry one can write

$$A = A_b + A_w \tag{4-6}$$

Eliminating A, A_b and A_w from Equation (4-6) by means of Equations (4-3), (4-4) and (4-5), one obtains

$$f_b = \frac{p}{p_b} f - \frac{p_w}{p_b} f_w \tag{4-7}$$

The cross section of the flume used in this investigation is rectangular with width, b , and with the depth of flow, d, so that $p = 2d + b$, $p_b = b$ and $p_w = 2d$. Substituting these relationships into Equation (4-7), one obtains

$$f_b = f + \frac{2d}{b}(f - f_w) \tag{4-8}$$

Before f_b can be determined, one must estimate the wall friction factor, f_w. This can be obtained through the following considerations.

Reynolds numbers for the channel are defined as

$$R = \frac{4rU}{\nu} \qquad \text{and} \qquad R_\omega = \frac{4r_\omega U}{\nu} \tag{4-9}$$

in which R is the Reynolds number for the entire channel.

R_w is the Reynolds number for the wall area,

r is the hydraulic radius for the entire channel,

r_w is the wall hydraulic radius and

ν is the kinematic viscosity of the flowing fluid.

From Equation (4-9) one obtains

$$\frac{R_\omega}{R} = \frac{r_\omega}{r} \tag{4-10}$$

Using Equations (4-3) and (4-5), one can solve for $\frac{A}{p}$ and $\frac{A_w}{p_w}$ which are equal to r and r_w respectively. Then one substitutes r and r_w into Equation (4-10) to obtain

$$\frac{R_\omega}{f_\omega} = \frac{R}{f} \tag{4-11}$$

If the walls are smooth, as they are in the flumes used in this study, one can apply the classical relations for friction factor of smooth pipes to obtain the value of f_w. This calculation is facilitated by Fig. (4-2) which is a graph of f against R/f for smooth pipes prepared by Brooks[15]. Knowing the value of R/f which is equal to R_w/f_w the graph will give directly the value of f_w as long as the wall is hydrodynamically smooth.

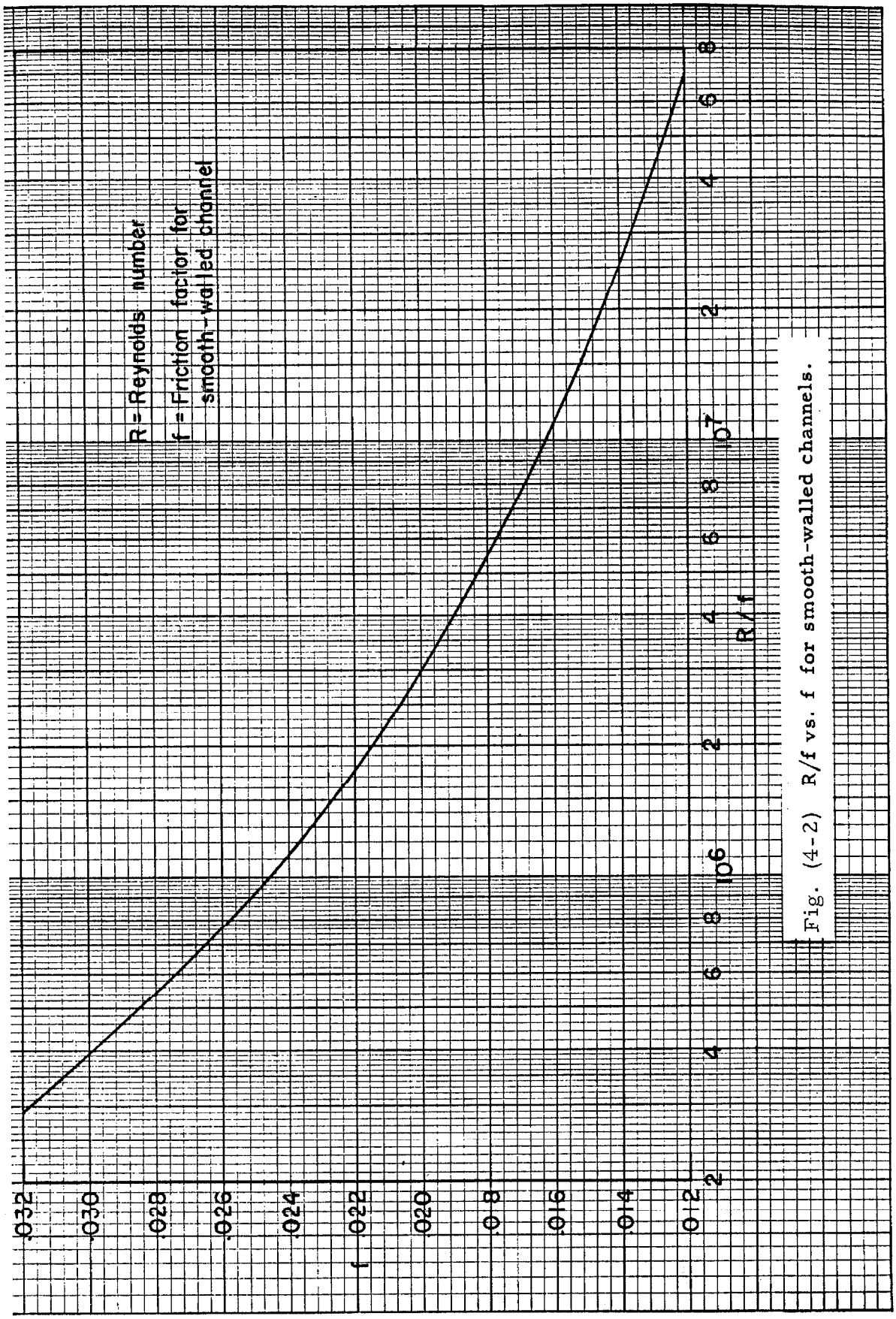

Fig. (4-2) R/f vs. f for smooth-walled channels.

F. Measurements of Point Velocities

A schematic diagram of the instruments used in measuring velocities is shown in Fig. (4-3). The procedure followed in using this apparatus was the following. The pressure transducer and the Prandtl pitot tube were flushed thoroughly by connecting the lines B, D, C and B', D', C' to the "Flushing Tank" which was about 5 feet above the pressure transducer. The objective of this operation is to remove all air bubbles from the system since they create undesirable damping effects due to their compressibility. After the flushing was completed, the calibration was started by connecting each side of the pressure transducer to a leg of a micromanometer and disconnecting the lines D and D' to the pitot tube. The water in the two pots of the micromanometer was brought to the same elevation by connecting them and the Sanborn recorder was started, thus establishing a zero reading. The two pots were then disconnected and the head differential on the system was increased in small steps by adding water to the manometer pot used to read the dynamic head of the pitot tube. The head differential at each step was read with the micromanometer and also recorded on the Sanborn recorder chart. Through this process, a calibration curve of head against chart reading was obtained which usually was linear as shown in Fig. (4-4). After finishing the calibration, the system was ready for use in measuring velocity. Since such measurements usually took half a day, several intermediate calibrations were made to ensure that the calibration was not changing with time.

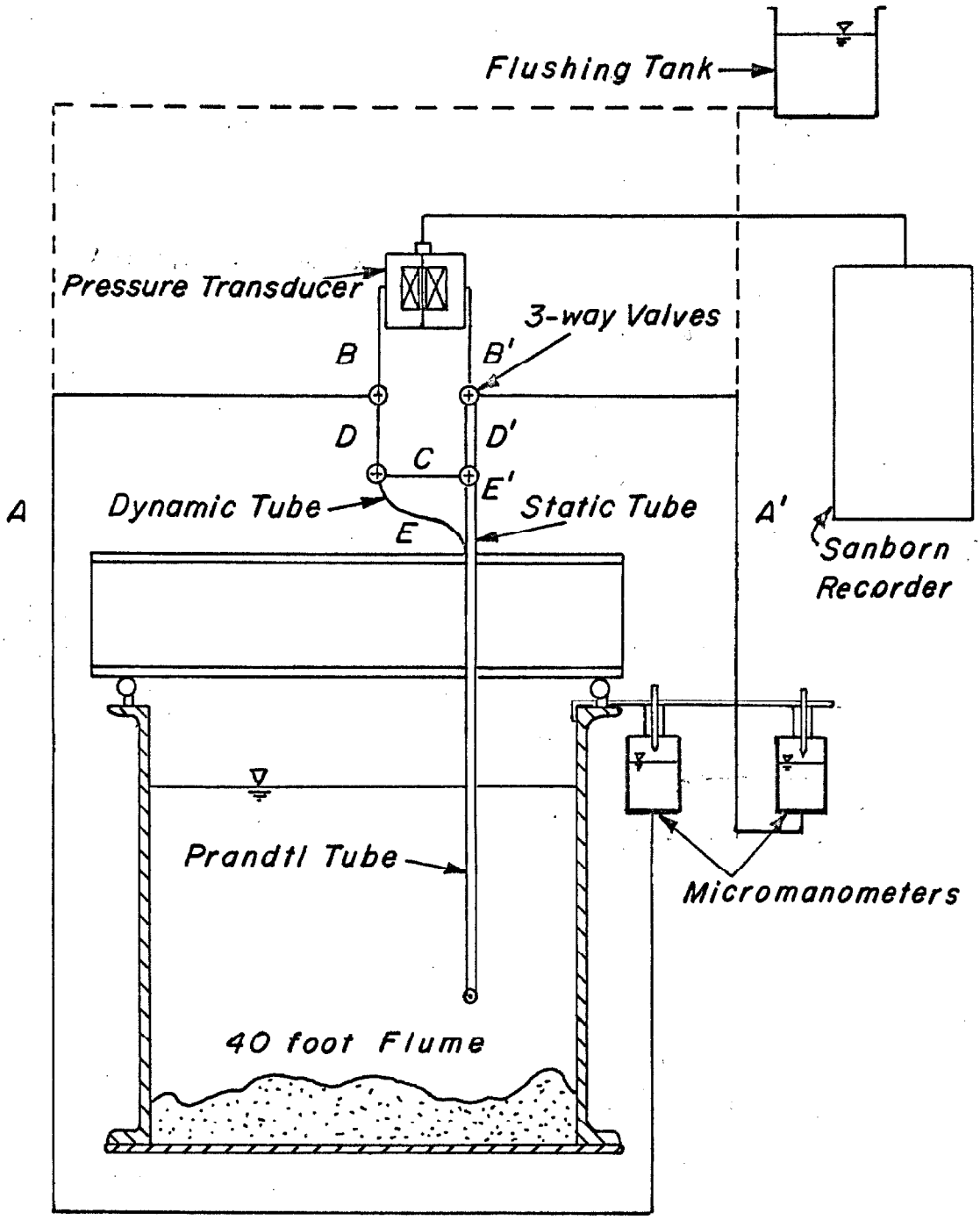

Fig. (4-3) Schematic diagram of the instruments for measuring point velocities.

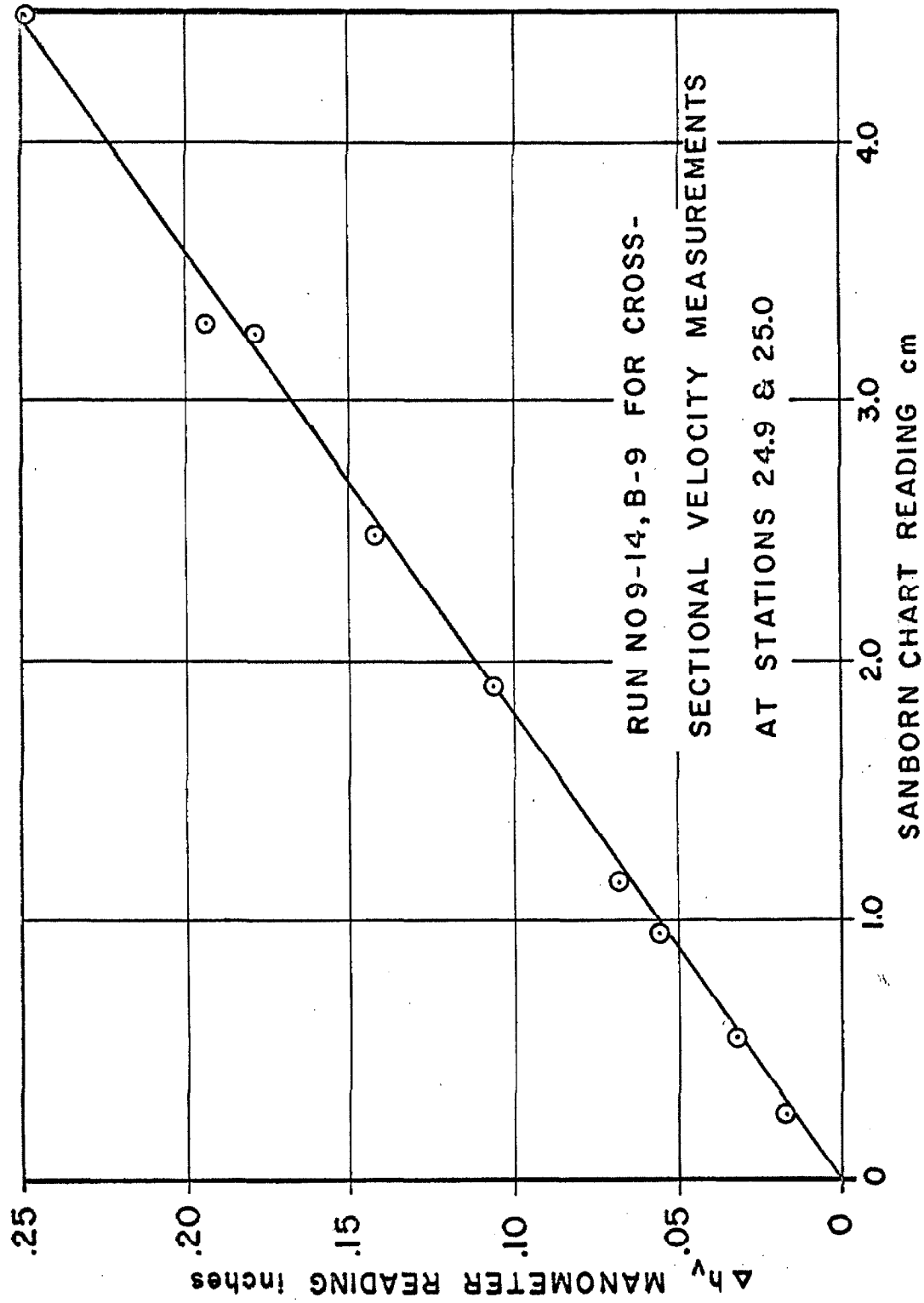

Fig. (4-4) Typical calibration curve of recorder chart reading against manometer head.

The Prandtl pitot tube was allowed to stay at the measuring point for a sufficient length of time to obtain a proper average reading. Since fluctuations were always present, the time for each measurement depended upon the amplitude of these fluctuations. Usually 40 seconds of record for each point was needed to give a proper average. A portion of the record traced by the Sanborn recorder for three positions in Run No. 9-14, B-9 is shown in Fig. (4-5). The paper speed for these measurements was 1 mm. per second as indicated by the mark at the margin of the paper. A long, dark block was marked during the change of the position of the Prandtl tube. The trace within the dark block was not used in obtaining the average. The three mean values of the head indicated on the chart show how averages were taken.

The accuracy of the transducer and recorder system was checked by comparing results of simultaneous measurements with the recording system and the micromanometer. Fig. (4-6) shows velocity profile data measured simultaneously at one vertical profile by the two methods. As will be noted, the two sets of data agree closely.

G. Measurements of the Sediment Discharge Concentration

In the experiments performed in the 40-foot flume, the sediment discharge concentration was taken in the inlet with the sediment discharge sampler shown in Fig. (3-14). Since the sampler can be moved in one direction only, the location of the sampling points are limited to one line. Five sampler locations were chosen, spaced 1 1/8 inches apart. At each location two liters of sample were taken. No definite concentration gradient was observed along the line. The point

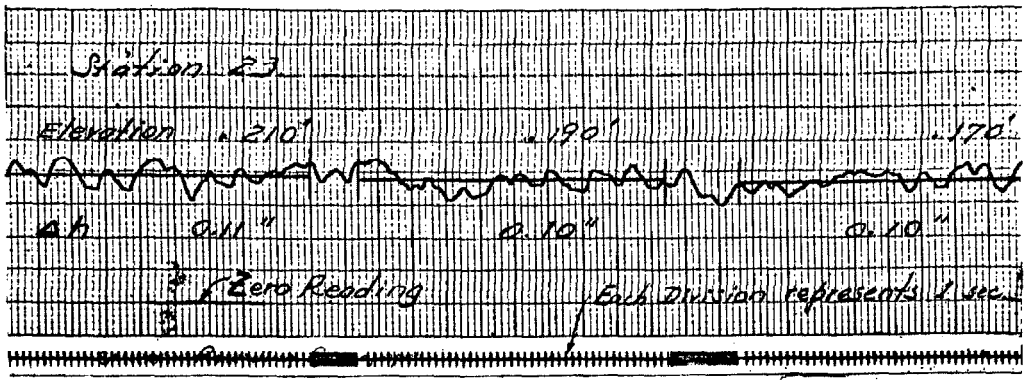

Fig. (4-5) A portion of Sanborn chart showing recording of head differential on pitot tube. (Run 9-14, B-9)

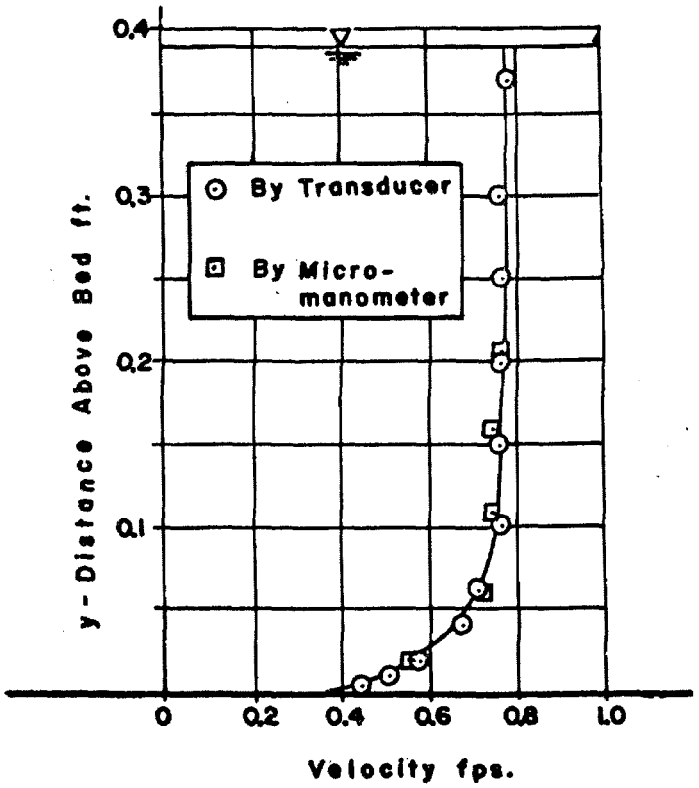

Fig. (4-6) A comparison of velocities measured by pressure transducer and by micromanometer.

concentration deviated randomly from the mean concentration. The sediment discharge concentration was taken to be the arithmetic average of the concentrations of all the samples.

In the 130-foot flume, samples (except for Run Nos. 1 and 3) were taken at 22 or more points with the sampler described in the previous chapter. Most of the sampling points were chosen at the outer portion of the sampling area where the highest concentration occurred. The sediment discharge concentration $\overline{C}$, was calculated according to the following formula

$$\overline{C} = \frac{1}{Q} \sum_{i=0}^{n} \frac{(CV)_i + (CV)_{i+1}}{2} \cdot a_i \qquad (4\text{-}12)$$

in which Q is the total water discharge,

$\overline{C}$ is the sediment discharge concentration,

c is the concentration of the sediment at a certain sampling point,

v is the velocity at the corresponding sampling point,

$(c \cdot v)_i$ is the value of $c \cdot v$ on the i^{th} contour,

a_i is the area between contour i and contour i+1,

n is the number of contours, and

i = 0 is the contour of the maximum value of $c \cdot v$.

The rate of sampling was regulated to make the velocity of the flow entering the tip of the sampler equal to the stream velocity at the sampling point. The importance of following this procedure has been demonstrated by Vanoni[17].

CHAPTER V

EXPERIMENTAL RESULTS

A. Introduction

The flume experiments can be divided into three major groups as follows:

1. Experiments in the 40-foot flume with stabilized beds.
2. Experiments in the 40-foot flume with loose sand (Runs 9-1 through 9-15).
3. Experiments in the 130-foot flume with loose sand (Runs 1 through 8).

The first group of experiments in the 40-foot flume was performed with two different stabilized dune beds and with no sediment being transported. The results of this are presented in Section B (Results of the Experiments with Stabilized Beds). The second and third groups of experiments were performed with loose sand, and were designed to clarify the effect of the exposure parameter, e, on the friction factor for a constant water depth. In these two groups, a total of 23 experiments were made; 15 of which were performed in the 40-foot flume and 8 in the 130-foot flume. Results of these experiments together with those of two series of experiments performed by Vanoni and Brooks in the 60-foot flume(*) are presented in Section C (Results of the Experiments with Loose Sand). All experiments in these three groups were designed to clarify the nature of dune resistance

---

*These experiments were made in 1957 with the sponsorship of The National Science Foundation Grant G-1709.

and to establish a correlation between quantities, such as flow parameters, dune size, dune geometry, and flow resistance.

B. Results of the Experiments with Stabilized Beds

1. Gross Measurements:

Two bed configurations generated by two different flows were stabilized in the 40-foot flume for this investigation. The first bed was generated by the flow of Run No. 9-14 which had an average velocity of 0.749 fps., a depth of 0.231 feet and a sediment discharge concentration of 0.007 grams per liter. The bed was composed of Sand No. 1 which had a geometric sieve size of 0.23 mm. Detailed information on the sand characteristics appears in Section C. Top and side views of the bed configuration taken before the bed was stabilized are shown in Fig. (5-1). These pictures were taken at station 25 through the glass window in the side wall. After the first bed was stabilized, four series of experiments, denoted by Series A, B, C, and D, were performed with flow depths of 0.17, 0.23, 0.35 and 0.47 feet respectively. Each series contained 11 or more runs. Each run is given a number made up of the number of the run in which the dune bed was generated, the letter denoting the series and a numeral denoting the run in the series. For example, Run 9-14, B-1 is the first run in B series of experiments with the first stabilized bed. A summary of the data from these experiments is presented in Table I. The runs with glycerine-water mixtures are denoted in Table I with two asterisks before the run number, while those with elevated water temperature are denoted with a single asterisk before the run number.

(a) Top view.

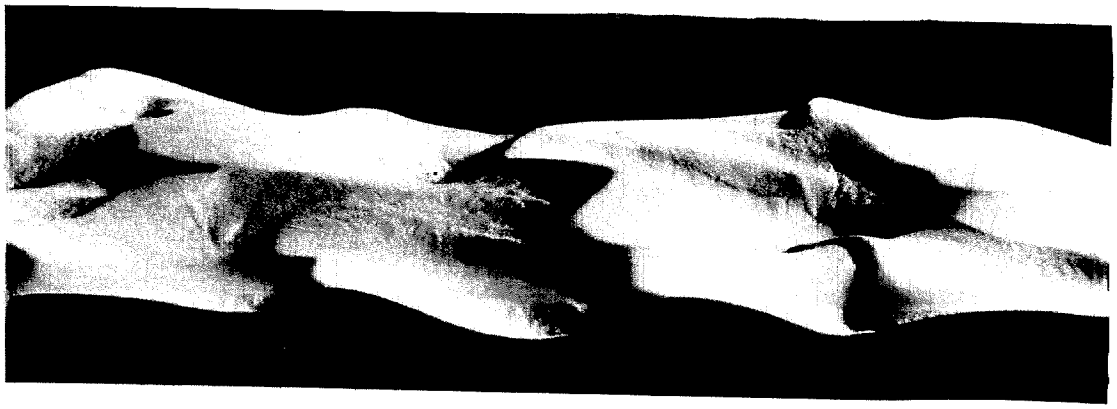

(b) Side view.

Fig. (5-1) Pictures of the sand bed of Run No. 9-14 before stabilization. (Flow is to the left.)

Table I. Summary of Data from the First Set of Experiments with a Stabilized Bed.

Run No	Q Discharge cfs	d Depth ft.	r Hydr. Radius ft.	S Slope $\times 10^{-4}$	U Ave. Vel. fps	f Frict. Factor	T Temp. °C	ν Kinematic Viscosity ft/sec 10^{-5}	r_b Bed Hyd. Radius ft.	f_b Bed Frict. Factor	F Froude Number	R_b Reynolds Number 10^{-5}
Set No. 1 Bed Configuration Generated by Run No. 9-14 U=0.749 fps d=0.231 ft. Flume Width=10.5 in.												
A-Series Water Depth=0.17 ft.												
A- 1	0.084	0.171	0.123	15.7	0.561	0.158	22.7	1.018	0.159	0.204	0.239	0.352
2	0.099	0.170	0.123	21.4	0.665	0.154	22.5	1.022	0.161	0.201	0.284	0.419
3	0.127	0.170	0.123	36.7	0.853	0.159	22.3	1.026	0.161	0.208	0.365	0.537
4	0.160	0.169	0.122	61.5	1.089	0.163	21.8	1.038	0.161	0.215	0.467	0.661
5	0.185	0.171	0.123	78.2	1.233	0.163	23.7	1.016	0.162	0.215	0.525	0.786
6	0.202	0.170	0.123	87.6	1.353	0.152	23.2	1.006	0.162	0.200	0.578	0.877
* 7	0.176	0.170	0.123	71.1	1.182	0.161	33.5	0.805	0.162	0.212	0.505	0.950
* 8	0.145	0.169	0.122	49.8	0.976	0.163	33.8	0.800	0.159	0.213	0.415	0.775
** 9	0.142	0.172	0.124	46.4	0.959	0.161	20.6	4.04	0.159	0.207	0.406	0.152
**10	0.121	0.172	0.124	29.9	0.802	0.149	21.1	2.79	0.159	0.192	0.340	0.183
**11	0.112	0.171	0.123	29.0	0.750	0.163	21.4	2.60	0.159	0.211	0.319	0.184

Table I cont.

Run No	Q	d	r	S	U	f	T	ν	r_b	f_b	F	R_b
B-Series Water Depth= 0.23 ft.												
B- 1	0.101	0.231	0.151	7.4	0.498	0.116	24.5	0.977	0.208	0.160	0.182	0.308
2	0.130	0.230	0.151	12.1	0.643	0.114	24.0	0.988	0.209	0.158	0.236	0.403
3	0.156	0.231	0.151	17.0	0.771	0.111	23.0	0.972	0.210	0.155	0.282	0.479
4	0.182	0.231	0.151	23.2	0.900	0.111	23.0	0.972	0.210	0.155	0.330	0.560
5	0.197	0.230	0.151	27.4	0.978	0.111	22.5	1.022	0.210	0.155	0.360	0.577
6	0.218	0.230	0.151	34.1	1.083	0.113	22.5	1.022	0.211	0.158	0.398	0.641
7	0.249	0.230	0.151	43.4	1.235	0.111	22.0	1.034	0.211	0.155	0.454	0.721
8	0.291	0.227	0.149	65.9	1.490	0.114	22.0	1.034	0.209	0.159	0.549	0.859
9	0.152	0.231	0.151	16.6	0.753	0.114	24.3	0.984	0.209	0.159	0.276	0.462
10	0.250	0.232	0.153	41.3	1.250	0.104	21.5	1.045	0.213	0.145	0.458	0.732
*11	0.220	0.230	0.151	33.0	1.091	0.111	30.2	0.866	0.211	0.156	0.401	0.762
*12	0.293	0.229	0.150	64.3	1.146	0.116	33.7	0.802	0.212	0.164	0.421	1.090
*13	0.183	0.232	0.153	22.0	0.901	0.107	34.0	0.798	0.210	0.149	0.330	0.690
**14	0.130	0.232	0.153	12.2	0.642	0.117	20.6	2.47	0.208	0.159	0.235	0.159
**15	0.140	0.231	0.151	14.5	0.693	0.118	20.8	1.97	0.207	0.161	0.254	0.213
**16	0.195	0.231	0.151	29.0	0.965	0.121	20.5	1.97	0.209	0.167	0.353	0.296

Table I cont.

Run No	Q	d	r	S	U	f	T	ν	r_b	f_b	F	R_b
C-Series Water Depth=0.35 ft.												
C- 1	0.134	0.351	0.195	2.9	0.436	0.765	24.0	0.988	0.292	0.115	0.129	0.516
2	0.173	0.350	0.194	4.7	0.563	0.742	24.0	0.988	0.292	0.112	0.167	0.664
3	0.240	0.350	0.194	9.0	0.783	0.734	23.6	0.996	0.295	0.112	0.233	0.925
4	0.336	0.349	0.194	17.3	1.100	0.714	23.5	0.998	0.298	0.110	0.328	1.310
5	0.426	0.348	0.193	29.0	1.397	0.738	23.6	0.996	0.294	0.113	0.417	1.652
6	0.522	0.346	0.193	42.2	1.723	0.708	23.5	0.998	0.299	0.110	0.516	2.062
* 7	0.414	0.349	0.194	25.2	1.355	0.686	35.6	0.771	0.300	0.106	0.404	2.107
* 8	0.474	0.350	0.194	34.0	1.546	0.711	36.0	0.762	0.304	0.111	0.459	2.462
** 9	0.141	0.352	0.195	3.2	0.457	0.766	20.5	2.55	0.280	0.110	0.136	0.201
**10	0.188	0.351	0.195	5.9	0.612	0.789	20.5	2.55	0.286	0.116	0.182	0.276
**11	0.260	0.350	0.194	11.0	0.849	0.762	20.5	2.55	0.280	0.110	0.252	0.373

Table I cont.

Run No	Q	d	r	S	U	f	T	ν	r_b	f_b	F	R_b
D-Series Water Depth= 0.47 ft.												
D- 1	0.136	0.472	0.227	1.0	0.328	0.054	24.4	0.978	0.346	0.083	0.084	0.465
2	0.178	0.472	0.227	1.8	0.430	0.057	24.2	0.982	0.358	0.090	0.110	0.626
3	0.246	0.472	0.227	3.3	0.595	0.055	23.8	0.992	0.361	0.087	0.152	0.867
4	0.323	0.471	0.227	5.8	0.783	0.055	23.8	0.990	0.368	0.090	0.200	1.165
5	0.425	0.472	0.227	10.1	1.028	0.056	23.7	0.994	0.370	0.091	0.263	1.530
6	0.580	0.469	0.226	18.8	1.410	0.055	23.5	1.002	0.376	0.092	0.362	2.110
7	0.701	0.468	0.226	27.4	1.708	0.055	23.4	1.002	0.379	0.092	0.442	2.580
8	0.426	0.472	0.227	10.1	1.030	0.056	24.4	0.978	0.375	0.092	0.264	1.546
* 9	0.644	0.469	0.226	23.0	1.569	0.054	32.0	0.830	0.381	0.092	0.403	2.867
*10	0.512	0.470	0.226	14.6	1.245	0.055	32.2	0.828	0.377	0.091	0.320	2.268
**11	0.267	0.471	0.227	4.2	0.648	0.058	20.8	2.18	0.350	0.090	0.166	0.416
**12	0.340	0.470	0.226	6.9	0.828	0.059	20.8	2.18	0.355	0.092	0.213	0.540
**13	0.563	0.470	0.226	17.4	1.368	0.054	20.9	2.18	0.363	0.087	0.352	0.912

* Temperature of water was raised to decrease the viscosity
** Glycerine was added to increase the viscosity

The bed for the second set of experiments with stabilized dune bed was generated by the flow of Run No. 9-15 which had an average velocity of 1.250 fps., a water depth of 0.241 feet and a sediment discharge concentration of 0.448 grams per liter. The bed was composed of Sand No. 1 as in the first stabilized bed,but as will be noted,the velocity of the generating flow is higher than that for the first bed. Four series of experiments denoted by Series A, B, C and D were performed with water depths of 0.18, 0.24, 0.36 and 0.48 feet respectively. The data of the experiments are summarized in Table II. The runs with elevated water temperature are denoted in Table II by one asterisk. No glycerine was used in these experiments. Top and side views of the unstabilized bed for this set of experiments at station 25 are shown in Fig. (5-2).

2. Point Velocity-measurements:

(a) Velocity Profiles: Measurements of velocity profiles were made along the center line of the flume starting at a point 29.8 feet downstream from the inlet of the flume. The corresponding station numbers are shown in Fig. (5-3) which is a photograph of the unstabilized bed of Run 9-14 in the region where the velocity profiles were measured. The results of the measurements for Run No. 9-14, B-9 and Run No. 9-14, B-10 with the same mean depth but with average velocities of 0.753 fps. and 1.250 fps. respectively,are shown in Fig. (5-4). The bed profile along the center line in the region of the velocity profiles is also plotted in Fig. (5-4). As will be noted, all velocities were normalized with the average velocity. A comparison

Table II. Summary of Data from the Second Set of Experiments with a Stabilized Bed.

Set No. 2 Bed Configuration Generated by Run No. 9-15 U = 1.25 fps d = 0.241 ft. Flume Width = 10.5 in.												
Run No	Q Discharge cfs	d Depth ft.	r Hydr. Radius ft.	S Slope $x10^{+4}$	U Ave. Vel. fps	f Frict. Factor	T Temp. °C	ν Kinematic Viscosity ft/sec 10^{+5}	r_b Bed Hyd. Radius ft.	f_b Bed Frict. Factor	F Froude Number	R_b Reynolds Number 10^{-5}
A-Series Water Depth = 0.18 ft.												
A- 1	0.095	0.181	0.128	11.0	0.602	0.100	20.9	1.058	0.165	0.129	0.249	0.375
2	0.110	0.181	0.128	14.9	0.696	0.102	20.8	1.061	0.165	0.131	0.288	0.433
3	0.152	0.181	0.128	28.2	0.961	0.101	19.9	1.084	0.166	0.131	0.398	0.587
4	0.186	0.181	0.128	44.5	1.173	0.106	19.7	1.090	0.167	0.139	0.486	0.717
* 5	0.117	0.182	0.128	16.2	0.736	0.098	41.5	0.687	0.166	0.127	0.304	0.712
* 6	0.138	0.181	0.128	23.7	0.874	0.102	40.3	0.703	0.167	0.133	0.362	0.828
* 7	0.167	0.181	0.128	35.5	1.055	0.106	39.6	0.712	0.168	0.138	0.437	0.994

Table II cont.

Run No	Q	d	r	S	U	f	T	ν	r_b	f_b	F	R_b
B-Series Water Depth = 0.24 ft.												
B- 1	0.110	0.241	0.156	5.3	0.523	0.078	20.7	1.064	0.209	0.104	0.188	0.418
2	0.146	0.241	0.156	8.9	0.693	0.074	20.7	1.064	0.210	0.100	0.249	0.548
3	0.188	0.241	0.156	14.8	0.892	0.075	20.8	1.061	0.211	0.101	0.320	0.709
4	0.256	0.241	0.156	28.0	1.216	0.076	20.8	1.061	0.214	0.104	0.436	0.981
5	0.263	0.241	0.156	29.0	1.250	0.075	20.8	1.061	0.214	0.102	0.449	1.008
6	0.330	0.241	0.156	46.0	1.566	0.075	20.8	1.061	0.215	0.104	0.562	1.271
* 7	0.244	0.241	0.156	24.5	1.155	0.074	38.7	0.724	0.215	0.101	0.415	1.371
* 8	0.315	0.241	0.156	42.1	1.494	0.076	38.0	0.734	0.216	0.105	0.536	1.759
C-Series Water Depth = 0.36 ft.												
C- 1	0.146	0.361	0.198	2.3	0.462	0.055	21.3	1.050	0.281	0.078	0.135	0.501
2	0.203	0.361	0.198	4.2	0.642	0.052	21.3	1.050	0.285	0.074	0.188	0.696
3	0.279	0.362	0.198	8.0	0.881	0.053	21.3	1.050	0.289	0.077	0.258	0.972
4	0.385	0.361	0.198	14.7	1.220	0.051	21.0	1.057	0.284	0.073	0.358	1.309
5	0.510	0.361	0.198	24.8	1.616	0.048	21.1	1.054	0.292	0.072	0.474	1.794
* 6	0.306	0.361	0.198	9.3	0.970	0.050	36.8	0.725	0.292	0.075	0.284	1.564
* 7	0.410	0.361	0.198	15.8	1.296	0.048	36.2	0.760	0.293	0.071	0.380	1.998
* 8	0.500	0.361	0.198	23.4	1.582	0.048	36.7	0.752	0.296	0.072	0.464	2.452

Table II cont.

Run No	Q	d	r	S	U	f	T	ν	r_b	f_b	F	R_b
D-Series Water Depth = 0.48ft.												
D- 1	0.166	0.481	0.229	1.2	0.395	0.045	21.3	1.050	0.336	0.067	0.100	0.506
2	0.218	0.481	0.229	2.0	0.518	0.044	21.3	1.050	0.341	0.066	0.132	0.673
3	0.297	0.481	0.229	3.4	0.705	0.040	21.4	1.047	0.340	0.060	0.179	0.913
4	0.435	0.481	0.229	7.3	1.033	0.040	21.3	1.050	0.350	0.062	0.263	1.375
5	0.632	0.482	0.229	14.9	1.500	0.039	21.4	1.047	0.356	0.061	0.381	2.037
* 6	0.335	0.481	0.229	4.3	0.793	0.040	39.0	0.720	0.352	0.062	0.202	1.552
* 7	0.501	0.481	0.229	9.2	1.190	0.038	38.6	0.725	0.354	0.060	0.302	2.325
* 8	0.680	0.481	0.229	16.5	1.615	0.037	38.2	0.731	0.366	0.060	0.410	3.228

* Temperature of water was raised to decrease the viscosity

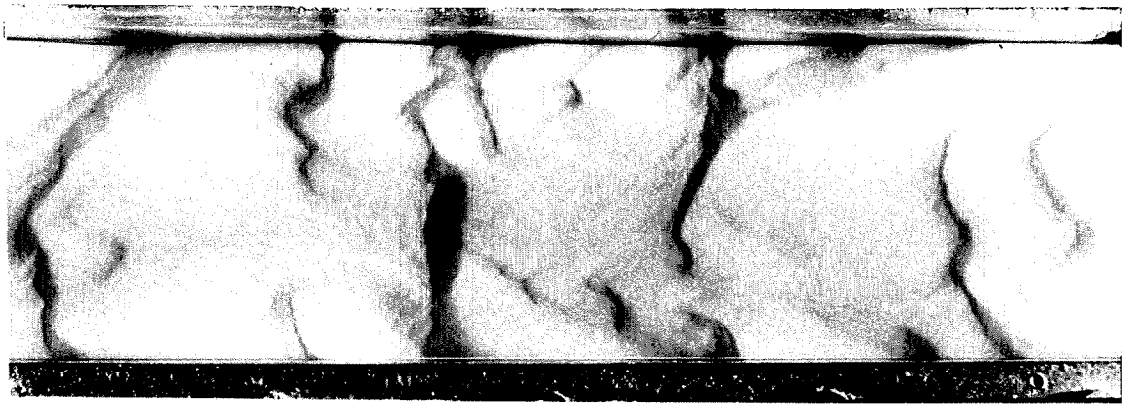

(a) Top view.

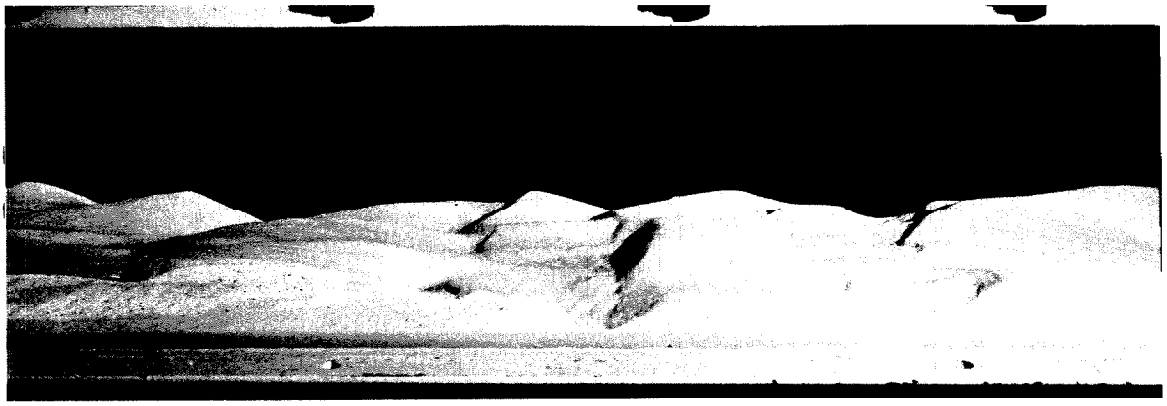

(b) Side view.

Fig. (5-2) Pictures of the sand bed of Run No. 9-15 before stabilization. (Flow is to the left.)

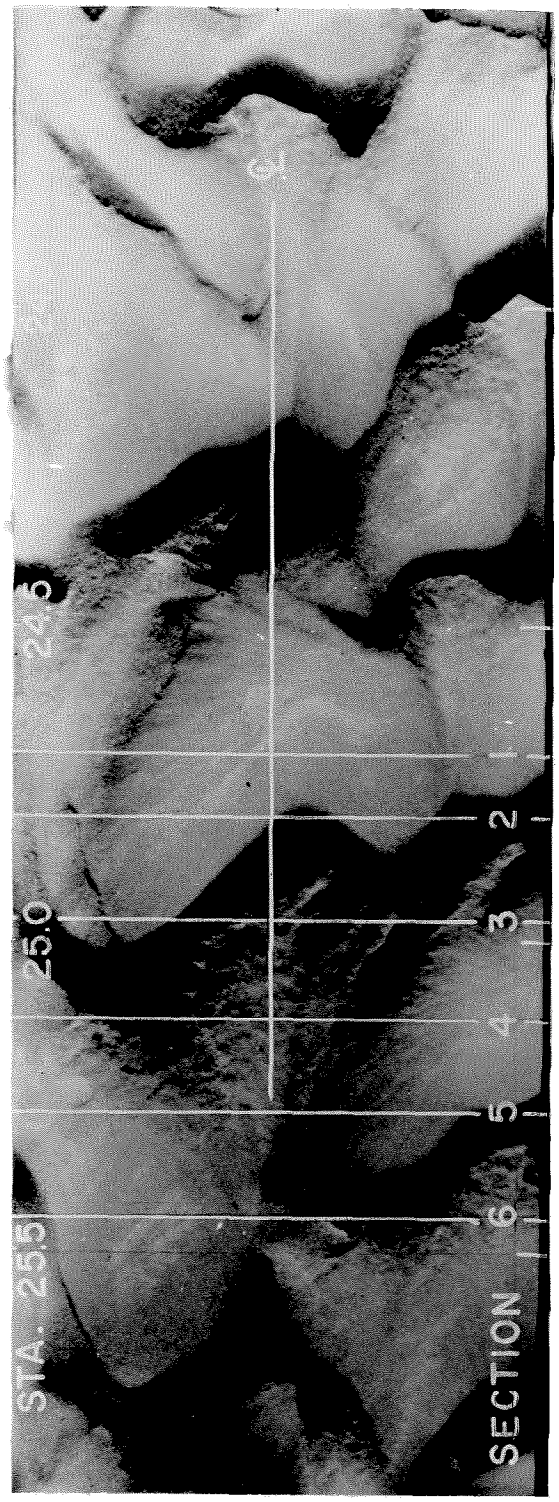

Fig. (5-3) Photograph of unstabilized bed of Run No. 9-14 showing positions of velocity measurements. Sections 1, 2, 3, 4, 5 and 6 are the locations for cross-sectional velocity distribution and section ℄ is the location for center line velocity profiles.

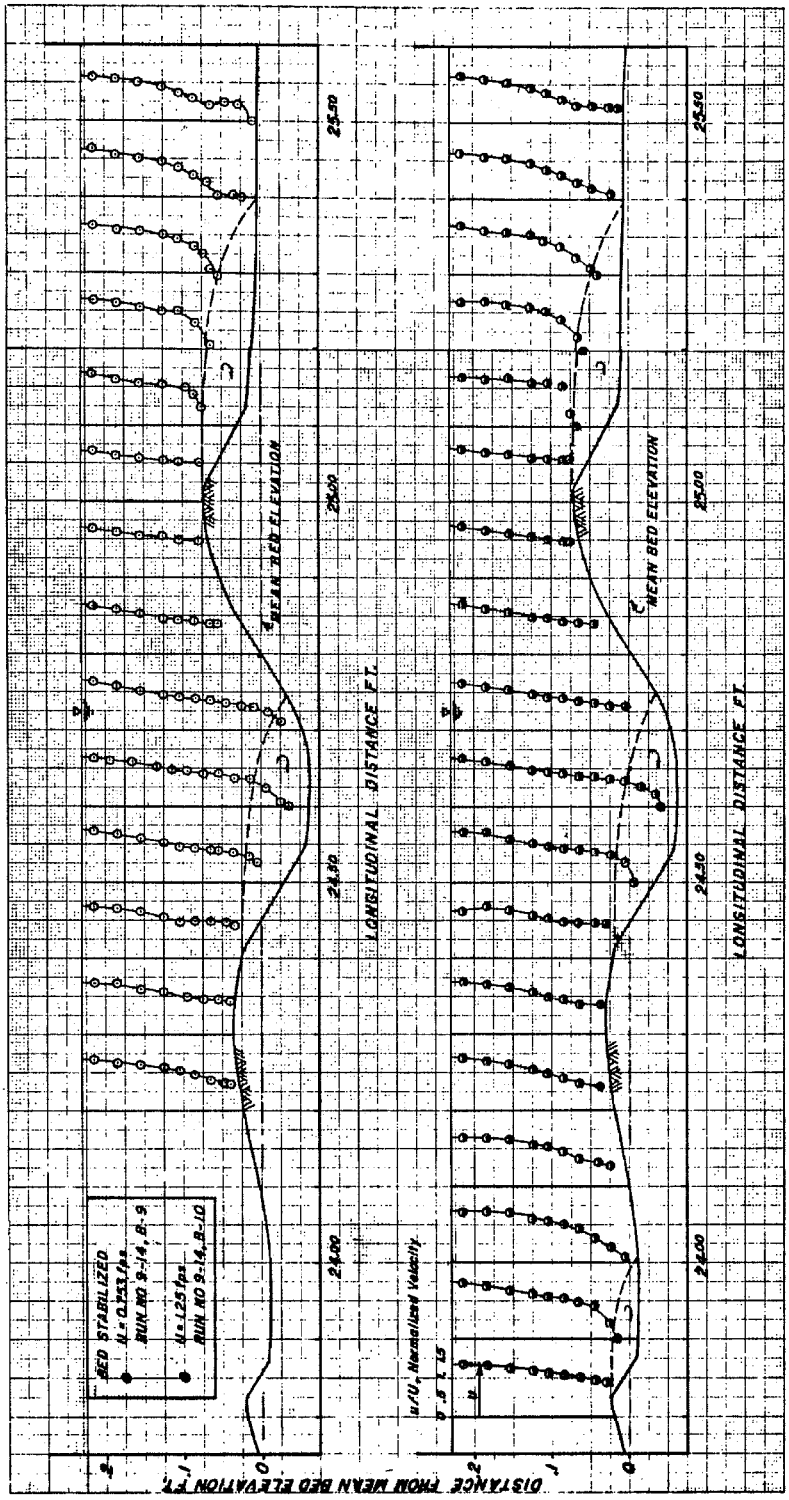

Fig. (5-4) Center line velocity profile over stabilized bed, Run No. 9-14.

of these two sets of normalized velocity profiles indicates that they are almost identical. This means that the velocity profiles of flows with different average velocities are similar.

The velocity profiles indicate that the velocity downstream from the dune crests reached zero at a small distance from the boundary. This point is at the core of the eddy in the lee of the dune. The presence of the eddy was verified visually with dye as was its upper boundary formed by the streamline dividing it from the main flow. This boundary is indicated in Fig. (5-4) for the three dunes over which velocity profiles were measured. The eddy or wake starts right behind the crest of the dune and ends at the point about 4 to 5 times the dune height downstream. The nature of the wake observed resembles that of the flow downstream from a step as described by Toni[18] and Walker[19].

From Fig. (5-4) one can see that the velocity near the bed is strongly affected by the dune; the velocity on the upstream side of the dune accelerates locally due to the sloping dune surface and then decelerates due to the flow expansion downstream from the dune crest. Hence, close to the bed, the velocity is extremely non-uniform due to this local acceleration and deceleration. Far above the bed, this local non-uniformity is gradually evened out, and the velocity away from the bed gradually tends to become uniform as one can see from the velocity profiles in Fig. (5-4).

The velocity profiles of Run No. 9-14, B-9 are also plotted in Fig. (5-5) on a semi-logarithmic graph with the origin of y at the local mean bed elevation, that is, the mean bed elevation taken after the bed is leveled between stations 22 and 26. A straight line is drawn

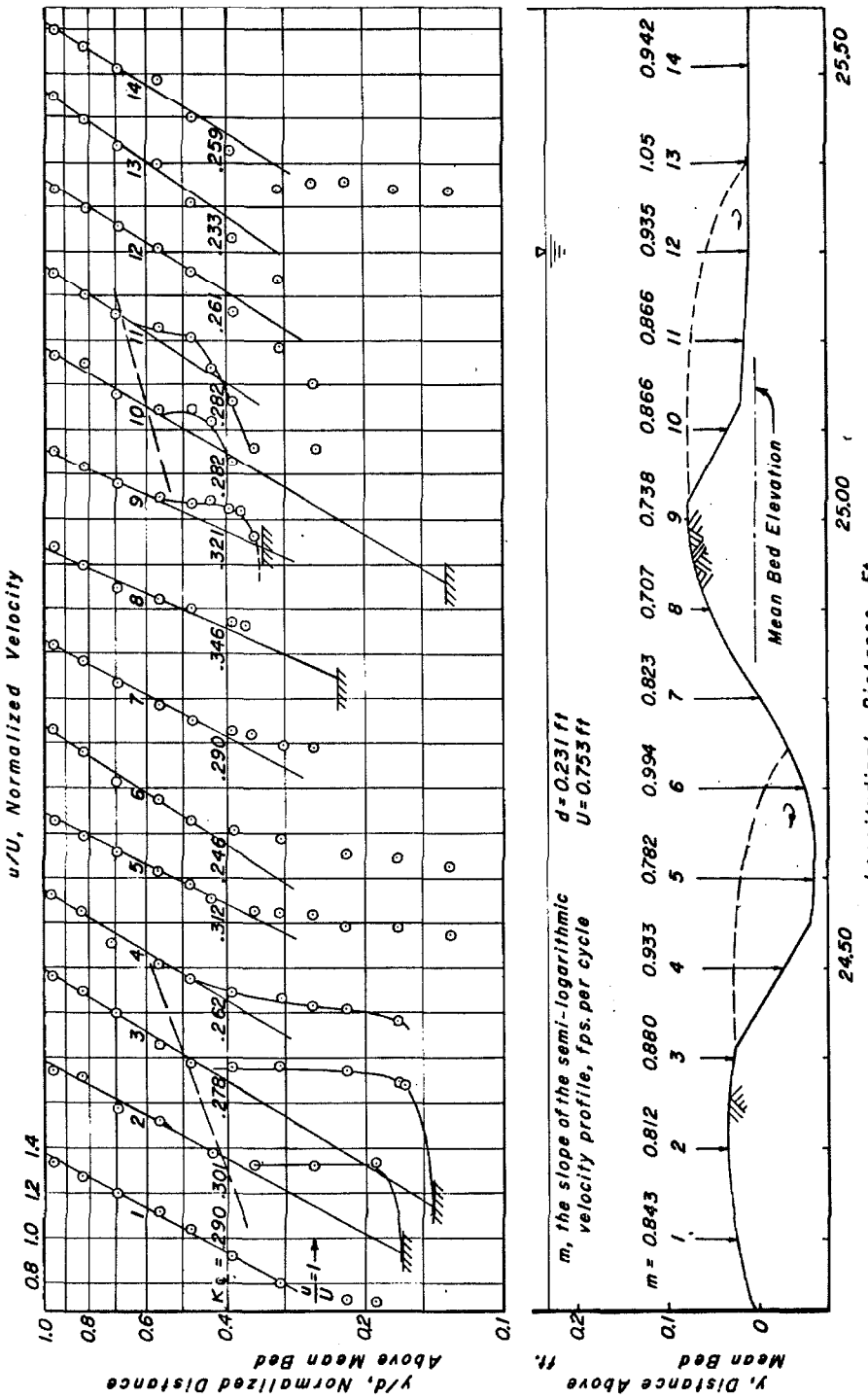

Fig. (5-5). Centerline Velocity Profiles and Bed Profile for Run No. 9-14, B-9.

to fit the upper portion of the points. As shown in the figure, the points near the bed deviate from the straight lines. It is interesting to note that near the bed the velocity profile over the upstream face of the dune falls ahead of the straight line near the trough but then turns back near the crest forming a hump. A possible explanation of the profile shapes is that the forward bending of the profile is caused by the contraction due to the sloping upstream side of the dune, and that the turning back of the velocity profile near the dune surface is caused by the frictional resistance of the dune surface. The point at which the profile departs from the semi-logarithmic line continues to penetrate further into the flow behind the crest of the dune as indicated by the dotted inclined straight lines in Fig. (5-5).

The horizontal lines over the cross-hatching at some of the profiles indicate the dune surface at the particular vertical.

It is clear from Fig. (5-5) that the velocity profiles near the dune surfaces do not follow the logarithmic law. Therefore, the calculation of von Karman's constant does not have the usual significance. But for convenience in comparing these results with those obtained from the field and the laboratory by other investigators, the von Karman constant is calculated according to the following procedure:

First, a straight line is drawn to fit the upper portion of the velocity profile.

Second, the value of m defined as the slope of the semi-logarithmic velocity profile in fps. per cycle is determined.

Third, the value of the von Karman constant, K_{cl}, is calculated by the following formula

$$K_{cl} = \frac{2.30\, U_{*cl}}{m} \tag{5-1}$$

where

$$U_{*cl} = \sqrt{\frac{f_b}{8}}\, U_{cl} \tag{5-2}$$

in which U_{*cl} is the mean shear velocity at the center line of the flume, U_{cl} is the average velocity determined from the centerline profile from which m was determined, and f_b is the bed friction factor. In case the mean center line velocity, U ,is less than the average velocity, U_{cl}, then $\sqrt{gr_b s}$ is used instead of U_{*cl}.

The values of von Karman's constant are shown in Fig. (5-5) at each profile. The values vary from one location to another, and range from 0.246 to 0.346 with an average of 0.282. The decrease of von Karman's constant in channels with large roughness has been observed by Rand[20] in the laboratory and by the U. S. Corps of Army Engineers[21] and Nordin and Dempster[22] in the field. The reason for this is not clear.

(b) Velocity Distribution in the Cross Section: Velocities were measured over the cross section at six stations in Run No. 9-14, B-9. The location of these velocity measurements is shown in Fig. (5-3). The results are shown as velocity contour maps in Figs. (5-6) and (5-7). In these figures the fact that the zero velocity line is away from the bed

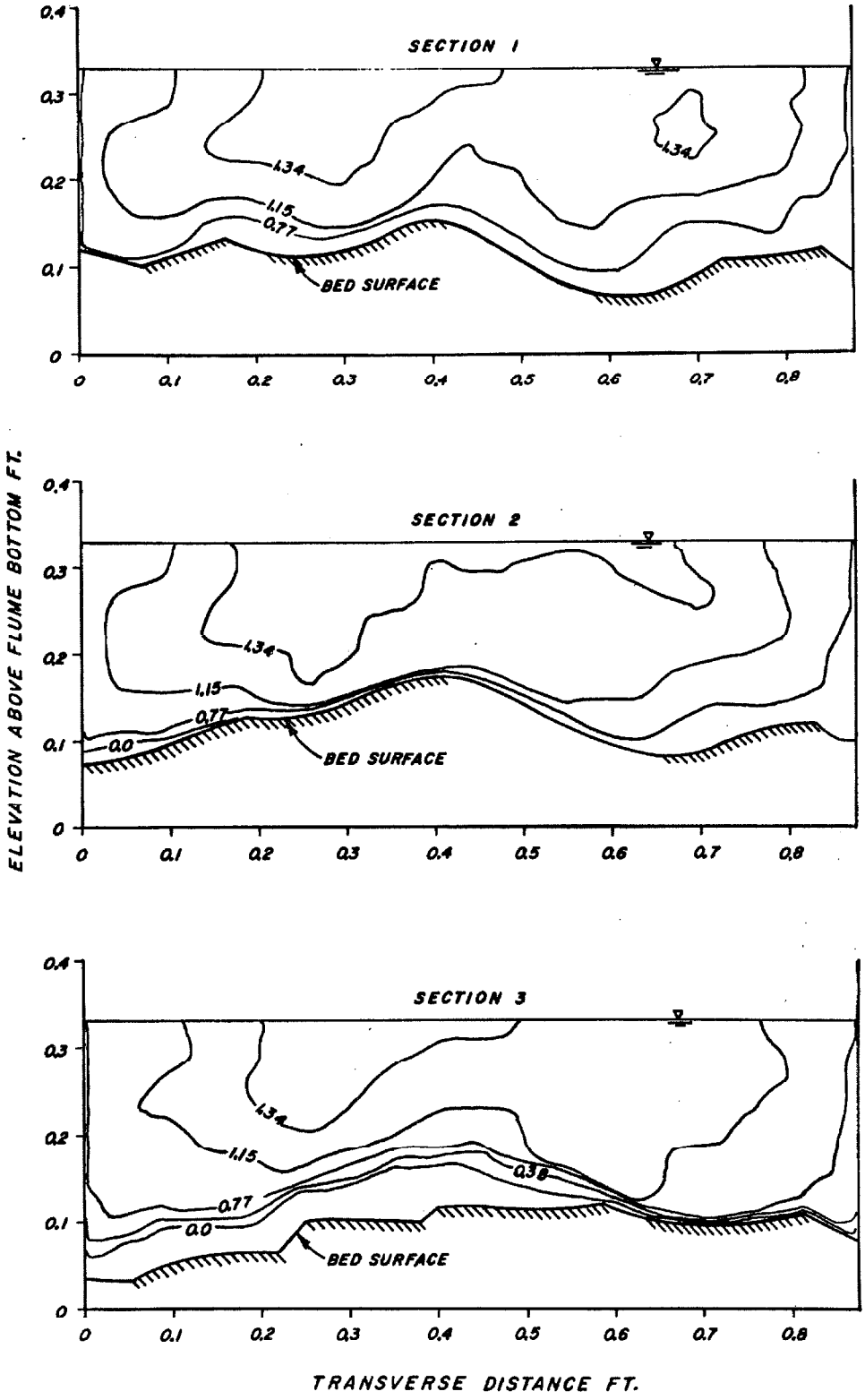

Fig. (5-6) Velocity distribution over dune bed for Run No. 9-14, B-9. The number on the velocity contour is the velocity divided by average velocity.

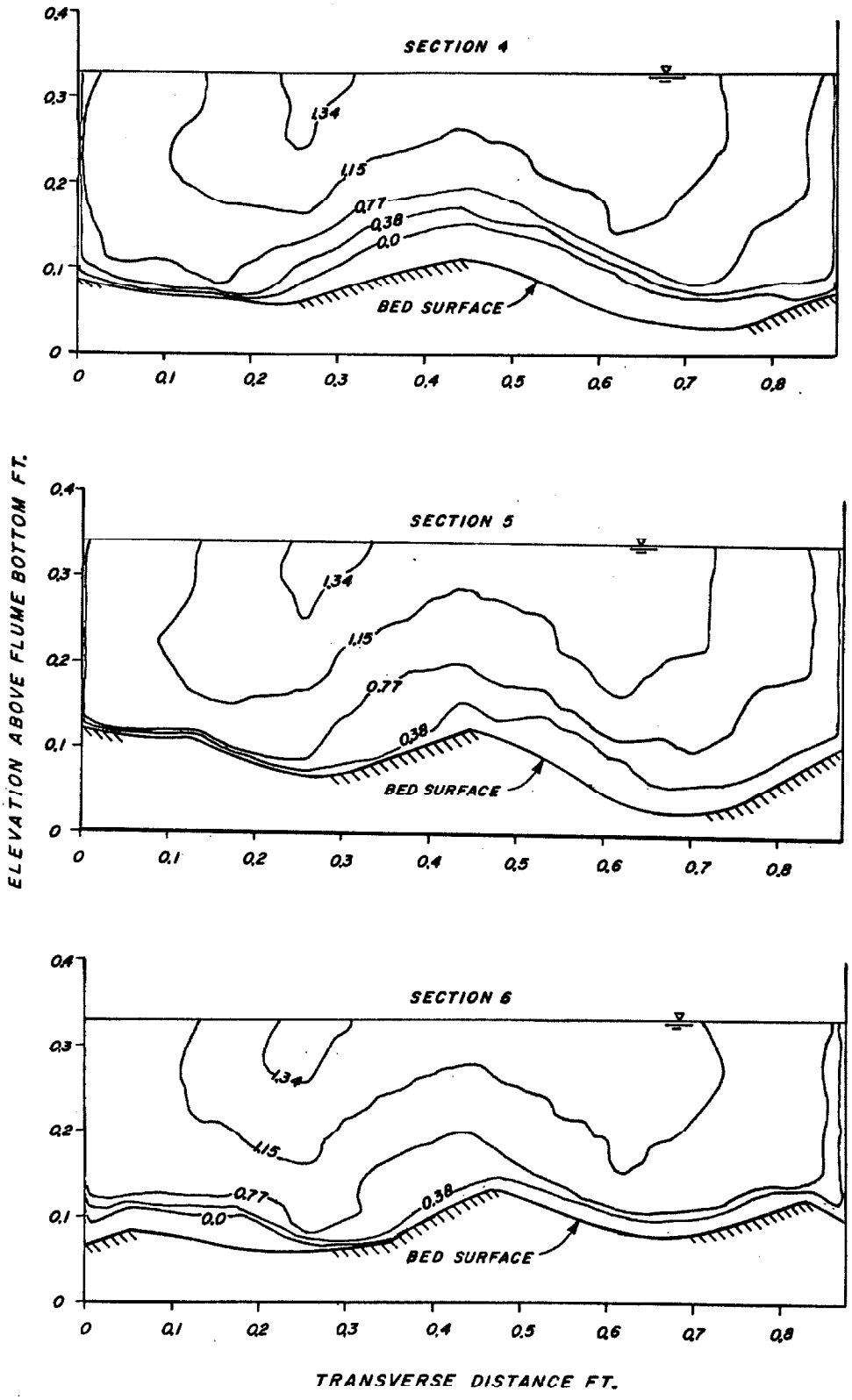

Fig. (5-7) Velocity distribution over dune bed for Run No. 9-14, B-9. The number on the velocity contour is the velocity divided by average velocity.

indicates that a reverse flow exists at the bed. This is especially noticeable in sections 3 of Fig. (5-6) and 4 of Fig. (5-7) where the flow direction is upstream in about 10 percent of the cross-sectional area. Due to the non-uniformity of the flow field the velocity near the bed at a station is strongly affected by conditions a short distance upstream. This is to say that the velocity profile at a station depends on the previous history of the flow.

Because the flow is strongly affected by the large roughness of the dune, the influence of the side wall is of small importance. The high velocity extends all the way out to the side wall where a very steep velocity gradient exists.

3. Pressure Distribution:

Since most of the resistance of a dune bed comes from the form drag of the dunes, it is very important to understand how the pressure distributes over the dune and how it varies with velocity and depth of flow. To determine the pressure distribution, 17 pressure taps were installed near station 25 0.58 in. off the center line in a typical part of the dune bed generated in Run No. 9-14. Fig. (3-15) is a photograph showing the bed configuration around the pressure taps. Pressure measurements were made in flows of different depths with several different average velocities for each depth. The pressure was measured by the micromanometer shown in Fig. (3-17) in terms of the height of a column of water. Plots of normalized pressure $P-P_r/\frac{1}{2}\rho U^2$ against position are presented in Fig. (5-8) for each of these three flow depths. The quantities P and P_r are respectively the local pressure and a reference pressure which was taken as the measured

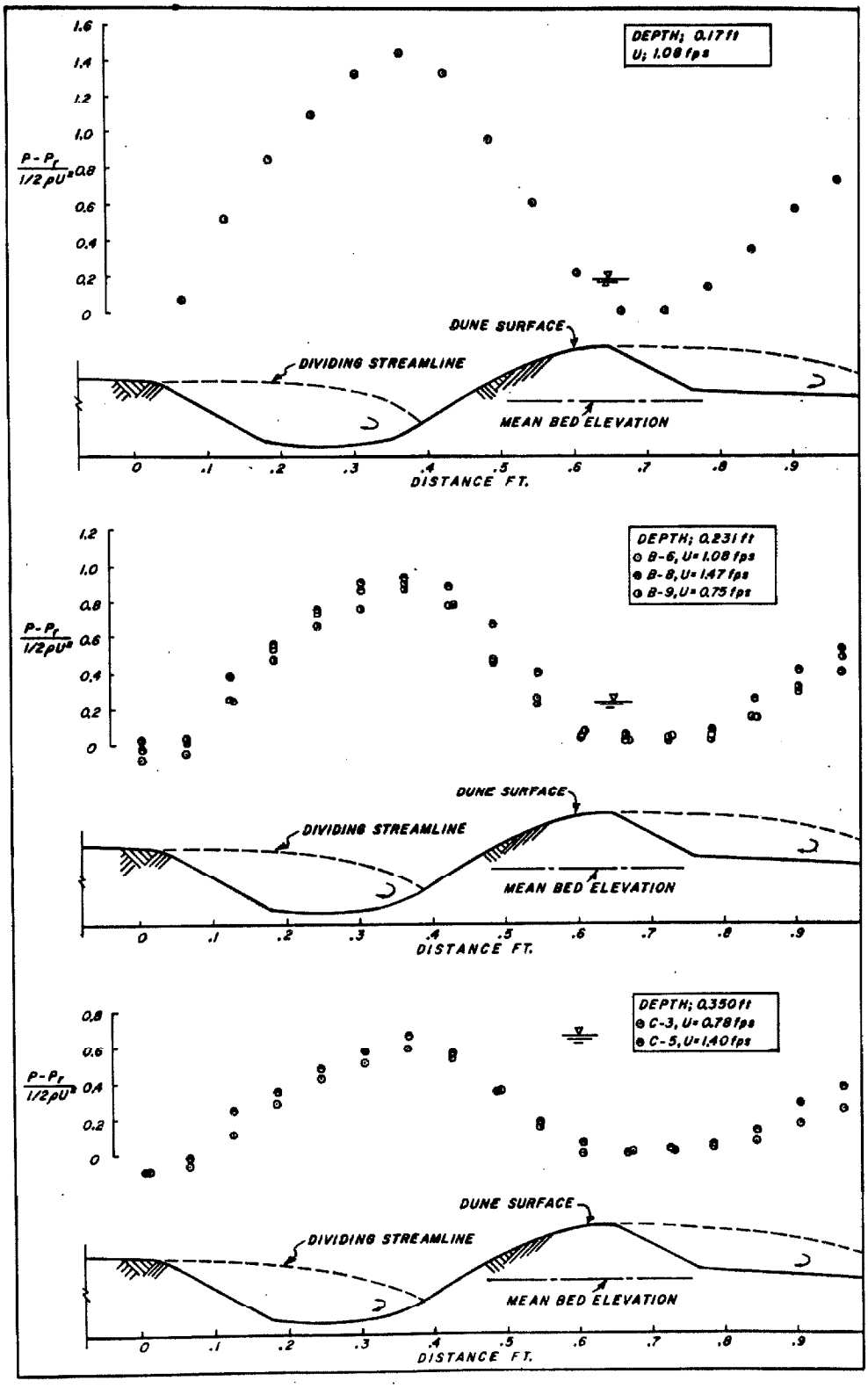

Fig. (5-8) Pressure Distribution over a Typical Dune.

pressure at the crest of the center dune and U is the average velocity, that is, the total discharge divided by the mean cross-sectional area. The results indicate that the shapes of the pressure distribution curves for all cases are roughly similar. The relative pressure, $P - P_r$, reaches a minimum near the crest where the flow separates from the boundary, and then increases as the dividing streamline diverges and finally reaches a maximum where the dividing streamline meets the boundary. This non-uniform distribution of the pressure over the dune results in a large resistance to flow. From the figure, one can see that for a given depth, the value of $\frac{P-P_r}{\frac{1}{2}\rho U^2}$ is related to the dune friction factor $f_b - f_b'$ according to

$$f_b - f_b' = 4\frac{\tau_D}{\frac{1}{2}\rho U^2} = \int_A \left(\frac{P-P_r}{\frac{1}{2}\rho U^2}\right) \hat{i} \cdot d\bar{\sigma} \qquad (5\text{-}3)$$

where τ_D is the average shear stress created by the dune, that is, the total shear stress minus the grain shear stress calculated from Nikuradse's resistance diagram, $\hat{i}$ is the unit vector in the main flow direction and $d\bar{\sigma}$ is the differential surface area with the direction normal to the dune surface. The right hand side of Equation (5-3) does not vary with the average velocity and therefore $f_b - f_b'$ is independent of average velocity at least for the range of velocities covered in Fig. (5-9).

A comparison of the normalized pressure, $P-P_r/\frac{1}{2}\rho U^2$, for flows with different depths will show that it decreases as the depth increases. This is because $P - P_r$ depends on the velocity impinging on the dune. Consider flows with different depths but with the same average velocity flowing over identical beds. Because of the nature of the velocity

profiles, the flow with higher depth will have smaller impinging velocity at the dune surface, and therefore a smaller $P-P_r/\frac{1}{2}\rho U^2$ and bed friction factor.

4. Effect of Reynolds Number and Froude Number on the Bed Friction Factor:

The data of the previous section indicate that the pattern of pressure distribution over dunes does not vary with flow velocity and therefore show that for the conditions of the experiments, f_b is also independent of velocity and hence of Reynolds number. To explore this idea, further experiments were made with flows over the two stabilized dune beds in which the Reynolds number range was expanded by changing the viscosity of the fluid. As already explained this was done by adding glycerine to the water to raise the viscosity and heating the water to lower the viscosity.

The experimental results are presented in Tables I and II appearing in a previous section of this chapter. The variation of bed friction factor f_b with Reynolds number for the two bed configurations are plotted in Figs. (5-9) and (5-10). The points for the high Temperature and Glycerine Runs can be identified from the figures. It is clear that for a given depth, f_b is independent of Reynolds Number, velocity, viscosity and temperature thus confirming the conclusions drawn from the pressure distribution. A comparison of Fig. (5-9) and Fig. (5-10) indicates that the bed of Run No. 9-14 generated by a flow with a velocity of 0.749 fps. has a much higher bed friction factor than that of Run No. 9-15 generated by a higher velocity of 1.25 fps. This illustrates a general trend in the friction factor of streams with dune covered beds. The bed friction factor for each unstabilized bed, measured during the runs which generated the bed, has been plotted

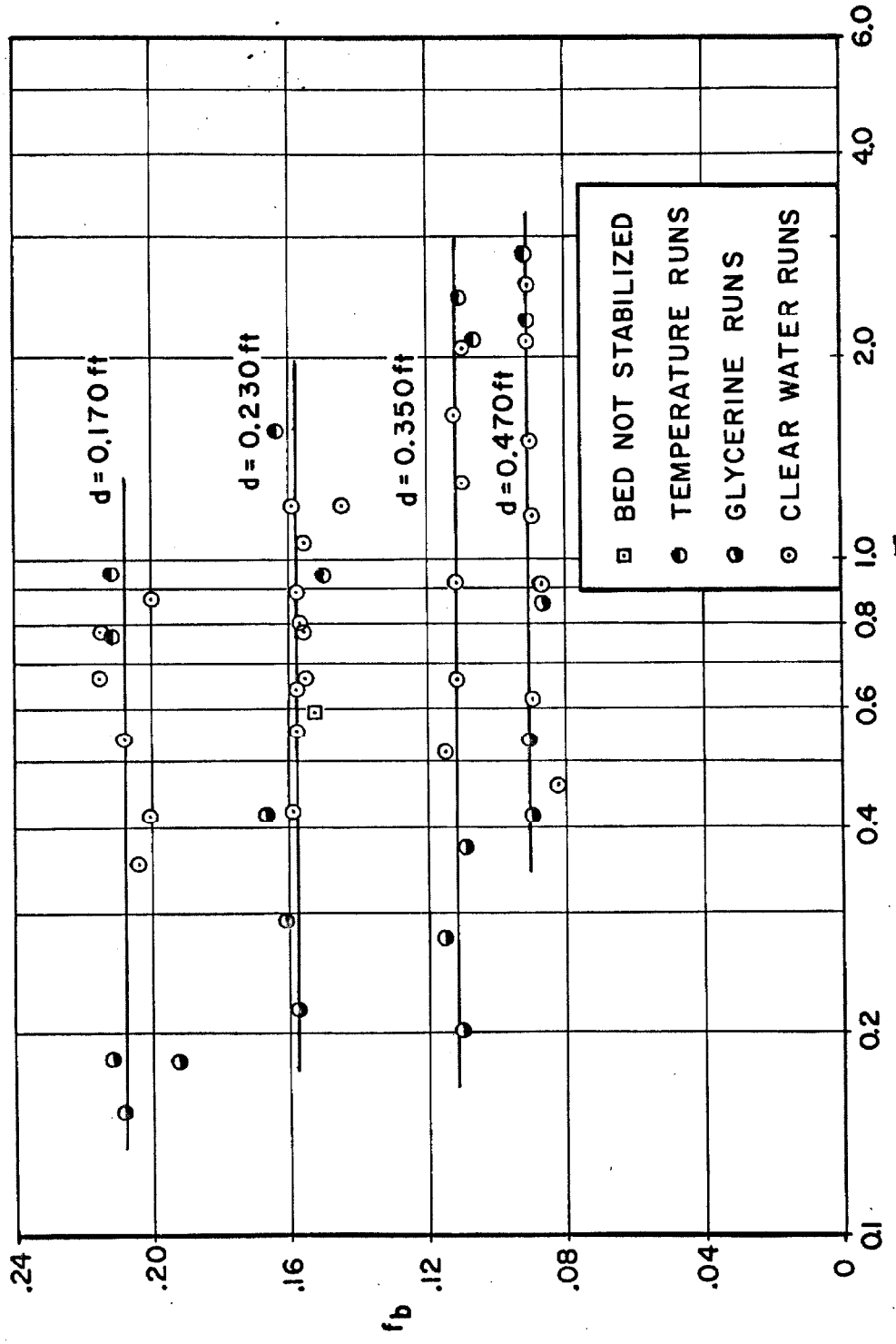

Fig. (5-9) Variations of bed friction factor with Reynolds number for several depths of flow over the stabilized dune bed generated by Run No. 9-14.

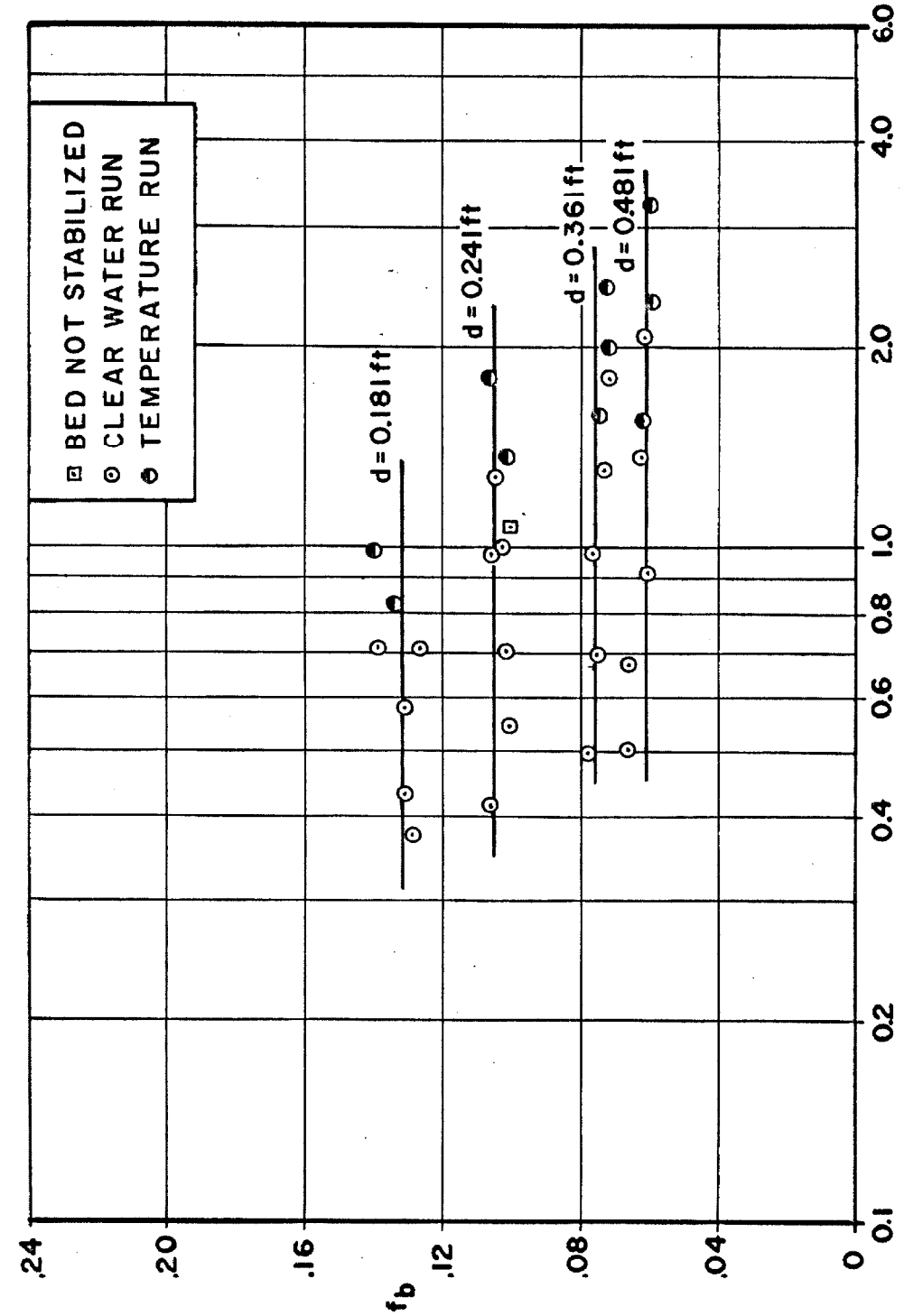

Fig. (5-10) Variations of bed friction factor with Reynolds number for several depths of flow over the stabilized bed generated by Run No. 9-15.

on each of the figures. It is pertinent to note that these values of f_b are not significantly different from those for the stabilized beds with the same flow depth.

In this investigation, Froude number, F, is defined as $\frac{U}{\sqrt{gd}}$ in which U is the average velocity, d is the depth of flow and g is gravitational acceleration. Values of f_b for the dune covered bed generated by the flow of Run No. 9-14 are plotted against F in Fig. (5-11) and those for the dune covered bed generated by the flow of Run No. 9-15 are plotted in Fig. (5-12). Within the range tested, the bed friction factor is essentially independent of Froude number as indicated in the above figures. This can also be deduced from Figs. (5-9) and (5-10).

Figures (5-9) through (5-12) indicate that for a given water depth and a given set of the dune features there is virtually no variation in the friction factor with Reynolds and Froude number. Certainly, this statement does not hold for very small Reynolds numbers. As Reynolds number is reduced, one may expect to have transition to laminar flow so that in this region the bed friction factor will depend on Reynolds number. Furthermore, for sufficiently high Froude numbers, f_b cannot be independent of the Froude number[23]. However, these two extreme conditions of very low Reynolds number and high Froude number will not occur in the usual alluvial stream with a dune bed. All alluvial streams with dune beds, including laboratory streams, are turbulent and hence well out of the transition range. Furthermore, the Froude number of streams with dune beds tend to be well below unity and out of the range where the bed friction factor is affected by Froude number.

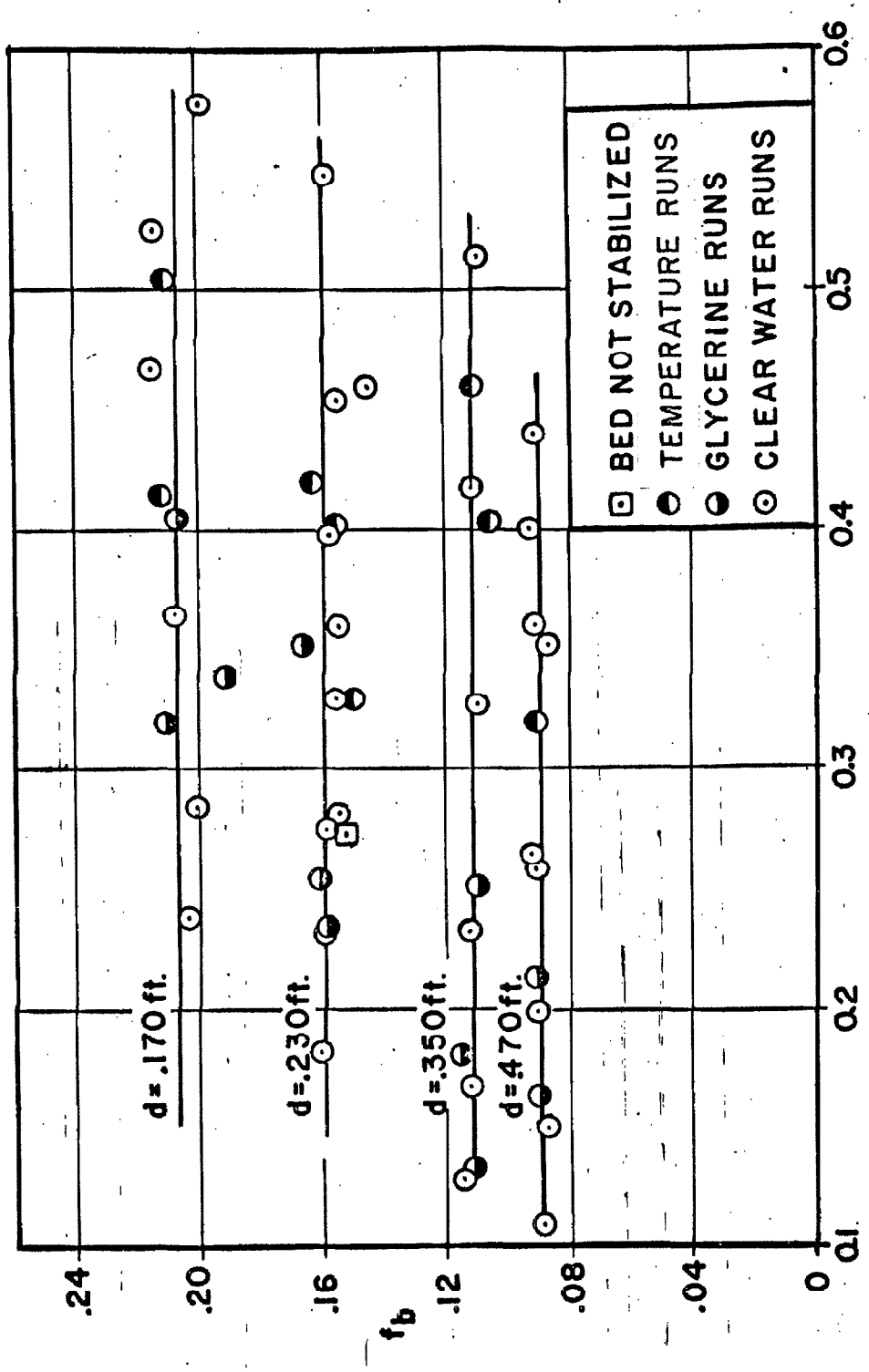

Fig. (5-11) Variation of the Bed Friction Factor with Froude Number for Several Depths of Flow over the Bed Generated by Run No. 9-14.

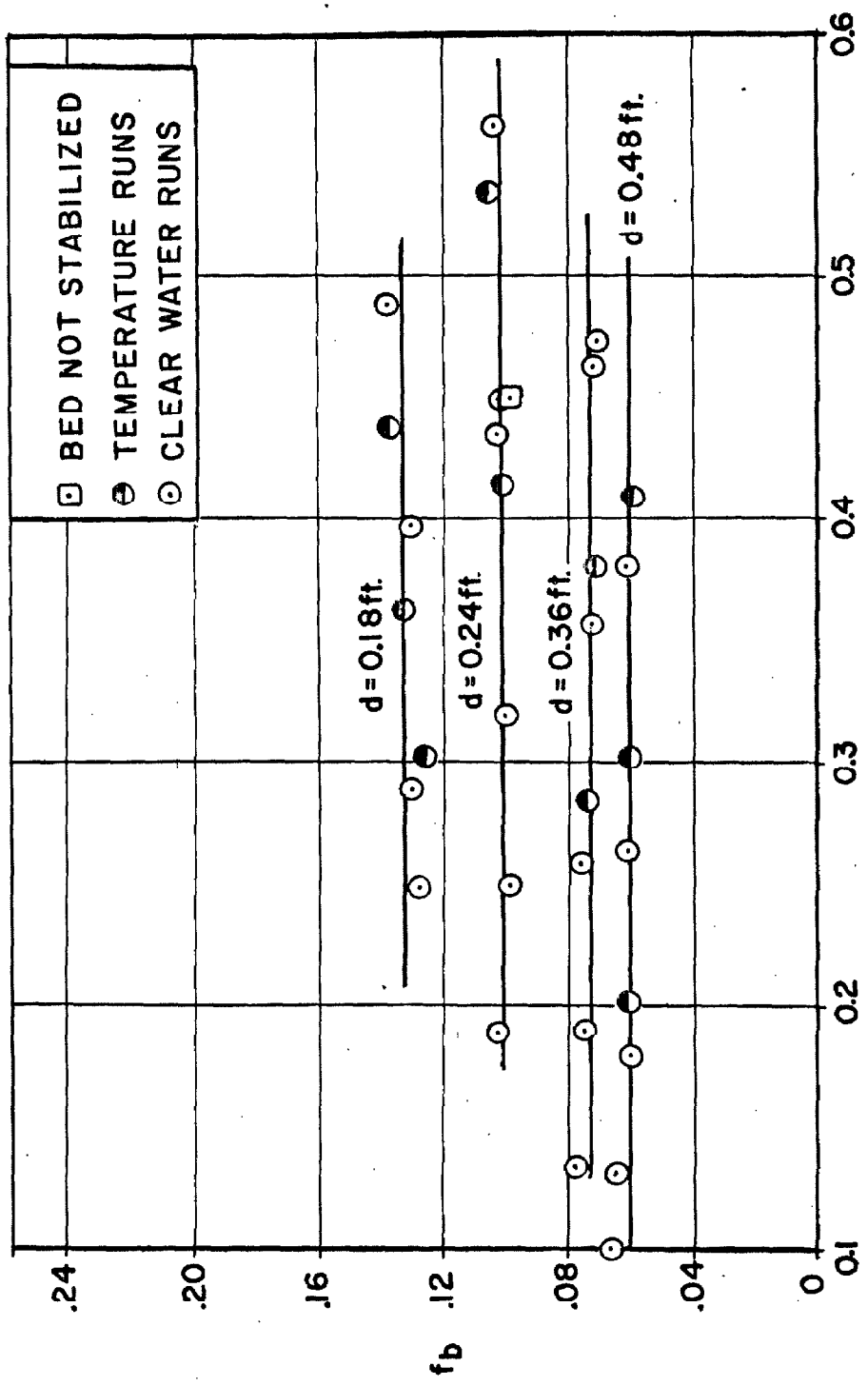

Fig. (5-12) Variation of the Bed Friction Factor with Froude Number for Several Depths of Flow over the Bed Generated by Run No. 9-15.

The lack of the dependence of the bed friction factor on Reynolds number and on Froude number indicates that the bed friction factor depends only on geometric quantities. The velocity and viscosity only play a role in the formation of the dune feature and do not directly affect the bed friction factor. This is a very important hydraulic characteristic of dunes and means that in the formulation of the resistance equation, only geometric quantities of the dune bed, such as depth and dune dimensions, are required.

5. Effect of the Bed Hydraulic Radius on the Bed Friction Factor:

As pointed out in the previous sections, dune resistance depends only on the water depth and dimensions of the geometric configuration of the bed. It is interesting to investigate the effect of the water depth on f_b for a fixed bed configuration. Fig. (5-13) is a plot of the friction factor, f_b, against the bed hydraulic radius, r_b, for each of the two bed configurations studied. The bed friction factor increases as the bed hydraulic radius decreases. The curves also indicate that for the shallower water depths, a small change in the bed hydraulic radius, r_b, causes a large change of the bed friction factor, f_b. This rate of change of the bed friction factor reduces gradually as the depth of water increases.

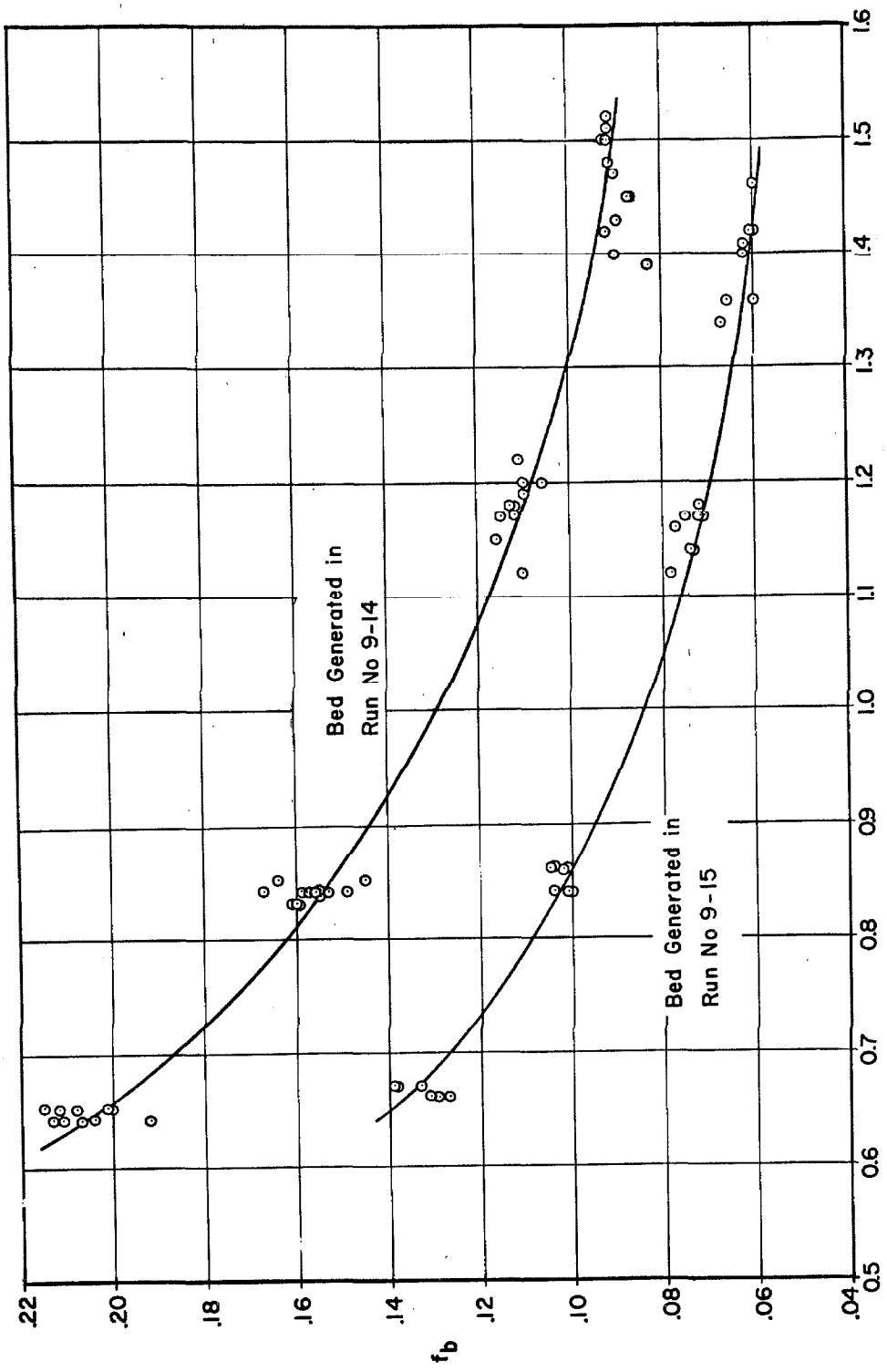

Fig. (5-13) Relationship between Bed Friction Factor and Bed Hydraulic Radius.

C. Results of the Experiments with Loose Sand

1. General Outline of the Experiments:

Each run reported in this section deals with a uniform flow over a loose sand bed. Uniform flow was established, measurements were made and the basic data were analyzed according to the procedure described in Chapter IV.

Tables III and IV list the most important measured and calculated quantities for each run. Table III gives the results obtained in the 40-foot flume, and Table IV gives those obtained in 130-foot flume. The entries missing in these two tables are the items not obtained. The notation at the top of each column gives the symbol for and a word description of the measured or calculated quantity which appears in the column. Quantities which are self-explanatory or can be calculated in a straight-forward way are not given further explanation below, while the others such as grain friction factor, f_b', mean sediment discharge concentration, $\overline{C}$, geometric mean sieve diameter, D_g, and geometric standard deviation, σ_g, will be explained in detail. Special explanations of the dune height, $\overline{H}$, and the exposure parameter, e, will be given in later sections.

The grain friction factor, f_b', is calculated by use of the pipe-friction diagram[24] for pipes artificially roughened with uniform sand. This diagram gives f as a function of relative roughness, D/k_s, and the Reynolds number, UD/ν, where D is the pipe diameter, k_s is the grain size of the sands used to roughen the pipe wall, U is the average velocity in the pipe and ν is the kinematic viscosity of the fluid. To use this chart for the present study, D is made equivalent to $4\,r_b$, k_s is taken

Table III. Summary of Data from Experiments with Loose Sand in the 40-foot Flume.

$D_g = 0.230$ mm. $\sigma_g = 1.43$

Run No.	Q Discharge cfs.	d Depth ft.	r Hydr. Radius ft.	S Slope $x10^{-3}$	U Ave. Vel. fps.	f Frict. Factor	T Temp. °C.	r_b Bed Hydr. Radius ft.	f_b Bed Frict. Factor	f'_b Grain Frict. Factor	$f_b - f'_b$ Dune Frict. Factor	$\bar{H}$ Ave. Dune Height ft.	e Exposure Parameter	$r_b / e\bar{H}$ Modified Relative Roughness	$\bar{C}$ Sed. Disch. Conc. gr/l	Analysis of Sediment Load	
																D_g mm.	σ_g
9- 1	0.195	0.248	0.158	2.30	0.899	0.1160	22.0	0.225	0.1653	0.0189	0.146	0.054	--	--	0.120	0.174	1.51
9- 2	0.171	0.242	0.156	2.00	0.806	0.1236	21.2	0.221	0.1753	0.0196	0.156	0.051	--	--	0.062	0.175	1.46
9- 3	0.130	0.241	0.155	1.20	0.616	0.1265	22.0	0.219	0.1786	0.0207	0.158	0.049	--	--	0.001	---	---
9- 4	0.260	0.241	0.155	2.80	1.232	0.0738	22.6	0.212	0.1009	0.0181	0.0828	0.050	--	--	0.488	0.180	1.53
9- 5	0.202	0.242	0.156	0.70	0.954	0.1191	25.5	0.222	0.1693	0.0185	0.151	0.052	--	--	0.265	0.183	1.55
9- 6	0.231	0.240	0.155	2.90	1.100	0.0956	21.7	0.217	0.1338	0.0184	0.115	0.049	--	--	0.417	0.188	1.55
9- 7	0.286	0.234	0.153	2.70	1.400	0.0542	21.9	0.200	0.0711	0.0180	0.0531	0.037	--	--	0.619	0.178	1.54
9- 8	0.127	0.242	0.156	1.20	0.599	0.1345	20.5	0.219	0.1888	0.0210	0.168	0.052	--	--	--	--	--
9- 9	0.118	0.237	0.153	0.90	0.570	0.1090	22.0	0.217	0.1510	0.0211	0.130	0.050	0.125	34.7	--	--	--
9-10	0.197	0.243	0.157	2.40	0.926	0.1130	20.8	0.217	0.1600	0.0191	0.141	0.053	0.144	28.4	--	--	--
9-11	0.242	0.235	0.153	2.89	1.180	0.0820	20.8	0.208	0.1130	0.0184	0.0946	0.050	0.118	35.3	--	--	--
9-12	0.250	0.238	0.154	2.80	1.240	0.0770	20.6	0.210	0.1050	0.0182	0.0868	0.050	0.101	41.5	--	--	--
9-13	0.280	0.232	0.152	2.39	1.380	0.0482	21.6	0.197	0.0622	0.0181	0.0441	0.038	0.062	83.7	--	--	--
9-14	0.152	0.231	0.151	1.59	0.749	0.1102	21.0	0.209	0.1525	0.0202	0.132	0.052	0.138	29.0	0.007	--	--
9-15	0.263	0.241	0.156	2.86	1.250	0.0735	20.9	0.213	0.1004	0.0178	0.0826	0.046	0.098	46.4	0.448	0.182	1.54

Table IV. Summary of Data from Experiments with Loose Sand in the 130-foot Flume.

$D_g = 0.206$ mm. $\sigma_g = 1.46$

Run No.	Q Discharge cfs.	d Depth ft.	r Hydr. Radius ft.	S Slope $x10^{-3}$	U Ave. Vel. fps.	f Frict. Factor	T Temp. °C.	r_b Bed Hydr. Radius ft.	f_b Bed Frict. Factor	f'_b Grain Frict. Factor	$f_b - f'_b$ Dune Frict. Factor	$\bar{H}$ Ave. Dune Height ft.	e Exposure Parameter	$r_b / e\bar{H}$ Modified Relative Roughness	$\bar{C}$ Sed. Disch. Conc. gr/l	Analysis of Sediment Load	
																D_g mm.	σ_g
1	2.26	0.598	0.450	0.642	1.045	0.0682	19.8	0.552	0.0839	0.0144	0.0695	0.043	0.125	103	0.031	0.127	1.33
2	3.09	0.589	0.444	1.055	1.452	0.0573	20.1	0.542	0.0699	0.0146	0.0553	0.052	0.110	100	0.180	0.155	1.34
*3	3.82	0.578	0.438	1.303	1.829	0.0439	20.7	0.522	0.0523	0.0144	0.0379	--	--	--	1.49	0.199	1.31
4	3.22	0.589	0.444	1.116	1.513	0.0556	21.0	0.535	0.0677	0.0145	0.0532	0.054	0.095	104	0.380	0.177	1.36
5	3.37	0.603	0.452	1.100	1.547	0.0538	19.2	0.555	0.0656	0.0145	0.0511	0.051	0.097	112	0.410	0.194	1.44
6	4.30	0.780	0.545	0.809	1.526	0.0487	18.8	0.699	0.0625	0.0139	0.0486	0.057	0.104	119	0.261	0.182	1.43
7	6.55	1.216	0.644	0.455	1.491	0.0339	20.0	0.870	0.0458	0.0133	0.0335	0.052	0.105	158	0.061	0.187	1.68
8	2.30	0.591	0.445	0.709	1.080	0.0705	19.2	0.548	0.0869	0.0154	0.0715	0.053	--	--	--	--	--

* Sand Wave

as D_g the geometric mean size of the sand in the flume, U is taken as the average velocity in the flume cross section and ν is taken as the kinematic viscosity of the water in the flume. From these quantities one calculates the relative roughness and Reynolds number, enters the chart with these values and reads f which is then taken as equivalent to f'_b.

The procedure for evaluating the sediment discharge concentration, $\overline{C}$, has been described in Chapter IV. The accuracy of this measurement for the 40-foot flume was described by Kennedy[23]. In the 130-foot flume the sampler device is much more precise than the one used in the 40-foot flume because it can reach most of the flow cross section. However, due to the extremely non-uniform concentration distribution resulting from the location of the sampler so near to the horizontal return pipe as shown in Fig. (3-7), some error may be introduced in plotting the c v contours. Nevertheless, it is believed that the error introduced above does not exceed 15 percent. However, no check was possible to prove that the error is within this limit.

In Run No. 4 in the 130-foot flume, a part of the sand was lost in a few samples during filtering. The value of the sediment discharge concentration was estimated from the rest of the samples and by comparing with the distribution patterns of the c v contours for other runs.

The last two columns of Tables III and IV show the geometric mean sieve size, D_g, and the geometric standard deviation of the sizes, σ_g, for the samples of the load. Sieve analyses were made of a composite of all sediment sampled during each run and then the results were plotted on logarithmic probability paper. The curves

plotted do not, in general, follow a straight line. Therefore, the geometric mean sieve diameter, D_g, is not equal to D_{50}, the median size. Values of D_g and the geometric standard deviation, σ_g, were determined by the method suggested by Otto[25], that is,

$$\sigma_g = \sqrt{\frac{D_{84.1}}{D_{15.9}}} \tag{5-4}$$

and

$$D_g = \frac{D_{84.1}}{\sigma_g} \tag{5-5}$$

where $D_{84.1}$ and $D_{15.9}$ are the sand sizes for which 84.1 percent and 15.9 percent, respectively, by weight are finer.

2. Sand Characteristics:

Both sands used in the experiments were obtained from a local foundry supply company and were commercially marked "Nevada 60". Sand No. 1 was first used by Kennedy[23] in his studies of the behavior of antidunes and Sand No. 2 was procured for this investigation in the 130-foot flume. As indicated in Fig. (5-14), Sand No. 1 had a slightly larger geometric mean size, D_g, than Sand No. 2.

The size distribution of the two sands was obtained by sieving in standard ten-inch Tyler Laboratory sieves. The sieves were shaken for 15 minutes in a Tyler Rotap Machine. The frequency distribution of sieve sizes for the two sands used in this study is shown on logarithmic probability paper in Fig. (5-14). The curves of Fig. (5-14) indicate that the distribution curve is almost a straight line except near the ends.

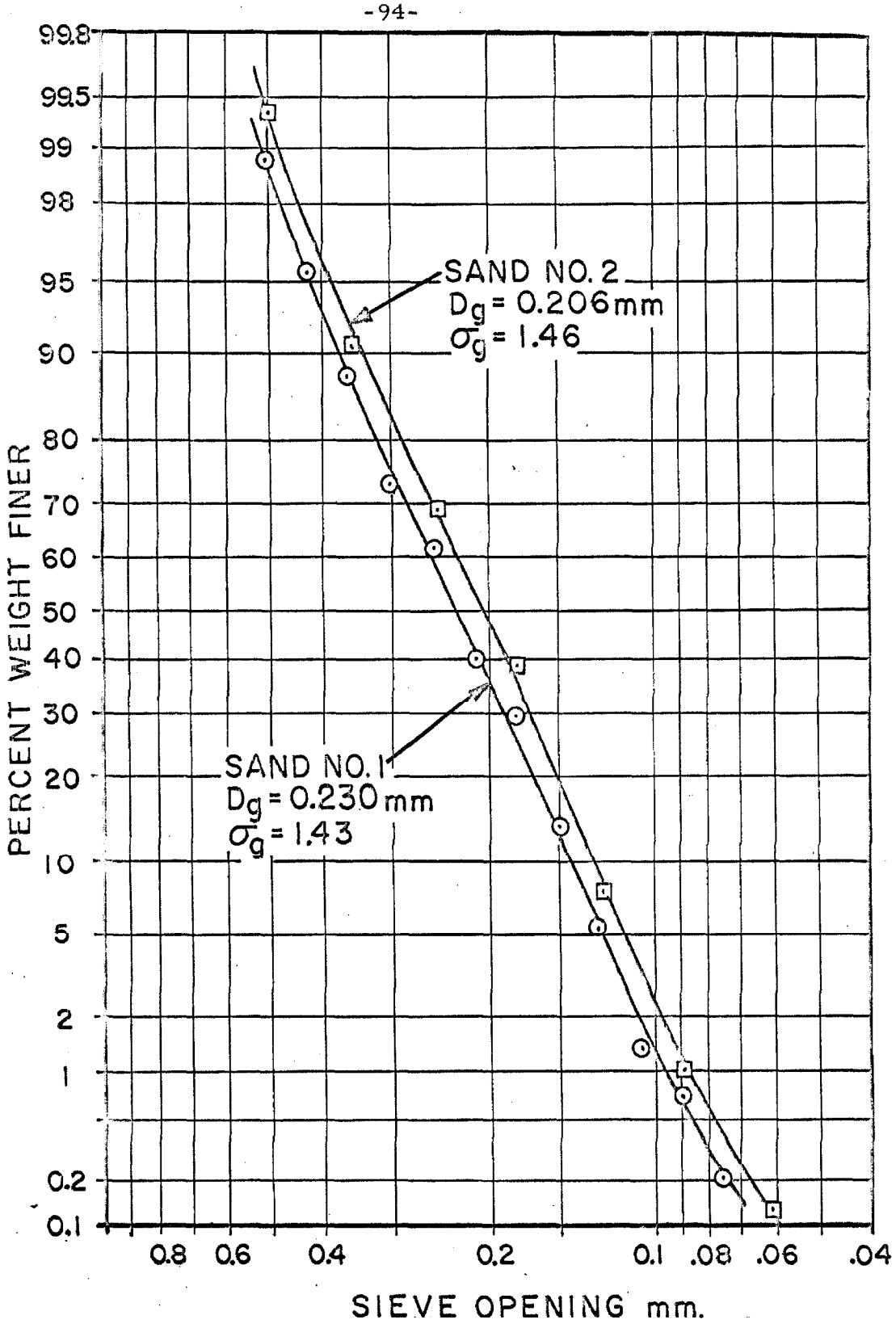

Fig. (5-14) Size-frequency distribution of sieve sizes of sands used in experiments.

This is to say that the logarithms of the sieve sizes of the sand grains are distributed according to the normal error law.

The shape and roundness of the sands may be judged from magnified photographs in Fig. (5-15). The grains of both sands are subrounded and somewhat angular, although Sand No. 2 is more angular than Sand No. 1. A summary of the properties of both sands is given in Table V.

TABLE V SUMMARY OF SAND PROPERTIES

	Sand No. 1	Sand No. 2
Geometric Mean Sieve Size, D_g, mm.	.230	.206
Geometric Standard Deviation σ_g	1.43	1.46
Specific Gravity	2.65	2.67
Flume in Which Sand Was Used	40-foot flume	130-foot flume

The specific gravity was measured by use of a specific weight bottle of known volume and distilled water, which was placed under vacuum to remove dissolved air. The procedure for this measurement is first to pour a known weight of sand into the specific weight bottle and then to fill the bottle with distilled water observing the volume of water required to fill the bottle. The volume or displacement of the sediment is given by the difference between the volume of the bottle and the water added. Finally, the specific gravity was determined by dividing the weight of the sand by its displacement.

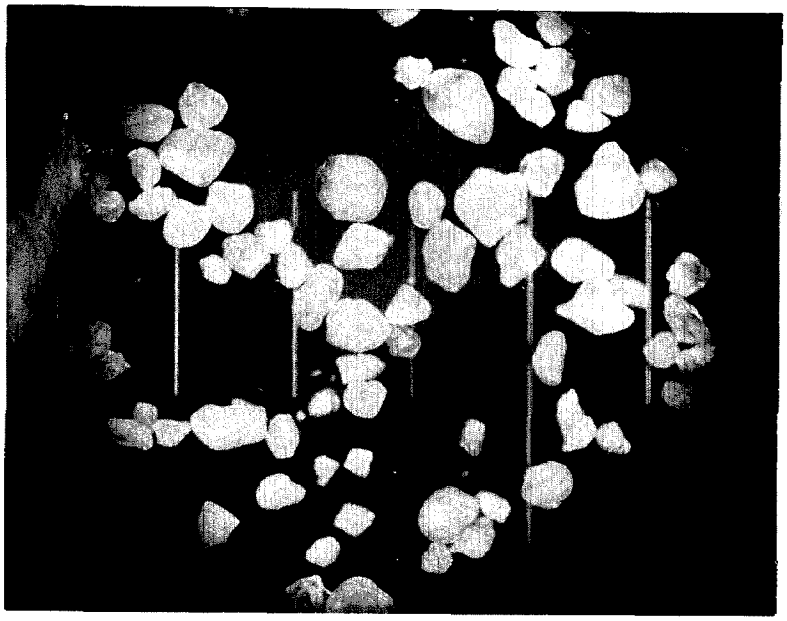

(a) Sand No. 1 D_g=0.230 mm., σ_g=1.43

(b) Sand No. 2 D_g=0.206 mm., σ_g=1.46

Fig. (5-15) Microphotographs of sands used in experiments. (Magnification: 30 times.)

3. Dunes and Sand Waves:

Two views of dunes generated in the 130-foot flume by a flow 0.598 ft. deep with an average velocity of 1.04 fps. are shown in Fig. (5-16). As may be seen,the dunes have a gentle upstream slope, a sharp crest and a steep downstream or lee slope. As the average velocity of flow over a dune bed is increased, the dunes change in shape and size but still retain most of the features shown in Fig. (5-16) until the limiting velocity is reached,at which point the bed form is no longer uniform along the length of the flow. Under these conditions a reach of the bed may become flat and free of dunes and the rest of the bed may be covered by dunes. The part of the flow with flat bed has a higher velocity and lower depth than the part with dune bed and where the two parts join, a sudden change often occurs in the bed elevation. Since this break in bed elevation moves downstream, it has the appearance of wave. Brooks[1], who first reported this phenomenon, called it a "sand wave".

Both top and side views of a sand wave in the 130-foot flume are shown in Fig. (5-17). The side view was taken with water flowing and shows the water surface clearly. The top view was taken after the water was removed. As shown in the photographs, the long sand wave has a length of more than 30 feet. The bed features on the wave front are very irregular and one can see that dunes on the right side are much larger than those on the left. As shown in the side view of Fig. (5-17), the depth of flow over the sand wave varies greatly. In this case, the mean depth upstream from the sand wave is about 0.457 feet and downstream of the wave front the depth is 0.664 feet, which

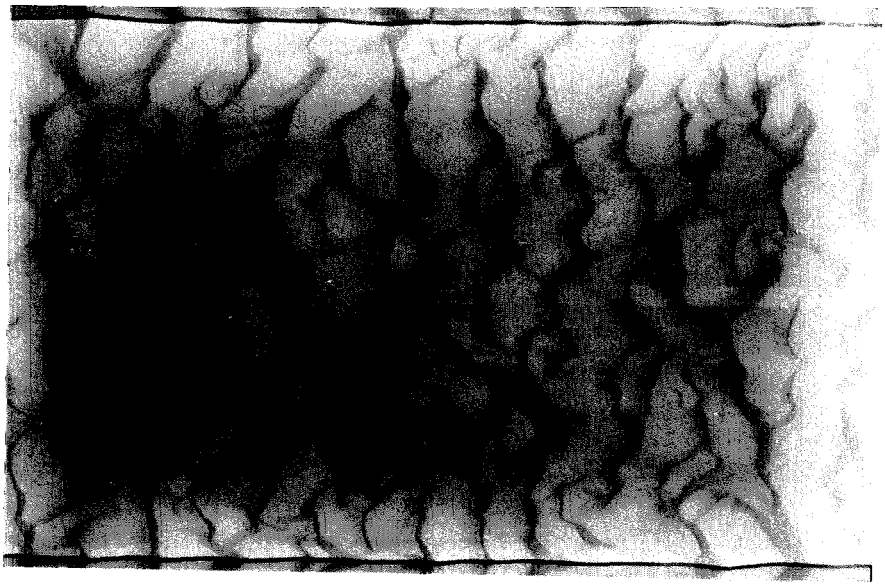

(a) Top view.

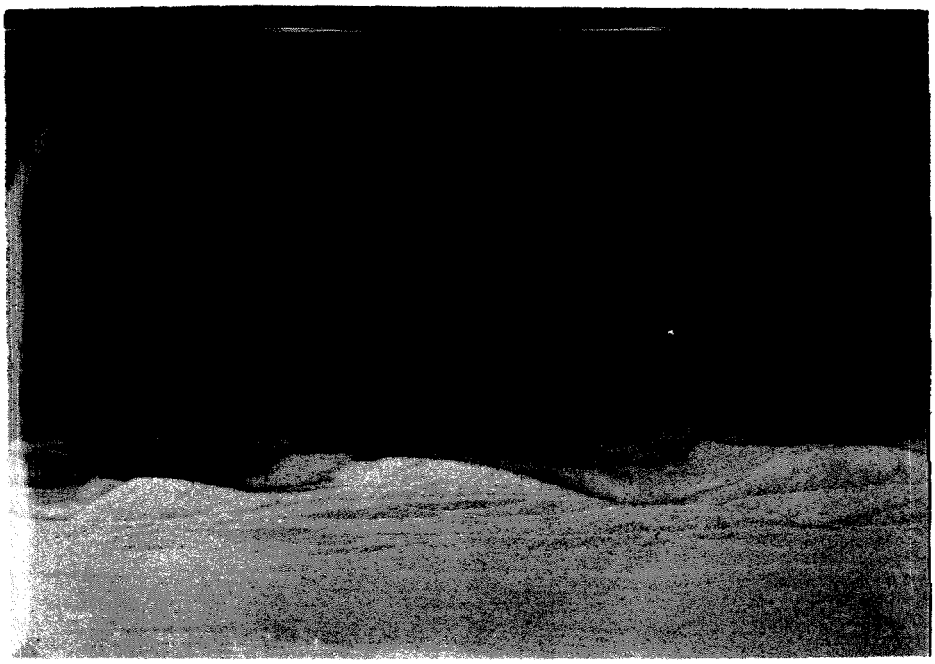

(b) Side view.

Fig. (5-16) Typical dune bed configuration in 130-foot flume. (Flow is from right to left.) U=1.05 fps. d=0.598 ft., D_g=0.206 mm., σ_g=1.46.

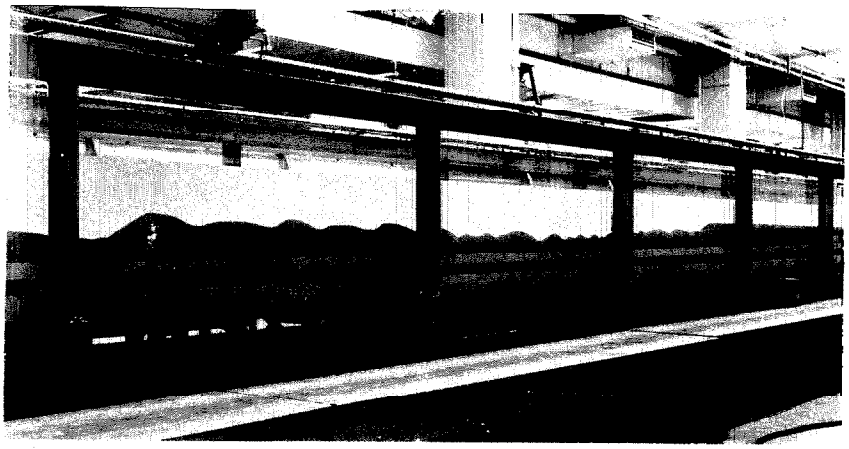

(a) Side view.

(b) Top view.

Fig. (5-17) Sand wave bed configuration. Flow is from right to left in (a) and from bottom to top in (b).

results in a change in average velocity from 2.31 fps. upstream of the sand wave to 1.59 fps. at the downstream end of the sand wave. Because of the difference in the depth of flow caused by this unsteady phenomenon, essentially there exist two equilibrium bed configurations in one flume.

Fig. (5-18) shows another sand wave which is more or less like a dune and has a relatively short length of only about 2 feet and a height of about 0.25 feet from the toe of the steep face to the crest of the curved top. This sand wave was generated by Run No. 3 with an average velocity of 1.83 fps. and a mean depth of 0.578 feet. It is interesting to note that this feature has a convex profile with its maximum elevation upstream from the crest of the steep front. Dunes of this shape are also observed in beds entirely covered with dunes.

Due to the complication of unsteady conditions in runs with sand waves, no useful resistance data could be obtained from such runs. Information on this phenomenon is reported here because it is of interest to these concerned with the development of bed forms.

4. Velocity Measurements:

To measure the velocity with loose sand is quite difficult, especially near the sand bed. This is because the dune configuration moves and changes continuously. As shown by the velocity measurements obtained with the stabilized bed, the velocity profile near the bed is greatly modified by the dune configuration. Consequently, the measured velocity profiles near a bed of loose sand are subject to considerable error due to the movement of the dune in the time required to

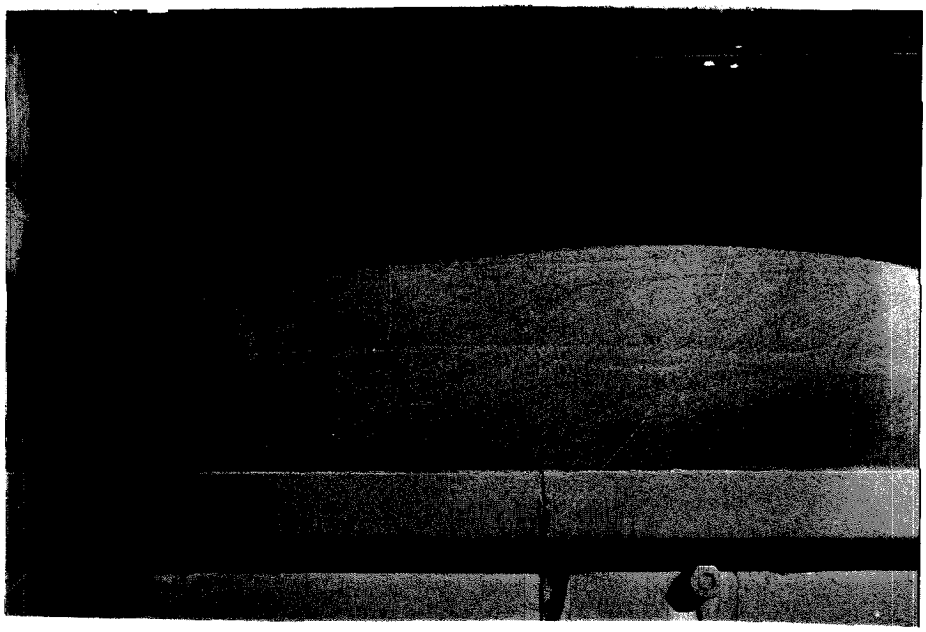

Fig. (5-18) A sand wave with convex surface, relatively smaller height at the crest than at the top of the wave. Flow from right to left.

make the measurements. However, some gross conclusions can still be made from such measurements.

At station 30, that is, 30 meters from the inlet of the 130-foot flume, measurements of the velocity distribution over the entire cross-sectional area were made for Run No. 8. The results are shown as isovels in Fig. (5-19). To locate the isovels, vertical velocity profiles were first plotted for each of 17 verticals and a smooth curve was fitted to each graph. The location of the contour line or isovel was then determined from the smoothed velocity curve.

As shown in Fig. (5-19), the velocity distribution over the cross section is close to symmetrical about the center line. The velocity in the vicinity of the bed is higher near the side walls than near the center line. The reason for this is not clear.

Fig. (5-20) shows the centerline velocity profiles at several stations along the flume in Run No. 8 in the 130-foot flume. The data are plotted on semi-logarithmic paper and the origin of y the distance above the bed is at the local mean bed elevation. As shown in the figure, the points are fitted with a straight line. The von Karman constant, κ, which is calculated according to the procedure outlined in Section B of this chapter varies from 0.27 to 0.43 and has an average value of 0.33.

Since the flow was over a loose sand bed and was carrying some suspended sediment, the value of this constant is affected both by the sediment of the suspension and the large roughness of the dunes.

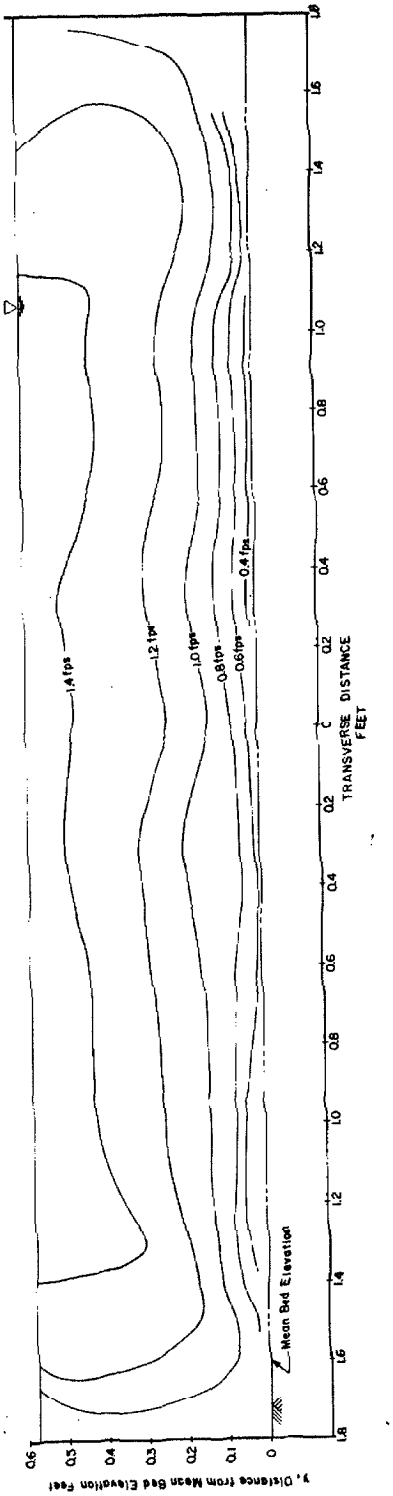

Fig. (5-19) Velocity distribution over dune bed of Run No. 8 with loose sand in the 130-foot flume. Looking downstream at station 30.

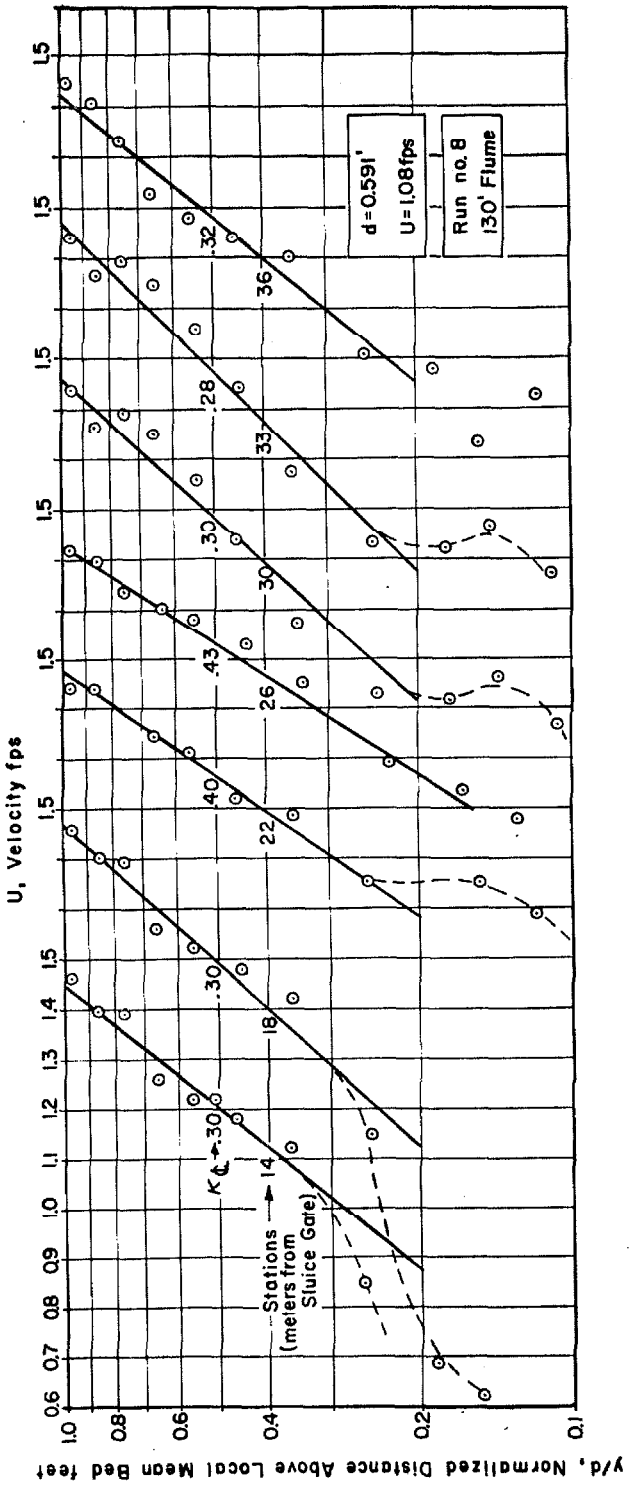

Fig. (5-20) Centerline velocity profiles for Run No. 8 along the 130-foot flume.

5. Evaluation of the Dune Height:

The dunes in general are triangular in shape with gentle upstream slopes and steep lee side slopes. They are distributed in a very irregular pattern. The size of dunes varies and the troughs just upstream and downstream from a crest are usually not at the same elevation. Therefore, to get a representative dune height is rather difficult. A method suggested by Brooks was followed in this work. In this method the dune height is defined as follows:

Let T_i, T_{i+1}, T_{i+2} .....

be the successive elevations relative to the flume of the troughs of the dunes determined by point gage, and C_i be the elevation of the crest of the dune between the troughs T_i and T_{i+1}. Then the height, H_i, of the i^{th} dune is defined as

$$H_i = C_i - 1/2\ (T_i + T_i + 1) \qquad (5\text{-}7)$$

Once the individual dune heights are calculated, a study of the height distribution of the dunes can be made.

In the 130-foot flume, the bed elevations relative to the rail of the flume were measured along the center line in a length of more than 10 meters. Histograms of dune height frequency for Runs 4, 5, 6 and 7 in the 130-foot flume are shown in Fig. (5-21). These show that the dune heights tend roughly toward a bell shaped distribution with a large range of sizes. The arithmetic average dune height, $\overline{H}$, was chosen as the representative height. In order to determine an accurate representative dune height, a great number of the dunes has to be measured. From a study of running averages of the height of the first 10, 15, 20...

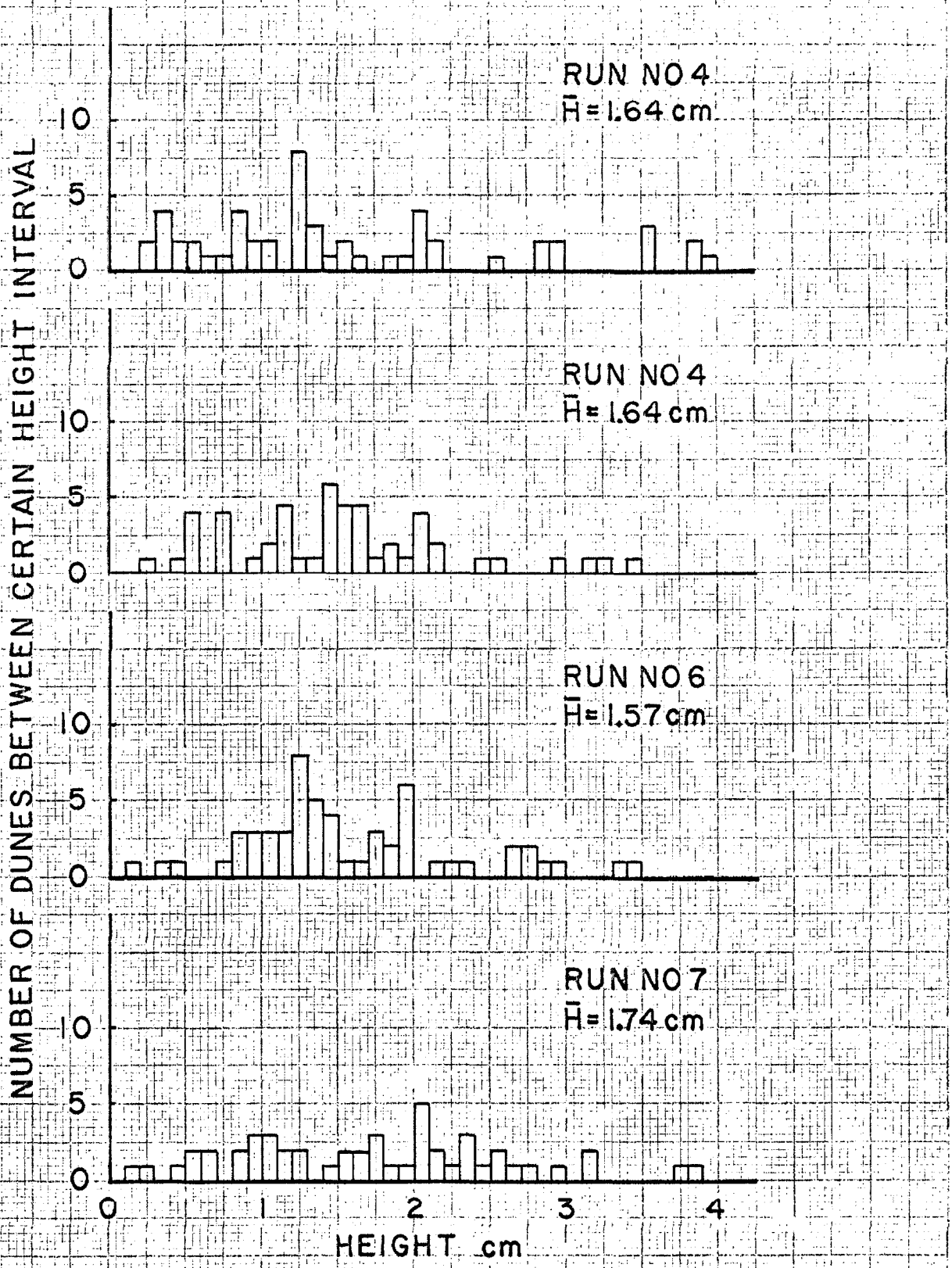

Fig. (5-21) Histogram of Dune Heights Measured in the 130-foot Flume.

dunes etc., it appears that at least 30 dunes have to be measured in order to obtain a reasonably good average.

Fig. (5-22) shows a plot of the average dune height, $\overline{H}$, against the average velocity, U, for experiments in the present investigation in the 40-foot and 130-foot flumes and for some carried out by Vanoni and Brooks[13] with fine sand in a flume 60 feet long and 33.5 inches wide. This plot indicates that the average dune height, $\overline{H}$, shows no general trend of variation with the average velocity until the transition regime is reached. The solid line in this figure was drawn to fit the points obtained in the 40-foot flume with depth ranging from 0.231 to 0.248 ft. It starts to dip down suddenly as the velocity approaches 1.4 fps. where the bed is on the verge of becoming flat.

The dunes observed in these studies are of small size. Much larger dunes have been observed in flumes with larger sand size[26][27] and in the field where the depths are large, large dunes are found even in very fine sand[28]. The reason for the large variation in dune size is not clear.

6. Determination of the Exposure Parameter and Its Effect on the Bed Friction Factor:

After finishing the experiments on the stabilized bed generated by Run No. 9-14, a portion of the stabilized bed was painted white to make visible dye injected into the flow through the piezometer holes in the bed. Two photographs taken for two different flow conditions with dye injected at the bed are shown in Fig. (5-23). One can see that on the upstream side of the dune the dye stream closely follows the boundary, while on the lee side of the dune the dye stream separates

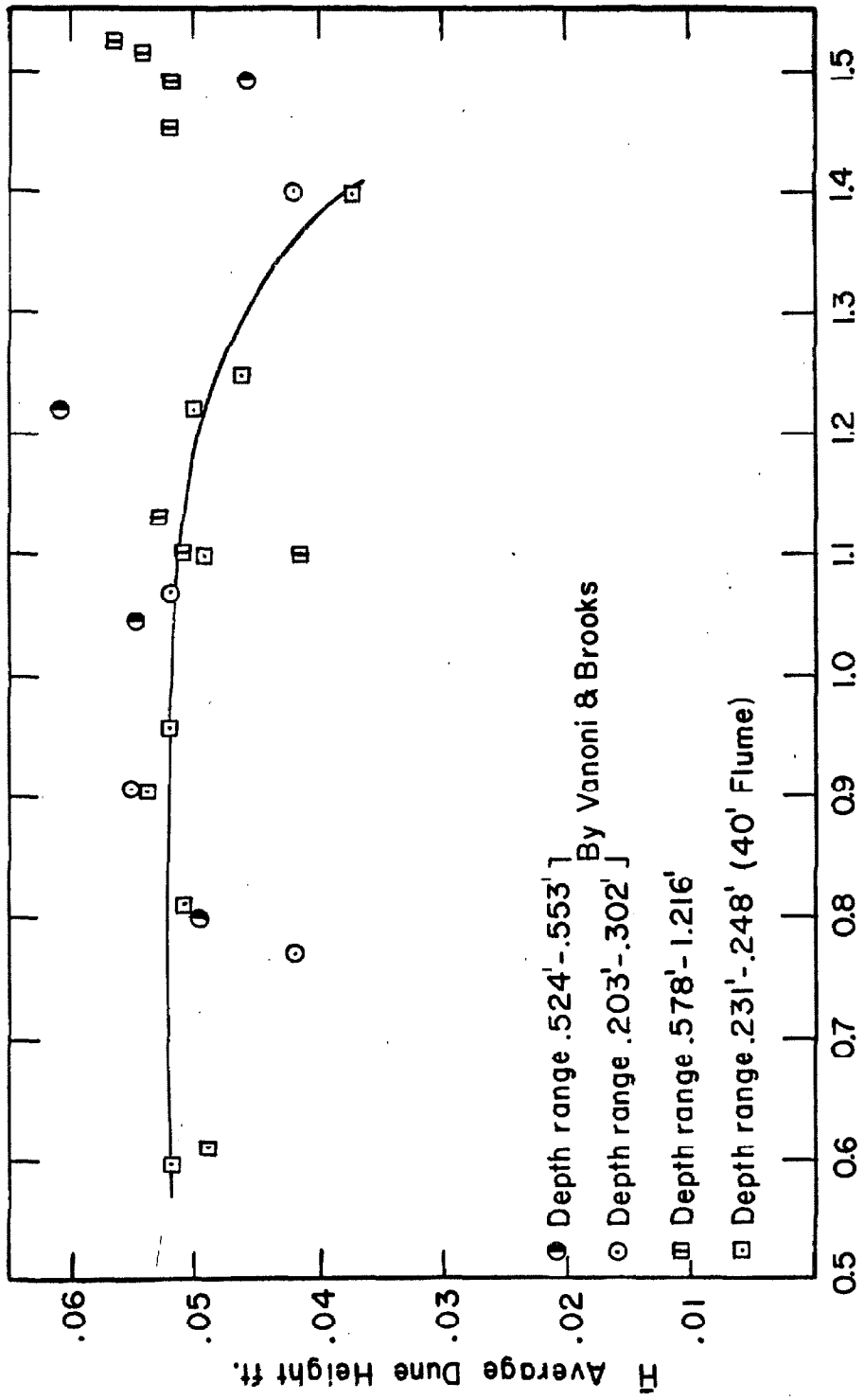

Fig. (5-22) Variation of the Average Dune Height with Average Velocity.

(a) Run No. 9-14, B-3.

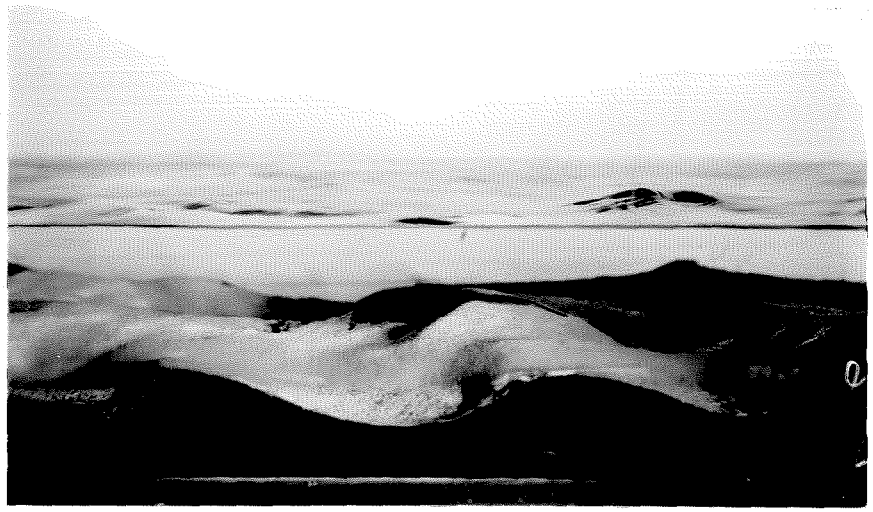

(b) Run No. 9-14, B-6.

Fig. (5-23) Flow field near a stabilized dune bed made visible by dye injected on the upstream face of the dune.

from the boundary and also tends to diffuse. Because of these characteristics of the flow field near the dune, the sand particles on the upstream side of the dune surface are acted upon by a tangential force. But this force will not exist where the flow separates from the boundary. At the separation point the sand particles will roll down the steep slope under action of the gravity force to form a distinct inclined surface. This surface provides a way to identify the location and the size of the lee side eddy or wake. A very convenient way to obtain a measure of this lee slope area is to measure its horizontal projection from a picture taken looking down on the dune. Fig. (5-24) shows a set of such photographs used in the determination of this area. The upper part of this figure shows an untouched photograph of dunes in the 40-foot flume generated by a flow 0.24 feet deep with an average velocity of 0.57 feet per second. The lee slopes of dunes in the lower picture were shaded to increase the contrast to facilitate the measurement of the horizontal area, a_s, by planimeter. Once this area, a_s, is determined over a certain bed area, A, the exposure parameter, c, can be obtained as the ratio of a_s to A.

Fig. (5-25) is a graph of dune friction factor, $f_b - f'_b$, against exposure parameter, e , for several values of r_b. One can see that the dune friction factor for a given r_b tends to increase with exposure parameter and for a given exposure parameter, e , the dune friction factor tends to diminish as r_b increases.

Photographs of six dune beds obtained from the experiments in the 40-foot flume are shown in Fig. (5-26). As may be seen from Table III, the depths for the six flows which generated the beds only from 0.231 to 0.241 ft, but the friction factors denoted below each photograph decrease as the exposure parameter, e , decreases.

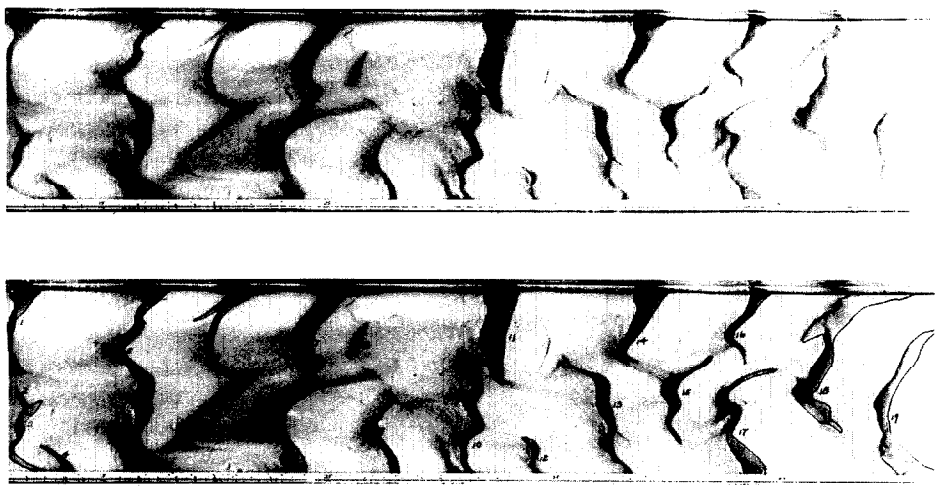

Fig. (5-24) Pictures used in determining the exposure parameter. Run No. 9-9. (Flow is to the left.)

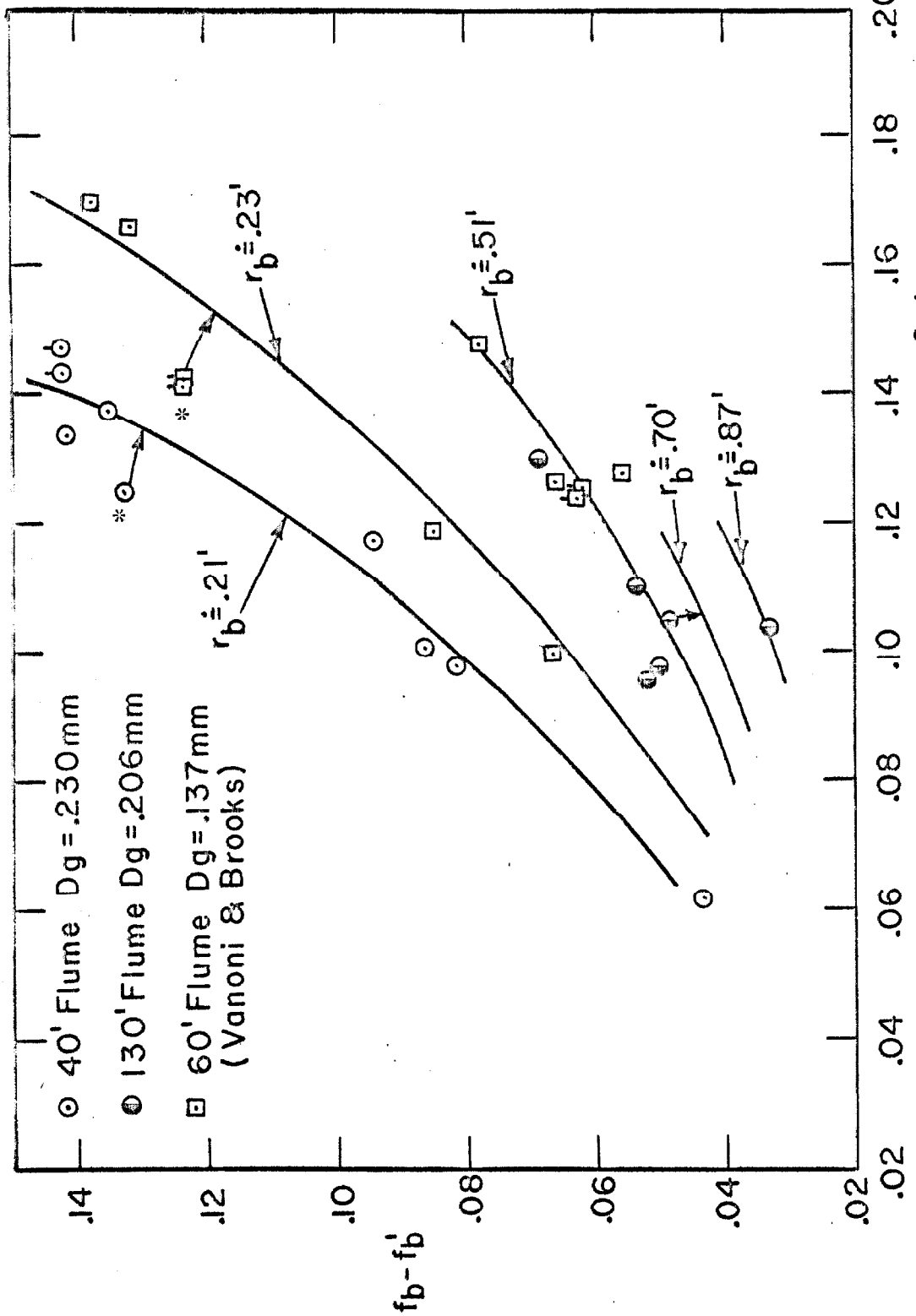

Fig. (5-25) Relationship between dune friction factor and exposure parameter.

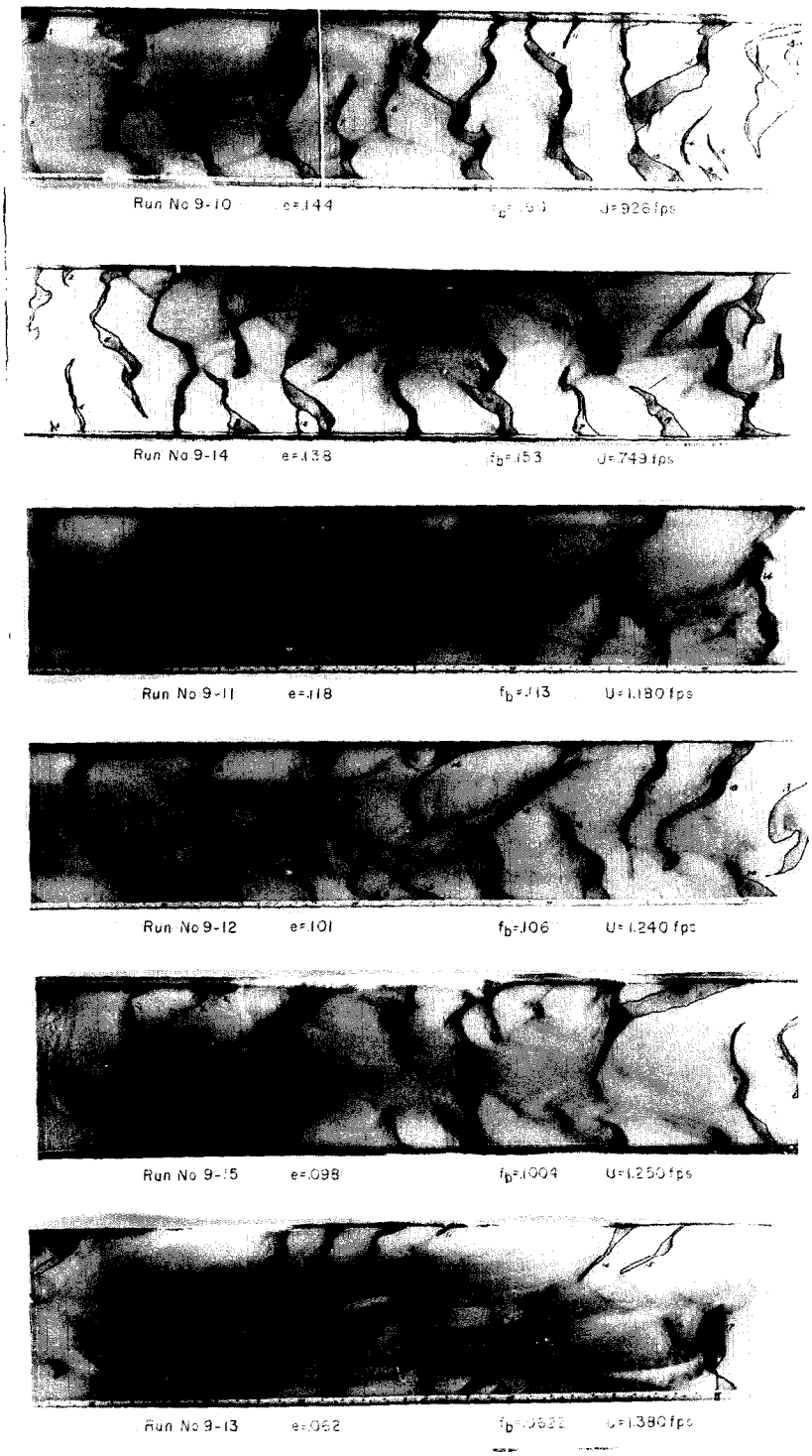

Fig. (5-26) Photographs of six dune beds in the 40-foot flume.

The shape of the upstream faces of the dunes depends to some extent on the velocity of flow. Careful measurements were made of some typical dunes generated by flows with different average velocities. These indicate that the upstream faces of dunes generated by low velocity flows are steeper near the point where the dividing streamline meets the boundary than those generated by flows of higher velocities. This is illustrated in Fig. (5-27) which shows pictures of dune beds generated by flows with different velocities. The profiles of dunes for two different velocities shown in Fig. (5-28) show the characteristic difference in shape. This difference in shape of upstream face of the dune might serve to explain the observed result that for a given exposure parameter, e, and bed hydraulic radius, the runs with lower velocity in general give slightly higher bed friction factor. This may be seen in Fig. (5-25) where the points for the flows with the lowest velocities have been denoted by an asterisk. However, no quantitative correlations can be made due to the difficulties in evaluating the slope variation.

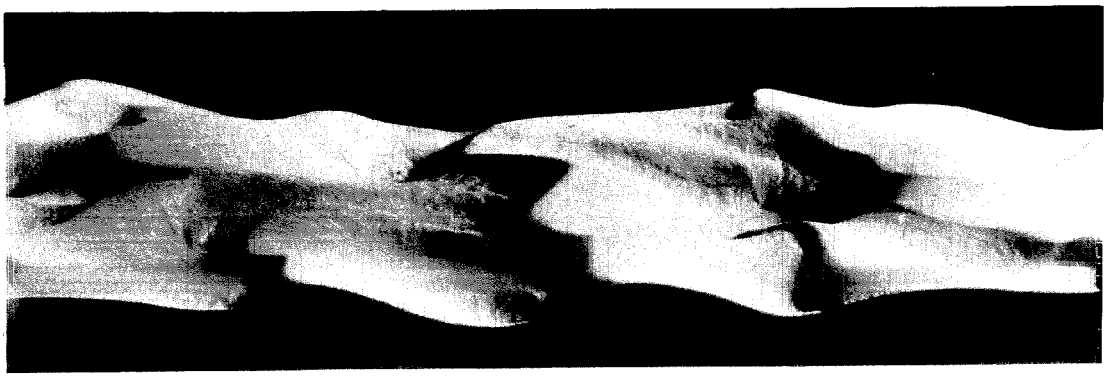

(a) Run No. 9-14, d = 0.231 ft. U = 0.749 fps.

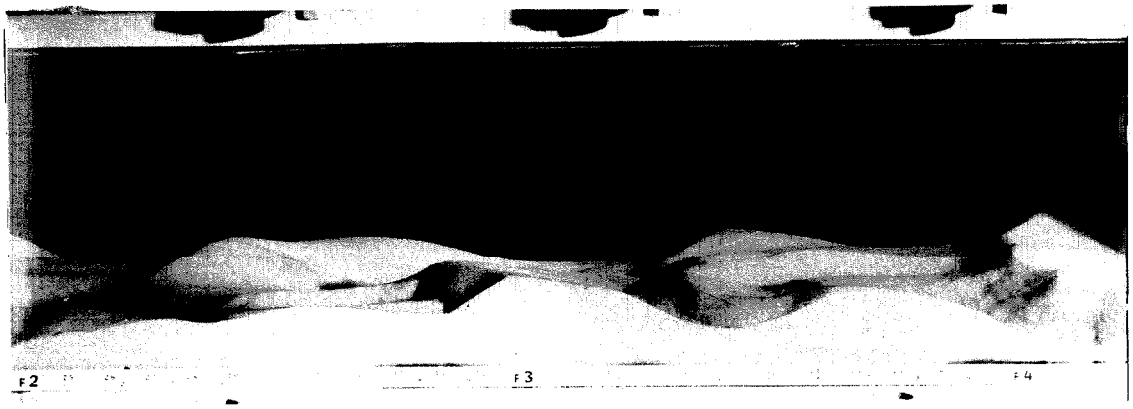

(b) Run No. 9-1, d = 0.248 ft. U = 0.899 fps.

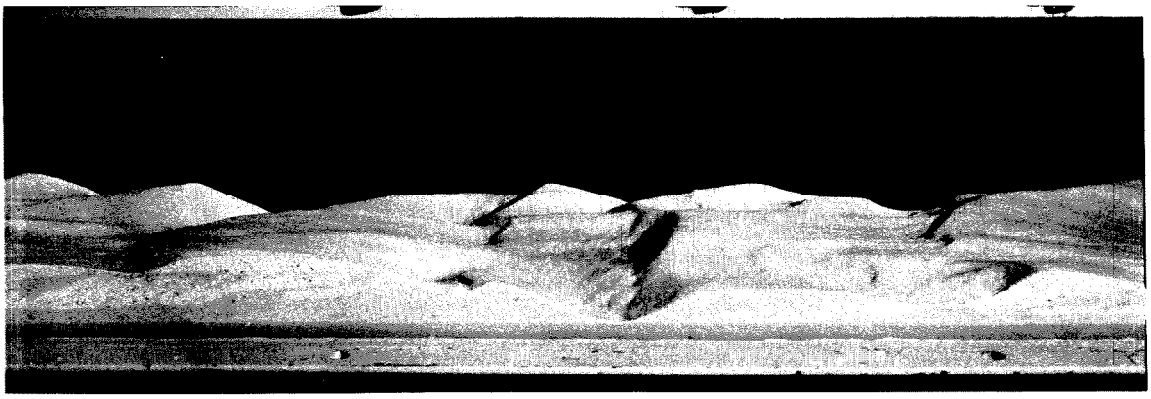

(c) Run No. 9-15, d = 0.241 ft. U = 1.250 fps.

Fig. (5-27) Dune Beds Showing Variation of Shape with Velocities.

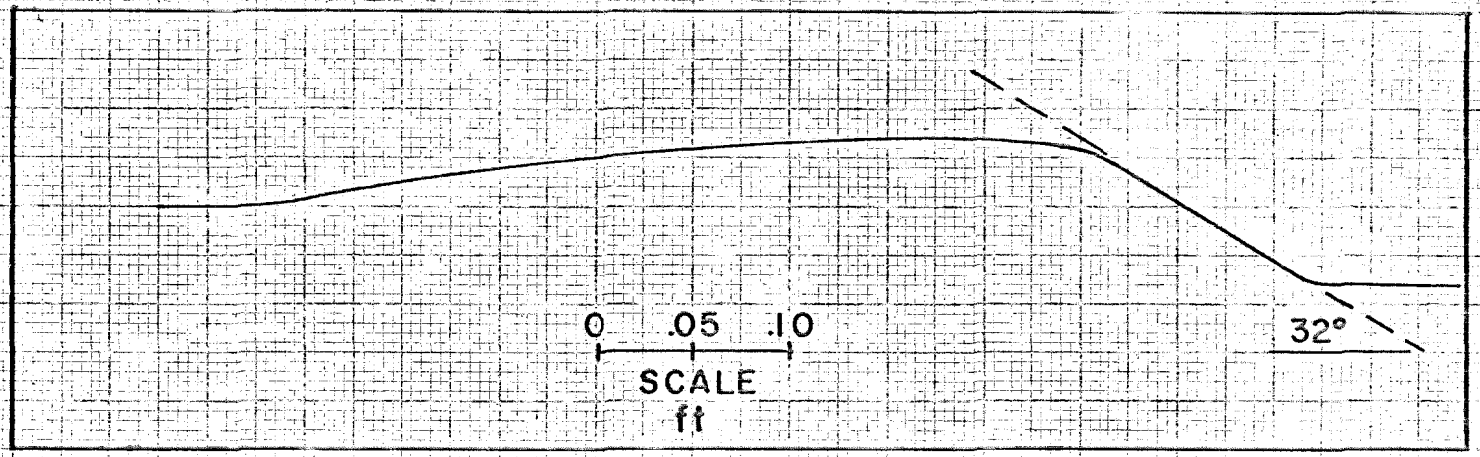

RUN NO 9-7 U=1.40 fps d=.234 ft

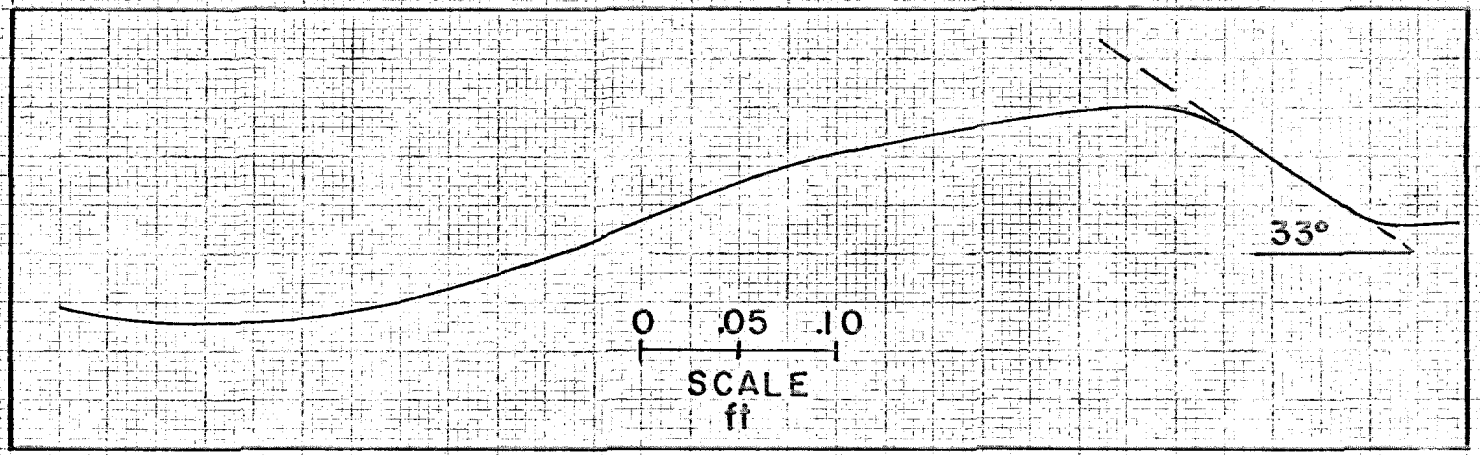

RUN NO 9-8 U=.599 fps d=.242 ft

Fig. (5-28) Diagram showing the difference of upstream shape of dunes generated by different velocities.

CHAPTER VI

RESISTANCE FUNCTION FOR STRAIGHT CHANNELS WITH DUNE COVERED BEDS

In Chapter II (Analytic Considerations), the modified relative roughness, $\frac{r_b}{e\overline{H}}$, has been identified as the important variable in the functional relationship for the dune friction factor, $f_b - f'_b$. The problem now remaining is to establish this functional relationship. For this purpose the experimental data obtained in the present study are presented in Table III and Table IV. Also experimental data on dune covered beds obtained in a flume 60 feet long and 33.5 inches wide by Vanoni and Brooks as mentioned in the last chapter are presented in Table VI.

Fig. (6-1) is an arithmatic plot of $f_b - f'_b$ against $r_b/e\overline{H}$ for all experimental results in Tables III, IV and VI. The fact that a line can be fitted to the points indicates that the dune friction factor is in fact a function of the modified relative roughness, $r_b/e\overline{H}$, as expressed by Equation (2-8). The graph shows that the dune friction factor, $f_b - f'_b$, will decrease as the bed hydraulic radius increases and that it will approach zero as $e\overline{H}$ becomes small compared to r_b, that is, as the bed becomes flat. The experimental results were also plotted on semi-logarithmic paper in Fig. (6-2) and as can be seen a straight line can be fitted to the points. This line has the following equation,

$$\frac{1}{\sqrt{f_b - f'_b}} = 3.5 \log_{10} \frac{r_b}{e\overline{H}} - 2.3 \qquad (6\text{-}1)$$

Table VI Summary of Data from Experiments in the 60-foot Flume with Dune Covered Beds (by Vanoni and Brooks, 1957).

$D_g = 0.137$ mm. $\sigma_g = 1.38$ (For The Dune Covered Bed)

Run No.	Q Discharge cfs.	d Depth ft.	r Hydr. Radius ft.	S Slope $x10^{+3}$	U Ave. Vel. fps.	f Frict. Factor	T Temp. °C.	r_b Bed Hydr. Radius ft.	f_b Bed Frict. Factor	f'_b Grain Frict. Factor	$f_b - f'_b$ Dune Frict. Factor	$\overline{H}$ Ave. Dune Height ft.	e Exposure Parameter	$r_b / e\overline{H}$ Modified Relative Roughness
Depth Range: 0.237 - 0.243 ft.														
2- 9	0.510	0.238	0.203	1.41	0.77	0.124	23.4	0.230	0.140	0.0194	0.121	0.042	0.143	38.3
2- 3	0.615	0.243	0.207	2.04	0.90	0.133	24.5	0.238	0.153	0.0185	0.135	0.055	0.170	25.4
2- 8	0.715	0.240	0.205	2.80	1.07	0.129	25.2	0.233	0.147	0.0178	0.129	0.052	0.166	27.0
2- 1	0.855	0.240	0.205	2.78	1.28	0.090	25.5	0.231	0.101	0.0172	0.0838	--	0.119	--
2- 7	0.930	0.237	0.203	2.77	1.40	0.074	22.4	0.227	0.083	0.0172	0.0658	0.044	0.100	51.6
Depth Range: 0.528 - 0.541 ft.														
2-12	1.21	0.541	0.390	0.39	0.80	0.061	24.6	0.488	0.076	0.0163	0.0597	0.050	0.125	78.1
2- 5	1.54	0.528	0.383	0.70	1.04	0.063	23.4	0.480	0.079	0.0156	0.0634	0.055	0.126	69.3
2-10	1.87	0.549	0.394	1.05	1.22	0.072	21.9	0.505	0.092	0.0151	0.0769	0.061	0.147	56.3
2-11	2.23	0.536	0.387	1.22	1.49	0.055	25.2	0.485	0.069	0.0144	0.0546	0.046	0.128	82.3

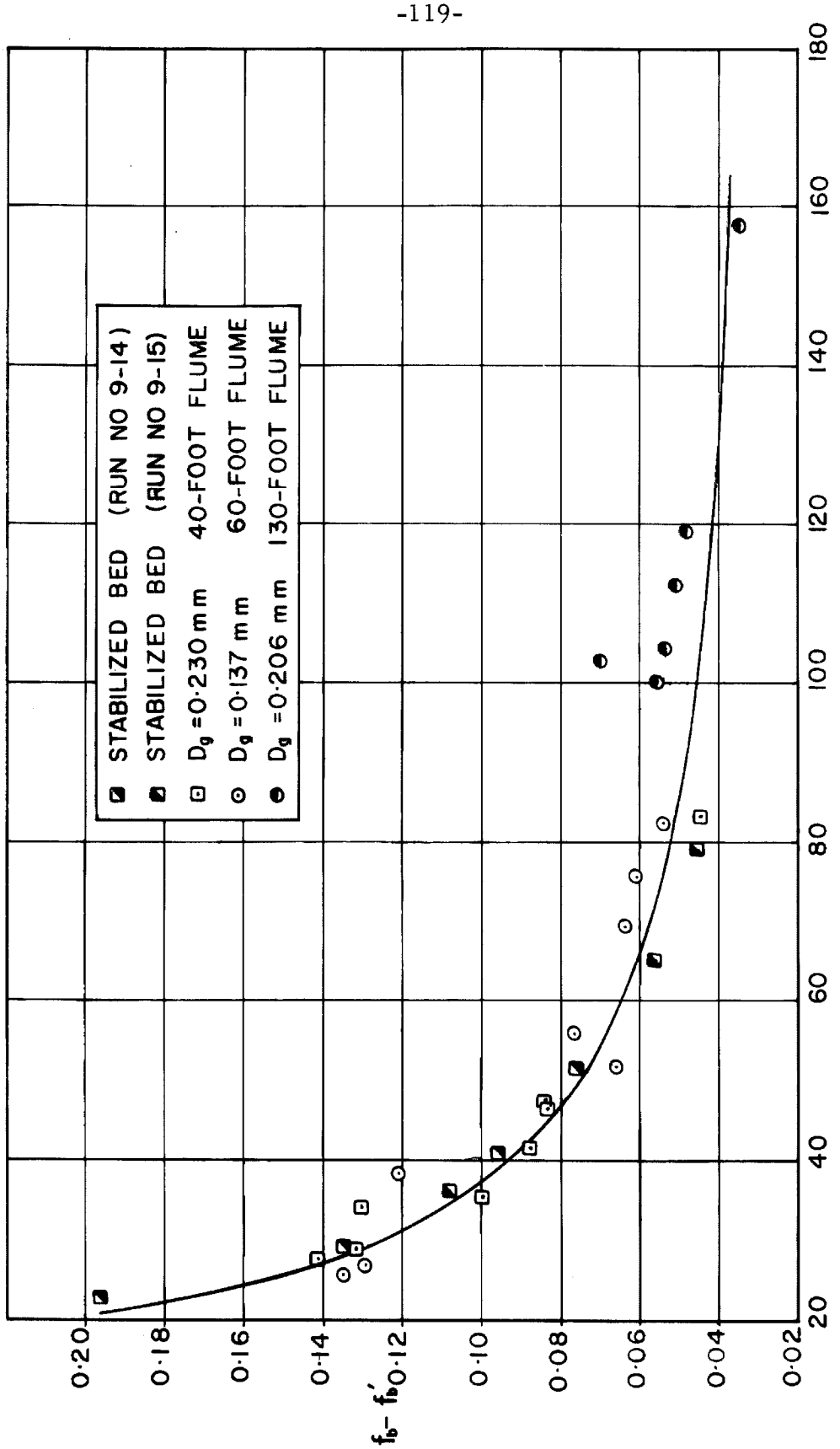

Fig. (6-1) Resistance Function for Straight Channels with Dune Covered Beds.

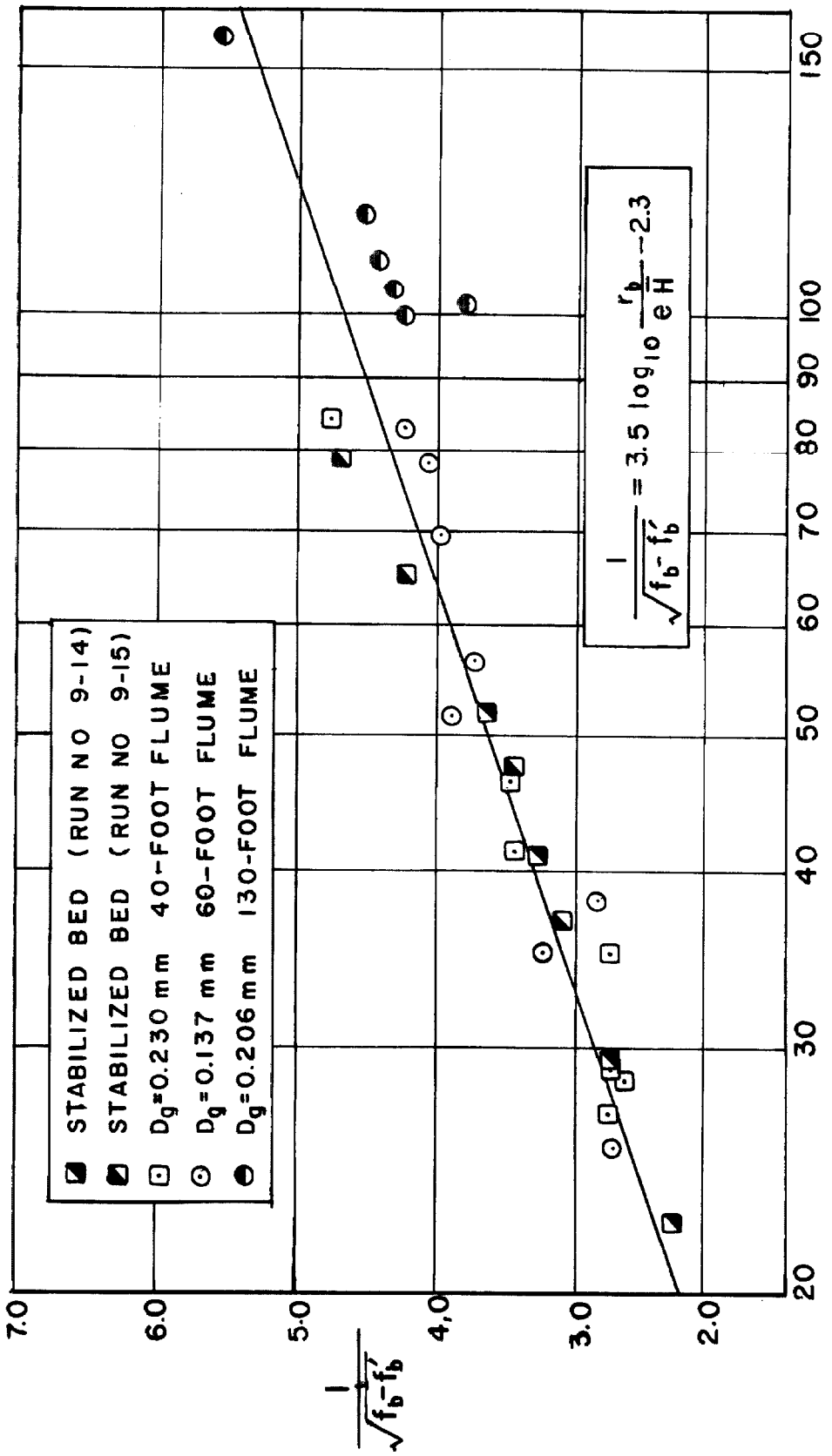

Fig. (6-2) Resistance Function for Straight Channels with Dune Covered Bcds.

The scatter of the points may be due to the following:

(a) The difficulties in determining a representative average dune height.

(b) Variation in dune shape, particularly of the upstream face as illustrated in Figs. (5-27) and (5-28).

Nevertheless, by use of this curve a reasonably accurate bed friction factor can be predicted for a straight laboratory channel covered with dunes of fine sand. To do this one needs to know the bed hydraulic radius, r_b, the exposure parameter, e, the average dune height, $\overline{H}$, and the geometric mean sieve size, D_g, of the sediment.

The dune friction factor, $f_b - f'_b$, is very sensitive to changes in the modified relative roughness, $\frac{r_b}{e\overline{H}}$, for low values of this relative roughness but much less sensitive at high values as indicated in Fig. (6-1). Therefore, for low values of the modified relative roughness, the evaluation of the average dune height, $\overline{H}$, and the exposure parameter, e, has to be quite accurate, otherwise a large error will result. For high values of $r_b/e\overline{H}$, the dune has a relatively flatter slope and effects of inaccuracy in determining the average dune height, $\overline{H}$, and the exposure parameter, e, will introduce relatively smaller error.

CHAPTER VII

DISCUSSION OF RESULTS

Much of the material in this report has been discussed under the presentation of experimental results (Chapter V). The present chapter is an extension of the discussions given previously to cover results obtained by various other workers. In the first section of this chapter, a discussion of the results of some field observations will be given and compared with the results obtained from Equation (6-1). In the second section, a discussion will be given of the effect of river meandering on friction factors. The discussions in the last two sections will cover equations for the bed friction factor in terms of geometrical properties of dune fields obtained by other investigators and the problems of using von Karman's pipe resistance formula to evaluate the equivalent sand roughness size in channels with relatively large roughness.

A. Friction Factors for Natural Streams Predicted from the Resistance Function Based on Flume Data

Equation (6-1) can not be expected to predict the bed friction factor of natural streams because the flume data on which it is based do not include the effect of meanders and lateral variation of bed roughness. Despite all these difficulties, the results calculated from this resistance function will still serve to explain some phenomena which exist in natural rivers as will be illustrated in the following.

Early in 1879, the Mississippi River Commission made some observations of the sand dunes at several stations in the lower

Mississippi River. The results were analysed by Eden [29] and Lane and Eden[30] and some of their results are presented in Table VII. It is interesting to calculate the bed friction factor for these cases through the use of Equation (6-1). In such calculations it was assumed (1) that the bed hydraulic radius was equal to the mean depth of flow in which the dune heights were observed, (2) that the exposure parameter, e , was equal to the average of the ratio of dune height to dune length, divided by tan θ where θ was the angle of repose of uniform sand and was taken as 30° and (3) that grain roughness size was equal to D_{50}. The results of this calculation are shown in the last three lines of Table VII.

Assumption (2) implies that the flow is separated behind each dune and tends to over-estimate the friction factor.

Despite the fact that the dune heights at Bullerton and Fulton are much larger than those observed in the flume experiments, these calculated results indicate that the ratio of the bed friction factor, f_b, to the grain friction factor, f'_b, is of the same order of magnitude as observed in the flume experiments[31]. The reason for this is that in the flume experiments, the exposure parameter, e , is much larger than in the Mississippi River at Bullerton and Fulton. In the flume, the exposure parameter, e , usually varies from 0.06 to 0.13 while the values of exposure parameter calculated through the assumption (2) above are only 0.026 and 0.024 at Bullerton and Fulton respectively.

In order to compare the result obtained from Equation (6-1) with actual measurements, the bed friction factor, f_b, for the Mississippi River near Fulton was calculated from the value of Manning's roughness

Table VII. Data on Dunes in the Mississippi River at Fulton, Tenn. and Bullerton and Helena, Ark.

	Bullerton	Fulton	Helena
Average Height of Crests ft.	4.4	4.7	5.0
Extreme Height of Crests ft.	13.0	12.0	8.0
Average Daily Movement, Perpendicular to Crests ft.	13.0	22.0	17.7
Extreme Daily Movement, Perpendicular to Crests ft.	20.0	35.0	--
Average Distance, Crest to Crest ft.	300	600	300
Extreme Distance, Crest to Crest ft.	--	--	500
Average Ratio, Length to Height	68	128	60
Depth of Water in Which Results Were Obtained ft.	10 to 30	45 to 60	13 to 30
Stage of the River Above Low Water ft.	12 to 26	12 to 26	12 to 18
Average Mean Velocity ft. per sec.	3.5	5.3	--
Size of Sand, D_{50} , mm.	0.3	0.5	--
Exposure Parameter, e	0.026	0.024	--
* Bed Friction Factor Calculated from Eq. (6-1), f_b	0.040	0.027	--
* Grain Friction Factor, f'_b	0.008	0.007	--
* Ratio of Bed Friction Factor to Grain Friction Factor, f_b/f'_b	5.0	3.9	--

coefficient, N , of 0.0305 reported by Eden[29]. This calculation yielded a value of 0.029 for f_b and agrees closely with the value of 0.027 calculated by Equation (6-1). However in calculating the latter value, it was assumed that the flow is separated behind each dune which tends to over-estimate the dune resistance and friction factor. This means that if the actual exposure parameter, e , is used in the calculation, the friction factor obtained by Equation (6-1) will be smaller than the measured value, 0.029. This result is not unexpected since, as already remarked, Equation (6-1) does not account for the effect of meanders and other irregularities in rivers.

In this connection, the work of Carey and Keller[28] should be mentioned. They observed the bed configurations of the Lower Mississippi River near Baton Rouge at two river stages by means of a sonic fathometer. They found that the largest dunes occurred at the higher stage. The largest dunes had lengths of as much as two miles and heights of the order of 30 feet and were covered with smaller dunes. At the low stage the dunes were from 20 to 50 feet long and 1 to 5 feet high and the long dunes had disappeared completely. This is shown in Fig. (7-1) reproduced from the work of Carey and Keller. The upper diagram shows a plan view of the reach of the river from mile 156 to mile 161 and the course of the ship carrying the fathometer. The next diagram shows a small scale reproduction of the fathometer trace over the reach for April 10, 1956. The other two diagrams are enlargements of the traces over the reach from mile 157.75 to mile 156.75 for April 10 and July 10, 1956 respectively. As noted on the diagrams, the gage at Donaldsonville read 18.3 feet on April 10, and 5.8 feet on

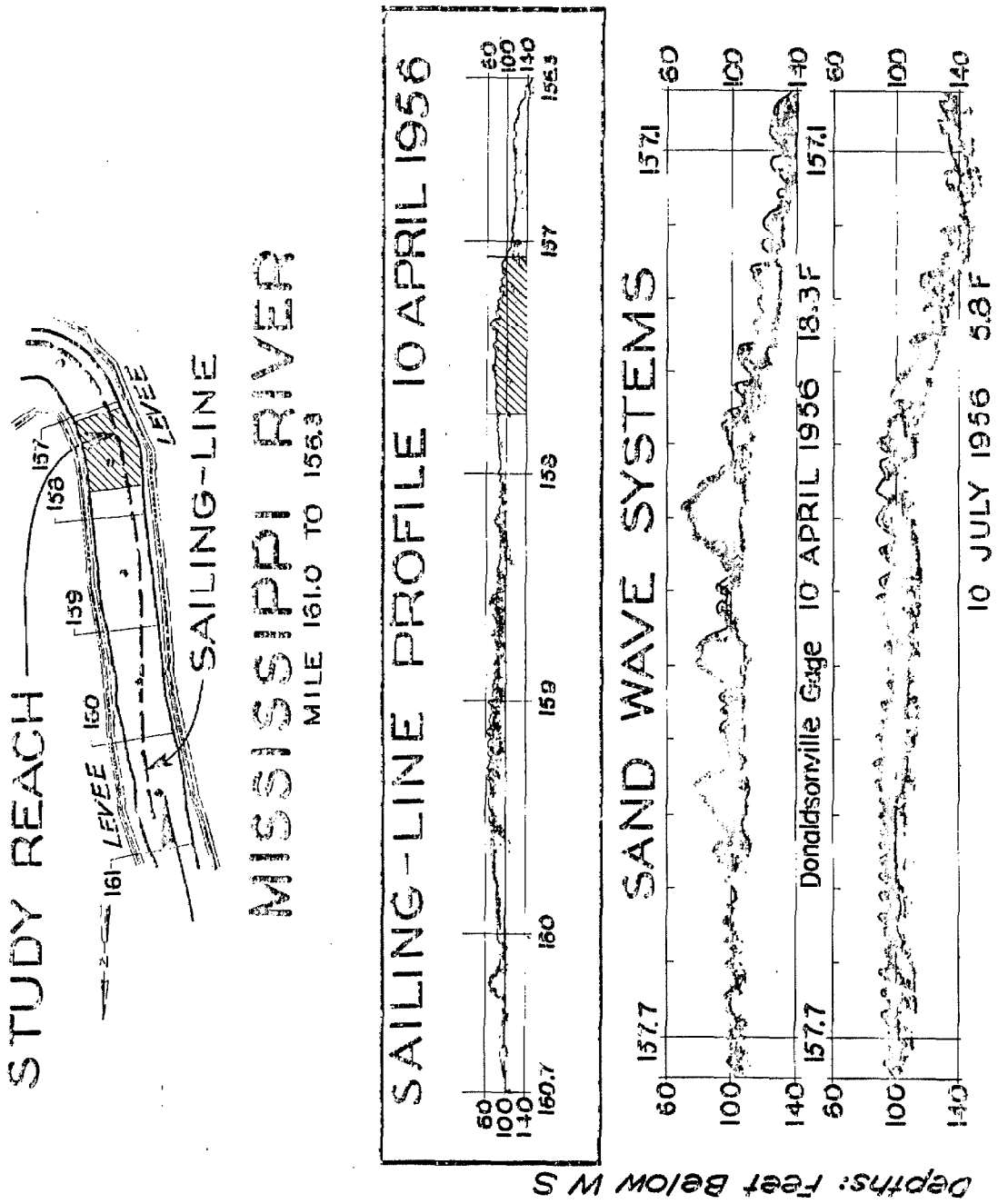

Fig. (7-1) Bed Profile for Lower Mississippi River from Carey and Keller.

September 10, 1956. The vertical scales on the traces show the distance below water surface.

In order to bring out the difference in the resistances of these two different roughness systems, the reach between miles 157.3 and 157.56 which had the largest difference in dune size for the two stages was chosen for evaluation. The friction factor for the two systems of roughness was calculated by use of Equation (6-1) under the assumptions made in a previous paragraph.

The dune height was taken to be equal to the average of the heights of all dunes within the reach, and the length of dunes was taken to be equal to the length of the reach divided by the number of the dunes in the reach. The hydraulic radius was taken to be equal to the depth of flow which, surprisingly, was 85 feet for the high stage and 90 feet for the low stage. The fact that the local depth of flow for the high stage is less than that for the low stage is not understood but it might be due to movement of sand from this location during the receding flood or to a change in the course of the ship carrying the fathometer.

The information obtained from Fig. (7-1) and the results of calculations using Equation (6-1) are presented in Table VIII. It is interesting to note that the relative roughness $r_b/\overline{H}$ for the low stage is about twice larger than that for the high stage but that the friction factor for the low stage is only 20 percent smaller. This small difference in friction factor can be explained in terms of the exposure parameter. The fact that e for the low stages is larger than that for the high stage tends to bring the values of the modified relative roughness and hence of $f_b - f'_b$ close together.

Table VIII Data on Dunes in the Lower Mississippi River at Donaldsonville Gage in the Reach between 157.3 to 157.56 Miles

	April 10, 1956 (high stage)	July 10, 1956 (low stage)
Water Depth, d , ft.	85	90
Number of Dunes	8	17
Average Dune Height, $\overline{H}$, ft.	12.5	7.7
Average Dune Length, ft.	171	80
Exposure Parameter, e	0.13	0.17
Relative Roughness, $r_b/\overline{H}$	7	12
Modified Relative Roughness, $r_b/e\overline{H}$	52	69
Calculated Dune Friction Factor, $f_b - f'_b$	0.073	0.058
Estimated Grain Friction Factor, f'_b	0.005	0.005
Bed Friction Factor, f_b	0.078	0.063

Eden[29] observed as did Carey and Kellar[28] that in the Lower Mississippi River, the largest dunes occurred at the highest stages. He also found that the Manning roughness coefficient, N , decreased as the stage increased. The reason for this can not be explained through the above calculation. However, some possible explanations can be outlined.

In Fig. (7-1) one can see that the lee slopes of the very large dunes tend to be less steep than those of most of the smaller ones. This indicates that the flow might follow the contours of these dunes without separation and consequently result in less pressure drag than assumed in the calculation. This would tend to decrease the friction factor for the high stage and bring the calculations in to closer agreement with the field observation by Eden[29]. Another factor which tends to reduce the friction factor for the high stage and which is not considered in the above calculation is the reduction of sinuosity of the river with increasing stage. Attention was called to this factor by Einstein and Barbarossa[32]. Additional remarks on this subject are presented in the next section.

B. River Meandering and Its Effect on Resistance to Flow

Nearly all natural channels exhibit some tendency to develop curves called meanders and meander patterns tend to be similar with their size approximately proportional to the size of the river[33]. Fig. (7-2) shows a photograph of a meandering river flowing in its alluvial valley. The resistance to flow due to meandering of a river has been studied both in the field[33] and in the laboratory[34]. The

Fig. (7-2) Photograph of a Meandering River in Central Alaska.
(photographed by Vanoni)

results of these studies indicate that as a river flows through a bend, a helicoidal or secondary flow (with top layer of water flowing outward and bottom layer of water flowing inward) is created. This secondary flow brings high surface velocity down to the bed of the channel and tends to cause higher shear stresses at the bed than in an equivalent straight channel.

Recently Bagnold[35] has established some quantitative relations between the friction factor due to a meander and the ratio of the radius of curvature, r_m, to the width of the river, w. Other studies[36] indicate that many rivers have a ratio r_m/w ranging from 2 to 3. However, r_m/w for the Mississippi River near Lake Providence, Louisiana, is equal to 2.8[36]. According to Bagnold's results, a curved river channel with r_m/w equal to 2.8 will have a friction factor that is around 60 percent larger than that of a straight channel with the same cross-section. This clearly indicates that the use of Equation (6-1) to predict the resistance of a natural stream is inadequate because it does not include the effect of river meandering on the friction factor.

C. *Use of von Karman's Resistance Formula to Evaluate the Equivalent Sand Roughness Size*

Von Karman's pipe resistance formula, Equation (2-3), has been used by many sediment workers[22] to evaluate the equivalent sand roughness size of channels. The data for flows with stabilized beds made it possible to check the validity of this equation for dune roughness. Calculations of these data showed that the equivalent sand roughness size of a dune bed evaluated from the von Karman's formula was not constant but that it actually depended on the bed hydraulic radius.

This is shown in Table IX where the results of calculations of data from eight runs with different depths but with the same dune bed are given.

As may be seen, the equivalent sand roughness size calculated by Equation (2-3) diminished rapidly as the depth and the bed hydraulic radius increased. Therefore, the use of equivalent sand roughness alone to describe the characteristic roughness length of the dune bed is inadequate. In contrast to this the values of $e\overline{H}$ calculated by using Equation (6-1) and the observed values of $f_b - f'_b$ vary only modulately as shown in the last columns of Table IX. The actual measured values of $e\overline{H}$ as in Table III, are .0072 and .0045 respectively for runs 9-14 and 9-15 and are seen to agree well with the calculated values.

D. Discussion of Channel Resistance Formulas

Most of the theories of river resistance relate the friction factor directly to flow parameters without knowing the bed configuration[32][36]. These have the advantage of convenience but they do not contribute to the understanding of the mechanism of the resistance offered by the different bed features.

The only formula known by the writer which attempts to relate the characteristics of a dune field to the friction factor was proposed by Laursen[38]. He followed von Karman's idea by choosing the height of the dune to be the roughness height and tried to establish the relationship between $\frac{1}{\sqrt{f_b}}$ and $\frac{2d}{\overline{H}}$, that is,

$$\frac{1}{\sqrt{f_b}} = F\left(\frac{2d}{\overline{H}}\right) \qquad (7-2)$$

Table IX. Calculated Values of Equivalent Sand Roughness for Stabilized Dune Beds.

Run No.	d Depth ft.	S Slope x 10^3	U Average Velocity fps.	T Temp. °C.	r_b Bed Hydr. Radius ft.	f_b Bed Frict. Factor	R_b Reynolds Number x 10^{-5}	f'_b Grain Frict. Factor	k_s Equivalent Sand Roughness Size ft.	$e\bar{H}$ modified Roughness Height [from Eq. (6-1)] ft.
Bed Configuration Generated in Run No. 9-14										
A-5	0.171	7.82	1.233	23.7	0.162	0.215	0.786	0.019	0.21	0.0081
B-5	0.230	2.74	0.978	22.5	0.210	0.155	0.577	0.020	0.17	0.0076
C-5	0.348	2.90	1.397	23.6	0.294	0.113	1.652	0.017	0.15	0.0077
D-5	0.472	1.01	1.028	23.7	0.370	0.091	1.530	0.015	0.12	0.0076
Bed Configuration Generated in Run No. 9-15										
A-5	0.182	1.62	0.736	41.5	0.166	0.127	0.712	0.020	0.096	0.0049
B-5	0.241	2.90	1.250	20.8	0.214	0.102	1.008	0.018	0.089	0.0049
C-5	0.361	2.48	1.616	21.1	0.292	0.072	1.794	0.016	0.060	0.0040
D-5	0.482	1.49	1.500	21.4	0.356	0.061	2.037	0.015	0.051	0.0036

in which $\overline{H}$ is the average dune height and d is the flow depth. The choice of the single dimensionless variable $\frac{2d}{\overline{H}}$ implies that dunes generated by different flows are similar. Or it is simply a statement that for a given depth of flow and a given dune height, the dunes with different exposure parameters will have the same bed friction factor. The experiments of the present investigation indicate that dune fields are not similar and that dunes with a certain height but different spacing or exposure parameter will offer different degrees of resistance to the flow. Therefore, any formula that does not consider the spacing between the dunes will certainly introduce large error in predicting the resistance. If such a formula were valid the exposure parameter would be constant. It is clear therefore that Equation (7-2) is inadequate.

For example, both Run No. 2-7 and Run No. 2-9 in Table VI have approximately the same values of $2e/\overline{H}$, but the bed friction factor, f_b, is 0.14 for Run No. 2-9 and 0.083 for Run No. 2-7. The reason for this difference is that the exposure parameters are different in these two runs. As can be seen the exposure parameter in Run No. 2-7 is 0.100 while in Run No. 2-9 it is 0.143.

CHAPTER VIII

SUMMARY OF CONCLUSIONS

1. The flow resistance created by the form drag of dune covered beds is independent of the viscosity of the fluid flowing over them. This indicates that the dune friction factor, $f_b - f'_b$, of a dune covered bed is a function of geometric quantities only.

2. The flow resistance offered by a dune bed can be expressed approximately in terms of two geometric characteristics of the dune field: (a) the average dune height, $\overline{H}$, and (b) the exposure parameter, e, defined as the fraction of the bed area occupied by the horizontal projections of the steep lee slopes of the dunes. The height, $\overline{H}$, is the characteristic roughness length for the dunes and e is a measure of the dune density or spacing.

3. It is not necessary to include parameters for the dune pattern or dune arrangement in the expression for resistance. It is believed that this is because the individual wakes behind the dunes are far enough apart so their flow fields do not interfere appreciably.

4. Experimental results indicate that for a straight channel with a dune covered bed, the dune friction factor, $f_b - f'_b$, is a function of the modified relative roughness $r_b / e\overline{H}$, that is,

$$f_b - f_b' = F\left(\frac{r_b}{e\overline{H}}\right) \qquad (8\text{-}1)$$

5. The pressure on a dune reaches a maximum on the upstream face where the dividing stream line of the eddy or the wake of the next

dune upstream meets the face and reaches minimum at the crest of the dune.

6. For a given dune bed configuration and a given depth of flow, the normalized velocity, u/U, at any point in the velocity field over the dunes was found to be independent of the average velocity.

7. The magnitude of the normalized pressure, $P-P_r/\frac{1}{2}\rho U^2$ over a dune decreases as the depth of flow increases, where P is the total pressure, P_r is a reference pressure on the dune, ρ is the density of the fluid and U is the average velocity in the cross section.

8. Equation (8-1) is expected to be valid for natural straight streams with regular cross section and dune covered beds.

9. The dune friction factor, $f_b - f'_b$, for the dune covered beds discussed in this study is given by,

$$\frac{1}{\sqrt{f_b - f'_b}} = 3.5 \log_{10} \frac{r_b}{e\bar{H}} - 2.3 \qquad (8\text{-}2)$$

This equation shows that a given change in the value of the modified relative roughness $r_b/e\bar{H}$ will produce a much larger change in the friction factor when $r_b/e\bar{H}$ is small than when it is large. This is also shown by Fig. (6-1).

10. Equation (8-1) can not give the friction factor of typical alluvial streams because it does not account for important effects such as those due to meandering.

11. Von Karman's equation (2-3) for the friction factor does not apply to channels with dune covered beds.

LIST OF SYMBOLS

A = area

A_r = dimensionless arrangement parameter

a_i = area between the i^{th} and $i+1^{th}$ c·v contours

a_s = sum of horizontal components of the lee side area of all dunes in the area A

b = width of flume (rectangular channel)

C = a constant

$\overline{C}$ = average sediment discharge concentration

C_i = point gage reading of the crest of the dune between the troughs T_i and $T_i + 1$

c = concentration of the sediment at a certain sampling point

D = pipe diameter

D_g = geometric mean sieve diameter (size)

D_{65} = grain size for which 65 percent by weight of sand is finer (similarly for D_{50}, $D_{84.1}$, etc.)

d = depth of flow

d_s = sand grain size

e = exposure parameter, a_s/A

e_s = elevation of the energy grade line

F = Froude number, $U/\sqrt{gd}$

f = Darcy-Weisbach friction factor for entire channel = $8(U_*/U)^2$

f_b = friction factor for the bed

f'_b = bed friction factor due to sand particles

f_w = friction factor for walls

g = gravitational acceleration

LIST OF SYMBOLS (cont'd)

$\overline{H}$ = average dune height

h = characteristic roughness length of the dune field

h_f = drop in piezometric head in a certain distance

h_v = differential piezometric head

$\hat{i}$ = unit vector in the main flow direction

k_s = equivalent roughness size

m = slope of velocity profile (units of velocity per cycle)

n = number of contours or number of dunes

N = Manning roughness coefficient

P = total pressure measured at a certain point

P_r = reference pressure

p = wetted perimeter

p_b = wetted perimeter for bed

p_w = wetted perimeter for walls

Q = water discharge (volume per unit time)

R = Reynolds number for the entire channel, $(4rU/\nu)$

R_b = Reynolds number for the bed, $(4r_bU/\nu)$

R_w = Reynolds number for the wall, $(4r_wU/\nu)$

r = hydraulic radius of cross section, $bd/(b+2d)$

r_b = hydraulic radius for the bed obtained by side-wall correction procedure

r_m = radius of curvature

r_w = hydraulic radius for the wall

S = slope of the energy grade line

LIST OF SYMBOLS (cont'd)

S_f = slope of the flume

T = temperature

T_i = point gage reading at the i^{th} trough of the dune

U = average velocity in the cross section, Q/bd

U_{cl} = average velocity at the centerline of the flume

U_{*cl} = mean shear velocity at the centerline of the flume $\sqrt{f_b/8}\ U_{cl}$

v = velocity at a certain sampling point

W = width of the stream

x = distance along the flume taken to be positive in the direction of flow

y_w = water surface elevation

δ = thickness of laminar sublayer

κ = von Karman's constant

κ_{cl} = von Karman's constant at centerline of a rectangular channel, $2.30U_{*cl}/m$

ν = kinematic viscosity of the flowing fluid

ρ = mass density of water

σ_g = geometric standard deviation of sand-size distribution

τ_D = total shear stress minus the grain shear stress calculated from pipe resistance diagram

REFERENCES

1. Brooks, N. H., "Mechanics of Streams with Movable Beds of Fine Sands", Proc. ASCE, Vol. 81, April 1955.
2. Keulegan, Garbis H., "Laws of Turbulent Flow in Open Channels", Research Paper RP1151, National Bureau of Standards, Vol. 21, December 1938.
3. Nikuradse, J., "Laws of Flow in Rough Pipes", Technical Memorandum 1292, NACA, Nov. 1950. Translation of "Stromungsgesetze in ranhen Rohreno", V. D. I., Gorschungsheft, p. 361, 1932.
4. von Kármán, Th., "Mechanische Ähnlichkeit und Turbulenz", Nach. Ges. Wiss. Göttingen, Math. Phys. Klasse, 58 (1930) and Proc. *3rd. Intern. Congress Appl. Mech., Stockholm*, Pt. 1, 85 (1930); NACA TM 611, (1931)
5. Morris, H. M., "Flow in Rough Conduits", Transactions, ASCE, Vol. 120, 1955.
6. Taylor, R. H. Jr., Unpublished Results.
7. Schlichting, H., "Experimentelle Untersuchungen zum Ranhigkeitsproblem", Ing.-Arch. 7, p. 1 (1936), English translation in Proc. ASME, 1936.
8. Colebrook, C. F. and White, C. M., "Experiments with Fluid Friction in Roughness Pipes", Roy. Soc. of London, Vol. 161, 1937.
9. Vanoni, V. A., and Nomicos, G. N., "Resistance Properties of Sediment-laden Streams", Transactions, ASCE, Vol. 125, 1960.

10. Einstein, H. A., "Formulas for the Transportation of Bed Load", Transactions, ASCE, Vol. 107, p. 561, 1942.

11. Johnson, J. W., "The Importance of Side-wall Friction in Bed-Load Investigations", Civil Eng., Vol. 12, No. 6, p. 329, June 1942.

12. Laursen, E. M., Etc., "Pressure and Shear Distribution on Schematic Dunes", Technical Report No. 2, M.S.U. Mich., 1962.

13. Vanoni, V. A., and Brooks, N. H., "Laboratory Studies of the Roughness and Suspended Load of Alluvial Streams", Report No. E-68, California Institute of Technology, Pasadena, California, 1957.

14. Vanoni, V. A., "130-Foot Precision Tilting Flume", Tech. Memo. No. 64-7, W. M. Keck Laboratory of Hydraulics and Water Resources, California Institute of Technology, Jan. 1964.

15. Brooks, N. H., "Laboratory Studies of the Mechanics of Streams Flowing over a Movable Bed of Fine Sand", Ph.D. Thesis, California Institute of Technology, Pasadena, California, 1954.

16. Vanoni, V. A., "Measurements of Critical Shear Stress for Entraining Fine Sediments in Boundary Layer", W. M. Keck Laboratory of Hydraulics and Water Resources, California Institute of Technology, Report No. KH-R-7, May 1964.

17. Vanoni, V. A., "Transportation of Suspended Sediment by Water", Transactions, ASCE, Vol. 111, 1946, pp. 67-133.

18. Toni, I., "Experimental Investigation on Flow Separation over A Step", Symposium on Boundary Layer Research, Germany, August 1957.

19. Walker, G. R., "A Study of the Two Dimensional Flow of Turbulent Fluid Past a Step", M. S. thesis, University of Auckland, Auckland, New Zealand, 1961.

20. Rand, W., Discussion of "Wind Tunnel Studies of the Movement of Sedimentary Material" by A. W. Zingg, Proceedings, Fifth Iowa Hydraulic Conference, 1952, pp. 132-133.

21. "Notes on Turbulence Function k", Missouri River Division, Corps of Engrs., U. S. Department of the Army, Omaha, Nebraska, 1953 (unpublished).

22. Nordin, C. F., Jr., and Dempster, G. R., Jr., "Vertical Distribution of Velocity and Suspended Sediment, Middle Rio Grande, New Mexico", Geological Survey Professional Paper 462-B, 1963.

23. Kennedy, J. F., "Stationary Waves and Antidunes in Alluvial Channels", Report No. KH-R-2, W. M. Keck Laboratory of Hydraulics and Water Resources, California Institute of Technology, Jan. 1961.

24. Rouse, H., Elementary Mechanics of Fluids , J. Wiley and Sons, New York, 1946.

25. Otto, G. H., "A Modified Logarithmic Probability Graph for the Interpretation of Mechanical Analysis of Sediments", Journal of Sedimentary Petrology, Vol. 9, No. 2, 1939, pp. 62-76.

26. Simons, D. B. and Richardson, E. V., "Resistance to Flow in Alluvial Channels", Transactions, ASCE, Vol. 127, 1962.

27. Simons, D. B. and Richardson, E. V., "Forms of Bed Roughness in Alluvial Channels", Transactions, ASCE, Vol. 128, 1963.

28. Carey, Walter C., and Keller, M. Dean, "Systematic Changes in the Beds of Alluvial River", Journal of Hydraulics Div., ASCE, Vol. 83, No. HY4, Aug. 1957.

29. Eden, Edwin W., "A Study of Bed Movement and Hydraulic Roughness Changes in the Lower Mississippi River", M.S. Thesis, Dept. of Mechanics and Hydraulics, State University of Iowa, June 1938.

30. Lane, E. W. and Eden, E. W., "Sand Waves in the Lower Mississippi River", Western Society of Engineers, 1940.

31. Taylor, R. Hugh and Brooks, Norman H., Discussion of "Resistance of Flow in Alluvial Channels", Trans. ASCE, Vol. 127, 1962, p. 982.

32. Einstein, Hans A. and Barbarossa, Nicholas L., "River Channel Roughness", Trans. ASCE, Vol. 117, 1952, p. 1121.

33. Leopold, Luna B., Wolman, M. Gordon and Miller, John T. Fluvial Processes in Geomorphology, W. H. Freeman and Co., San Francisco, 1964.

34. Leopold, Luna B., Etc., "Flow Resistance in Sinuous or Irregular Channels", Geologic Survey Professional Paper 282-D, U.S.A. 1960.

35. Bagnold, Ralph A., "Some Aspects of the Shape of River Meanders," Geologic Survey Professional Paper 282-E, U.S.A. 1960.

36. Leopold, Luna B. and Wolman, M., "River Meanders", Bulletin of the Geological Society of America, Vol. 71, pp. 769-794, June 1960.

37. Ali, Said M., and Albertson, Maurice L., "Some Aspects of Roughness in Alluvial Channels", Dept. of Civil Eng., Colorado A. and M. College, Fort Collins, Colorado, Aug. 1953, revised Aug. 1956.

38. Laursen, Emmett M., "The Total Sediment Load of Streams", Journal of the Hydraulics Division, ASCE, Paper 1530, HY1, Feb. 1958.